AFRL-AFOSR-VA-TR-2015-0263

REGENERATION AND REMODELING OF COMPOSITE MATERIALS

Scott White
UNIVERSITY OF ILLINOIS

08/27/2015
Final Report

Air Force Research Laboratory
AF Office Of Scientific Research (AFOSR)/ RTB2
Arlington, Virginia 22203
Air Force Materiel Command

REPORT DOCUMENTATION PAGE

Form Approved
OMB No. 0704-0188

PLEASE DO NOT RETURN YOUR FORM TO THE ABOVE ORGANIZATION.

1. REPORT DATE *(DD-MM-YYYY)*	2. REPORT TYPE	3. DATES COVERED *(From - To)*
18/08/15	Final	01/06/10-31/05/15

4. TITLE AND SUBTITLE

Regeneration and Remodeling of Composite Materials

5a. CONTRACT NUMBER

FA9550-10-1-0255

5b. GRANT NUMBER

5c. PROGRAM ELEMENT NUMBER

6. AUTHOR(S)

White, Scott R., Sottos, Nancy R., Moore, Jeffrey S.

5d. PROJECT NUMBER

5e. TASK NUMBER

5f. WORK UNIT NUMBER

7. PERFORMING ORGANIZATION NAME(S) AND ADDRESS(ES)

University of Illinois
Office of Business and Financial
1901 South First St., Suite A
Champaign, IL 61820-7406

8. PERFORMING ORGANIZATION REPORT NUMBER

9. SPONSORING/MONITORING AGENCY NAME(S) AND ADDRESS(ES)

USAF, AFRL
AF Office of Scientific Research
875 N. Randolph St. Room 3112
Arlington, VA 22203

10. SPONSOR/MONITOR'S ACRONYM(S)

AFOSR

11. SPONSOR/MONITOR'S REPORT NUMBER(S)

12. DISTRIBUTION/AVAILABILITY STATEMENT

A: Approved for public release: distribution unlimited

13. SUPPLEMENTARY NOTES

14. ABSTRACT

The Regeneration and Remodeling of Composite Materials (Regeneration) Program was supported by the Air Force Office of Scientific Research (AFOSR) through a Discovery Grant from 2010-2015. The program was conducted at the University of Illinois at Urbana-Champaign (UIUC). Regeneration was conceived to expand the function of materials containing microvascular networks to achieve autonomous response and adaptation to external stimuli. The central goal of Regeneration was to integrate bio-mimetic functions into synthetic, engineering materials realized through a synergistic combination of expertise in chemistry and engineering. The Regeneration and Remodeling of Composite Materials program was focused on replicating the function of regeneration in which natural systems rebuild or replace macroscopic structures autonomously. Inspired by this biological ability, vascular networks were designed to synthetically regrow load-bearing structures and replenishing protective surface coatings. Multistage polymerization reactions introduced a new paradigm in healing agent conceptual design where rapid rheological transformations and selective wetting resulted in new self-supporting fluids which build upon themselves in an accretive

15. SUBJECT TERMS

16. SECURITY CLASSIFICATION OF:			17. LIMITATION OF ABSTRACT	18. NUMBER OF PAGES	19a. NAME OF RESPONSIBLE PERSON
a. REPORT	b. ABSTRACT	c. THIS PAGE			Scott R. White
U	U	U	SAR	66	19b. TELEPHONE NUMBER *(Include area code)* 217-333-1077

Reset

Standard Form 298 (Rev. 8/98)
Prescribed by ANSI Std. Z39.18
Adobe Professional 7.0

INSTRUCTIONS FOR COMPLETING SF 298

1. REPORT DATE. Full publication date, including day, month, if available. Must cite at least the year and be Year 2000 compliant, e.g. 30-06-1998; xx-06-1998; xx-xx-1998.

2. REPORT TYPE. State the type of report, such as final, technical, interim, memorandum, master's thesis, progress, quarterly, research, special, group study, etc.

3. DATES COVERED. Indicate the time during which the work was performed and the report was written, e.g., Jun 1997 - Jun 1998; 1-10 Jun 1996; May - Nov 1998; Nov 1998.

4. TITLE. Enter title and subtitle with volume number and part number, if applicable. On classified documents, enter the title classification in parentheses.

5a. CONTRACT NUMBER. Enter all contract numbers as they appear in the report, e.g. F33615-86-C-5169.

5b. GRANT NUMBER. Enter all grant numbers as they appear in the report, e.g. AFOSR-82-1234.

5c. PROGRAM ELEMENT NUMBER. Enter all program element numbers as they appear in the report, e.g. 61101A.

5d. PROJECT NUMBER. Enter all project numbers as they appear in the report, e.g. 1F665702D1257; ILIR.

5e. TASK NUMBER. Enter all task numbers as they appear in the report, e.g. 05; RF0330201; T4112.

5f. WORK UNIT NUMBER. Enter all work unit numbers as they appear in the report, e.g. 001; AFAPL30480105.

6. AUTHOR(S). Enter name(s) of person(s) responsible for writing the report, performing the research, or credited with the content of the report. The form of entry is the last name, first name, middle initial, and additional qualifiers separated by commas, e.g. Smith, Richard, J, Jr.

7. PERFORMING ORGANIZATION NAME(S) AND ADDRESS(ES). Self-explanatory.

8. PERFORMING ORGANIZATION REPORT NUMBER. Enter all unique alphanumeric report numbers assigned by the performing organization, e.g. BRL-1234; AFWL-TR-85-4017-Vol-21-PT-2.

9. SPONSORING/MONITORING AGENCY NAME(S) AND ADDRESS(ES). Enter the name and address of the organization(s) financially responsible for and monitoring the work.

10. SPONSOR/MONITOR'S ACRONYM(S). Enter, if available, e.g. BRL, ARDEC, NADC.

11. SPONSOR/MONITOR'S REPORT NUMBER(S). Enter report number as assigned by the sponsoring/ monitoring agency, if available, e.g. BRL-TR-829; -215.

12. DISTRIBUTION/AVAILABILITY STATEMENT. Use agency-mandated availability statements to indicate the public availability or distribution limitations of the report. If additional limitations/ restrictions or special markings are indicated, follow agency authorization procedures, e.g. RD/FRD, PROPIN, ITAR, etc. Include copyright information.

13. SUPPLEMENTARY NOTES. Enter information not included elsewhere such as: prepared in cooperation with; translation of; report supersedes; old edition number, etc.

14. ABSTRACT. A brief (approximately 200 words) factual summary of the most significant information.

15. SUBJECT TERMS. Key words or phrases identifying major concepts in the report.

16. SECURITY CLASSIFICATION. Enter security classification in accordance with security classification regulations, e.g. U, C, S, etc. If this form contains classified information, stamp classification level on the top and bottom of this page.

17. LIMITATION OF ABSTRACT. This block must be completed to assign a distribution limitation to the abstract. Enter UU (Unclassified Unlimited) or SAR (Same as Report). An entry in this block is necessary if the abstract is to be limited.

Final Report

REGENERATION AND REMODELING OF COMPOSITE MATERIALS

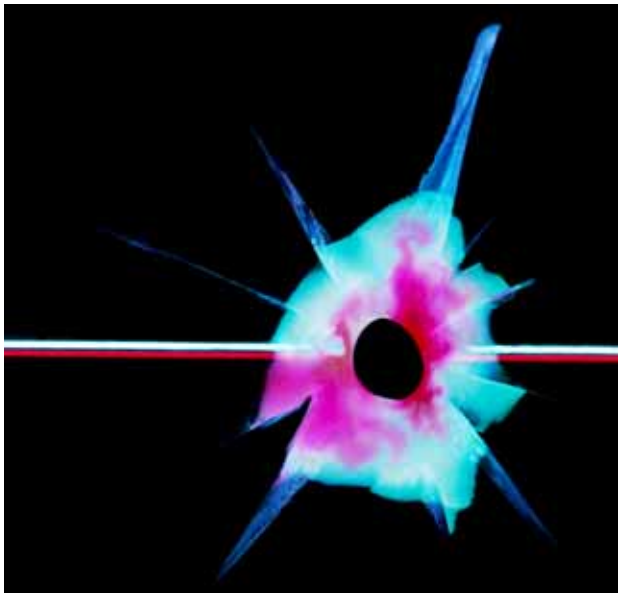

AFOSR GRANT # FA9550-10-1-0255

Scott R. White (PI)
swhite@uiuc.edu

University of Illinois at Urbana-Champaign
306 Talbot Lab, 104 S. Wright St.
Urbana, IL 61801

Co-PIs: Nancy R. Sottos, Jeffrey S. Moore

Materials Science & Engineering, Chemistry
University of Illinois at Urbana-Champaign

Table of Contents

1. Overview pg. 3

1.1. Archival publications resulting from the AFOSR Discovery grant pg. 4

1.2. Conferences presentations resulting from the AFOSR Discovery grant pg. 4

1.3. Patents resulting from the AFOSR Discovery grant pg. 5

2. Summary of Research

2.1. Damage Regeneration

2.1.1. Coating regeneration pg. 6

2.1.2. Fiber pullout pg. 9

2.1.3. PDMS hole sealing pg. 11

2.1.4. Restoration of large damage volumes in polymers pg. 12

2.1.5. Enhanced design and performance of restorative polymer systems pg. 23

2.1.6. Impact damage restoration pg. 35

2.2. New Healing Chemistries

2.2.1. UV curable healing agents pg. 39

2.2.2. Epoxy-thiol healing chemistry pg. 41

2.2.3. Reversible chemistries pg. 44

2.2.4. Two-stage polymer chemistry pg. 47

2.3. Advanced Vascular Delivery

2.3.1. Fluid-mediated Delivery pg. 58

2.3.2. Air assisted reagent delivery pg. 59

2.3.3. Accumulators for healing agent sequestration pg. 59

3. References pg. 63

1. Overview

The Regeneration and Remodeling of Composite Materials (Regeneration) Program was supported by the Air Force Office of Scientific Research (AFOSR) through a *Discovery Grant* from 2010-2015. The program was conducted at the University of Illinois at Urbana-Champaign (UIUC). Regeneration was conceived to expand the function of materials containing microvascular networks to achieve autonomous response and adaptation to external stimuli. The central goal of Regeneration was to integrate bio-mimetic functions into synthetic, engineering materials realized through a synergistic combination of expertise in chemistry and engineering.

The Regeneration and Remodeling of Composite Materials program was focused on replicating the function of regeneration in which natural systems rebuild or replace macroscopic structures autonomously. Inspired by this biological ability, vascular networks were designed to synthetically regrow load-bearing structures and replenishing protective surface coatings. Multi-stage polymerization reactions introduced a new paradigm in healing agent conceptual design where rapid rheological transformations and selective wetting resulted in new self-supporting fluids which build upon themselves in an accretive fashion to regenerate lost mass. Experimental procedures were developed to demonstrate system efficacy and repeatability in achieving functional homeostasis of structural materials. A detailed description of thematic research results for the research team as part of the Regeneration program are presented in the following sections.

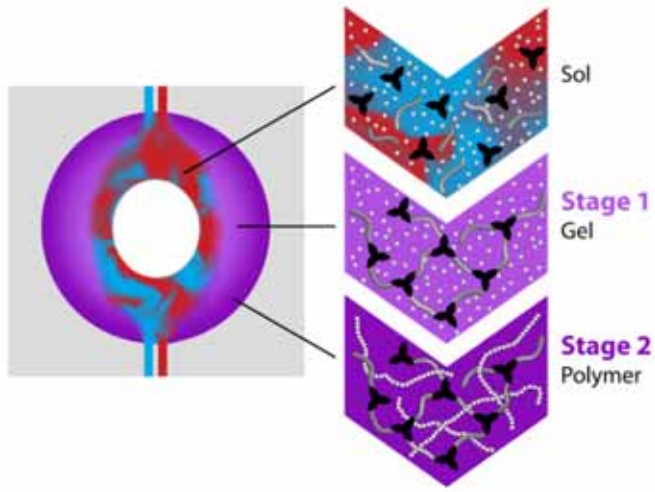

Schematic of multi-stage polymerization for repair of large damage volume.

1.1. Archival publications resulting from the AFOSR Discovery grant

1. H. Jin, K.R. Hart, A.M. Coppola, R.C. Gergely, J.S. Moore, N.R. Sottos, S.R. White, Self-Healing Epoxies and Their Composites, in: W.H. Binder (Ed.), Self-Healing Polymers From Principles to Applications. Wiley-VCH Verlag GmbH & Co. KGaA, Weinheim, Germany, 2013.
2. J.F. Patrick, K.R Hart, B.P. Krull, C.E. Diesendruck, J.S. Moore, S.R. White, N.R. Sottos. Continuous Self-Healing Life Cycle in Vascularized Structural Composites. Advanced Materials, 26 (2014) 4302-4308.
3. S.R. White, J.S. Moore, N.R. Sottos, B.P. Krull, W.A. Santa Cruz, R.C.R. Gergely, Restoration of Large Damage Volumes in Polymers. Science 344 (2014) 620–3.
4. R.C.R. Gergely, S.J. Pety, B.P. Krull, J.F. Patrick, T.Q. Doan, A.M. Coppola, P.R. Thakre, N.R. Sottos, J.S. Moore, S.R. White, Multidimensional Vascularized Polymers using Degradable Sacrificial Templates. Advanced Functional Materials 25 (2015) 1043–1052.
5. B.P Krull, J.F Patrick, K.R. Hart, S.R White, N. Sottos, Automatic Optical Crack Tracking for Double Cantilever Beam Specimens. Accepted by Experimental Techniques 3 March 2015.
6. B.P Krull, R.C.R. Gergely, W.A. Santa Cruz, Y. Fedonina, J.F. Patrick, J.S. Moore, S.R. White, N.R. Sottos, Enhanced Performance of Regenerative Polymers. In Preparation for Advanced Functional Materials.
7. R.C.R. Gergely, N.R. Sottos, J.S. Moore, S.R. White, Regenerative Polymeric Coatings via Pressure Responsive Surface Valves. In Preparation for Advanced Materials
8. W.A. Santa Cruz, B.P. Krull, R.C.R. Gergely, S.R. White, N.R. Sottos, J.S. Moore, Two-Stage Chemical Resins: A Broad Tool for Material Regeneration. In Preparation for ACS Macro Letters.

1.2. Conferences presentations and papers from the AFOSR Discovery grant

1. R.C.R. Gergely, J.S. Moore, N.R. Sottos, S.R. White, Regenerative Coatings, Society for Experimental Mechanics Annual Conference and Exposition. Lombard, IL, 6 June 2013.
2. R.C.R. Gergely, B.P. Krull, W.A. Santa Cruz, J.S. Moore, N.R. Sottos, S.R. White, Regenerative Polymeric Coatings. Presented at Fourth International Conference on Self-Healing Materials. Ghent, Belgium, 20 June 2013.
3. B.P. Krull, W.A. Santa Cruz, R.C.R. Gergely, S.R. White, J.S. Moore, N.R. Sottos, Autonomic Regeneration of Large Damage Volumes. Presented at Fourth International Conference on Self-Healing Materials. Ghent, Belgium, 20 June 2013.
4. W.A. Santa Cruz, B.P. Krull, R.C.R. Gergely, N.R. Sottos, S.R. White, J.S. Moore, Gap-Filling Fluids for Materials Regeneration. Presented at Fourth International Conference on Self-Healing Materials. Ghent, Belgium, 16-20 June 2013.
5. W.A. Santa Cruz, B.P. Krull, R.C.R. Gergely, N.R. Sottos, S.R. White, J.S. Moore, Gap-Filling Fluids for Materials Regeneration. Presented at 246th National Meeting of the American Chemical Society. Indianapolis, IN, September 8–12, 2013.

6. W.A. Santa Cruz, Material Regeneration by Two-Stage Chemical Resins. Beckman Graduate Student Seminar, Beckman Institute, October 30, 2013.
7. R.C.R. Gergely, W.A. Santa Cruz, B.P. Krull, N.R. Sottos, J.S. Moore, S.R. White, Two-Stage Polymers that Enable Structural Regeneration. The 9th International Conference on Mechanics of Time Dependent Materials. 29 May 2014.
8. B.P. Krull, W.A. Santa Cruz, R.C.R. Gergely, S.R. White, J.S. Moore, N.R. Sottos, Regenerative Polymers for Large Scale Damage. Presented at 16th European Conference on Composite Materials. Seville, Spain, 24 June 2014.
9. W.A. Santa Cruz, B.P. Krull, R.C.R. Gergely, N.R. Sottos, S.R. White, J.S. Moore, Material Regeneration using a Versatile Two-Stage Polymer Chemistry. Presented at 248th National Meeting of the American Chemical Society. San Francisco, CA, August 10–14, 2014.
10. R.C.R. Gergely, S.J. Pety, B.P. Krull, J.F. Patrick, T.Q. Doan, A.M. Coppola, N.R. Sottos, J.S. Moore, S.R. White, Multidimensional Vascular Polymers via Degradable Sacrificial Templates. Presented at Society of Engineering Science 51st Annual Technical Meeting. West Lafayette, IN, 3 October 2014.
11. B.P. Krull, R.C.R. Gergely, W.A. Santa Cruz, Y. Fedonina, J.S. Moore, S.R. White, N.R. Sottos, Restoration of Catastrophic Damage in Polymers. Presented at MRS 2014 Fall Meeting and Exhibit. Boston, MA, 1 December 2014.
12. B.P. Krull, R.C.R. Gergely, W.A. Santa Cruz, Y. Fedonina, J.F. Patrick, J.S. Moore, S.R. White, N.R. Sottos, Restoration of Catastrophic Damage in Polymers. Presented at Fifth International Conference on Self-Healing Materials. Durham, NC, 22 June 2015.

1.3. Patents from the AFOSR Discovery grant

1. Brett P. Krull, Windy A. Santa Cruz, Ryan C. R. Gergely, Nancy R. Sottos, Scott R. White, Jeffrey S. Moore. Multiple stage curable polymer system with controlled transition. US Provisional Patent Application 61/976,793
2. Jason F. Patrick, Brett P. Krull, Nancy R. Sottos, Jeffrey S. Moore, Scott R. White. Advanced Thermal Processing Techniques of 'Sacrificial' Polylactic Acid (PLA) for Fabrication of Microvascular Networks and Inverse Architectures in Polymers and Fiber-Reinforced Composites. US Provisional Patent Application 61/904,094
3. Jason F. Patrick, Kevin R. Hart, Brett P. Krull, Nancy R. Sottos, Jeffrey S. Moore, Scott R. White. Method of Making A Self-Healing Composite System. US Patent Application 14/607,759

2. Summary of Research

2.1. Damage Regeneration

The complexities present in large and multiscale damage, which require a new approach to repair beyond the capabilities of existing self-healing technologies are investigated using several different types of damage. These challenges are not exclusive to the damage modes tested here, thus we seek strategies that can be applied more generally to a variety of damage modes.

2.1.1. Coating regeneration

Abrasive damage of coatings presents challenges with geometric configuration of damage and vasculature, protection of healing agents, and formulation of the healing agent. Previous demonstrations of vascular coatings targeted small damage such as cracks or scratches and implemented a two-part healing agent. However, damage due to abrasion that results in complete removal of large areas of a coating, has not been addressed. A large volume of material is removed and must be restored. Abrasive damage of a coating enables isolation of the vasculature from the damage, facilitating the study of repeat damage and repair and the effect on vascular delivery.

Our concept for regenerative coatings, described in Figure 1, is subdivided into three stages: triggering, transport, and repair [1]. Initially, a protective coating is deposited on a vascularized substrate, a multi-layer model similar to the structure of skin. Upon damage-induced removal of the coating (triggering), the vasculature is exposed and uncured liquid healing agent is released onto the surface of the substrate (transport). Ultraviolet (UV) light from the sun cures the liquid healing agent, reforming the protective coating (repair).

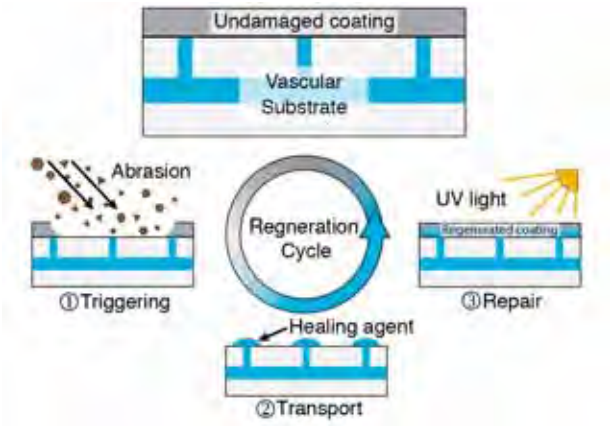

Figure 1. Coating regeneration cycle. Abrasive damage triggers the release of liquid healing agent stored in the underlying vasculature. The one-part healing agent reforms the protective coating when exposed to simulated sunlight. Protection of the vasculature enables multiple regeneration cycles.

Here a vascular system with a pressurized reservoir enables the delivery of adequate volume of healing material to the site of damage. A pressure sensitive valve is employed to mitigate potential blockage of vasculature. Lastly, in contrast to two-part chemistries that are commonly used in self-healing materials, the one-part UV curable healing agent employed here does not require mixing in-situ. The vascular system design in combination with one-part healing chemistry enables the regeneration of a protective coating in response to controlled abrasive damage.

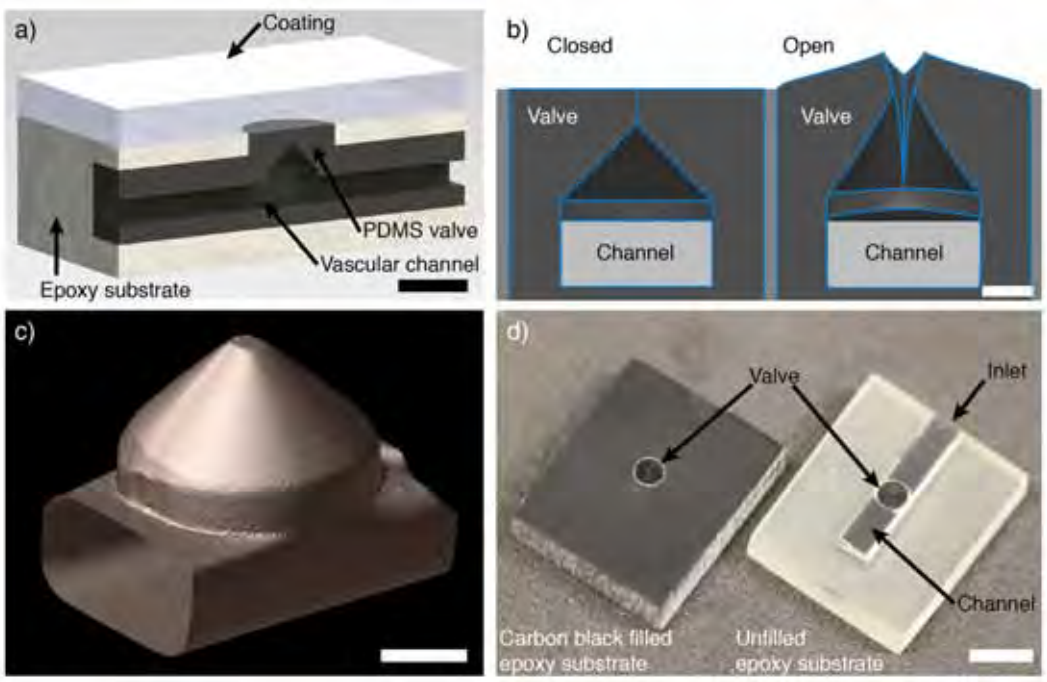

Figure 2. Embedded surface valve for coating regeneration: a) cross-sectional diagram of valve and vascular channel embedded in substrate (scale bar = 2 mm); b) model of valve opening deformation under pressure, undeformed shape (left), deformed shape (right) (SolidWorks Simulation, 276 kPa, scale bar = 0.5 mm); c) 3D x-ray computed microtomographic (microCT) reconstruction of channel and conical valve interior (filled with gallium, scale bar = 0.5 mm); d) valve specimens, embedded in carbon black filled epoxy (left) and unfilled epoxy (right) (scale bar = 5 mm).

A vascular substrate and valve is designed such that the flexible valve terminates at the interface between the substrate and coating (Figure 2). The coating constrains the valve until damage occurs, triggering the release of healing agent from the pressurized vasculature. The valve is constructed of a silicone elastomer, and closes to prevent penetration of UV into the underlying vasculature once the pressure is disengaged. Flow through the valves was characterized using solutions of water and glycerol to ensure non-reactivity of the test fluid. The correlation of pressure to flow rate is nearly linear ($R^2 = 0.990$). In addition, testing with glycerol and water solutions of various mass ratios shows that flow rate is inversely proportional to viscosity. We observed a reduction in flow rate over time when testing with epoxies, attributed to swelling of the silicone valve material.

We sought a one-part healing agent, to preclude the challenges imposed by two-part chemistries. Furthermore, photocurable chemistries can be selected to harness the UV light available in sunlight, removing the need for a non-autonomous post cure [2]. The healing agent is a solution of a diluted Bisphenol-A based epoxy (Epon 813) and a cationic photonitiator (4 wt% Irgacure 250). Upon exposure to UV light with comparable irradiance to sunlight (1 mW cm^{-2}, 365 nm peak wavelength), the coating material cures to full hardness in 12 h (Figure 3). This formulation has a cured hardness comparable to polymethyl methacrylate (~19 HV) [3]. Both the flexible valve and surrounding epoxy are filled with carbon black (a commonly used UV absorber [4]). The grade of carbon black selected disperses well in both PDMS and epoxy and reduces the transmitted UV irradiance (at 365 nm peak wavelength) of PDMS by ~97%.

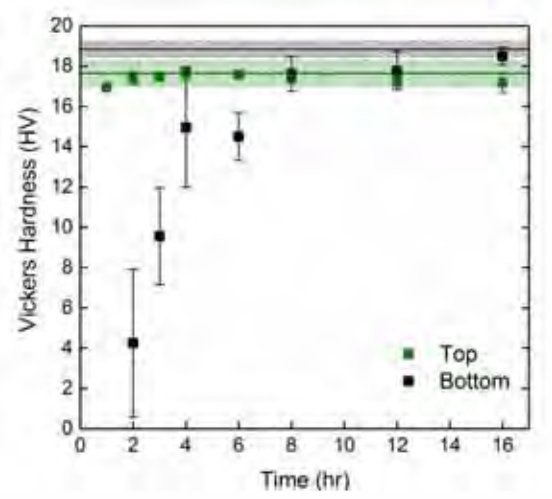

Figure 3. Vickers indentation hardness testing of UV cured coating (Epon 813, 4 wt% Irgacure 250). Exposed to simulated sunlight lamp (1 mW cm^{-2}) for various times and hardness tested on both top (green) and bottom (black) of 1 mm thick coating. Error bars represent one standard deviation (n = 3). Horizontal lines indicate hardness of specimen cured for 4 h using a high intensity lamp, bands represent one standard deviation of three measurements of the same specimen (n = 1, 6 mW cm^{-2}).

Coating regeneration is demonstrated in a simplified sample geometry consisting of a channel and single compliant valve embedded in epoxy (Figure 2d). The original coating (generation 0) is formed on the test specimen by pumping liquid through the valve using a constant static pressure (276 kPa) until the specimen is coated with a thin (~1.1 mm) layer of polymer (~100 μL). The specimen is subsequently irradiated with UV light to cure the coating. Each generation (0-4) of coating is cured with the simulated sunlight lamp (1 mW cm^{-2}, 12 h) and evaluated using Vickers indentation hardness. After evaluation, the vascular system is reconnected to a healing agent reservoir and pressurized. Damage is introduced by translating the specimen under an abrasive wheel until the coating is completely removed and the valve is re-exposed (Figure 4a), thus triggering release of liquid healing agent. The process of abrasive removal and coating regeneration is repeated a total of four cycles (generations 1-4). All specimens fully regenerated after each cycle, with hardness near the virgin cured coating for all regenerations (Figure 4b).

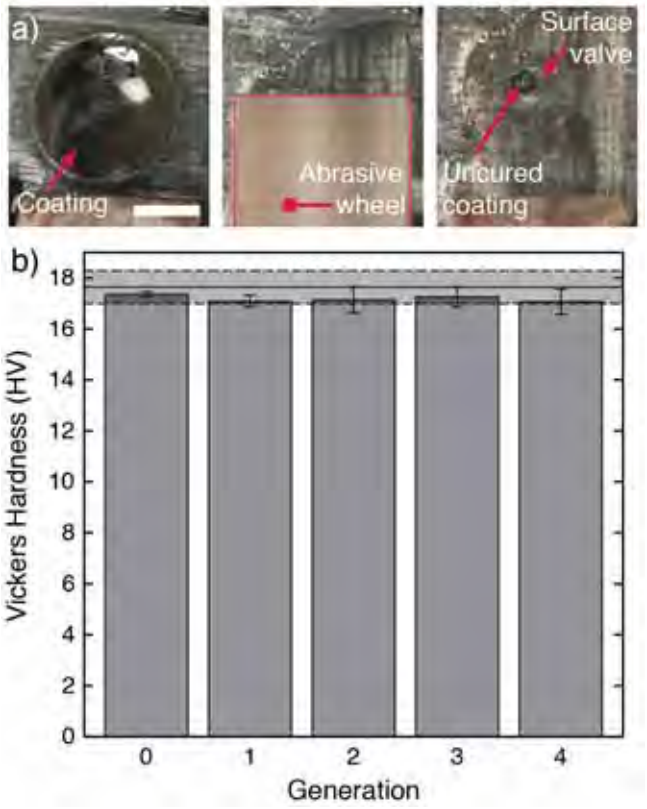

Figure 4. Regeneration process and results: a) top view images of specimen during abrasive removal of coating (scale bar = 5 mm), red outline indicates abrasive wheel; b) hardness of each generation, cured with simulated sunlight lamp (n = 3, cured 12 h at 1 mW cm^{-2}), horizontal bar indicates full cure, with high intensity lamp (6 mW cm^{-2}, 4 h). Error bars and dashed lines bound 1 standard deviation.

2.1.2. Fiber pullout

In order to recover large damage volumes one potential approach is to incorporate a scaffold that retains healing fluid in the damage volume. In fiber reinforced composite materials the phenomenon of fiber pullout and bridging occurs during some failures (Figure 5b). We developed a concept that incorporated fibers (nylon monofilament) that were intentionally designed to pullout after fracture of the surrounding matrix material (Figure 5a). Fibers run axially along the specimen and damage is introduced via single edge notched tension testing. The specimen fractures perpendicularly to the loading axis, and as the gap in the specimen grows larger, the fiber bridge the damage and act as a scaffold for fluid retention (Figure 5c).

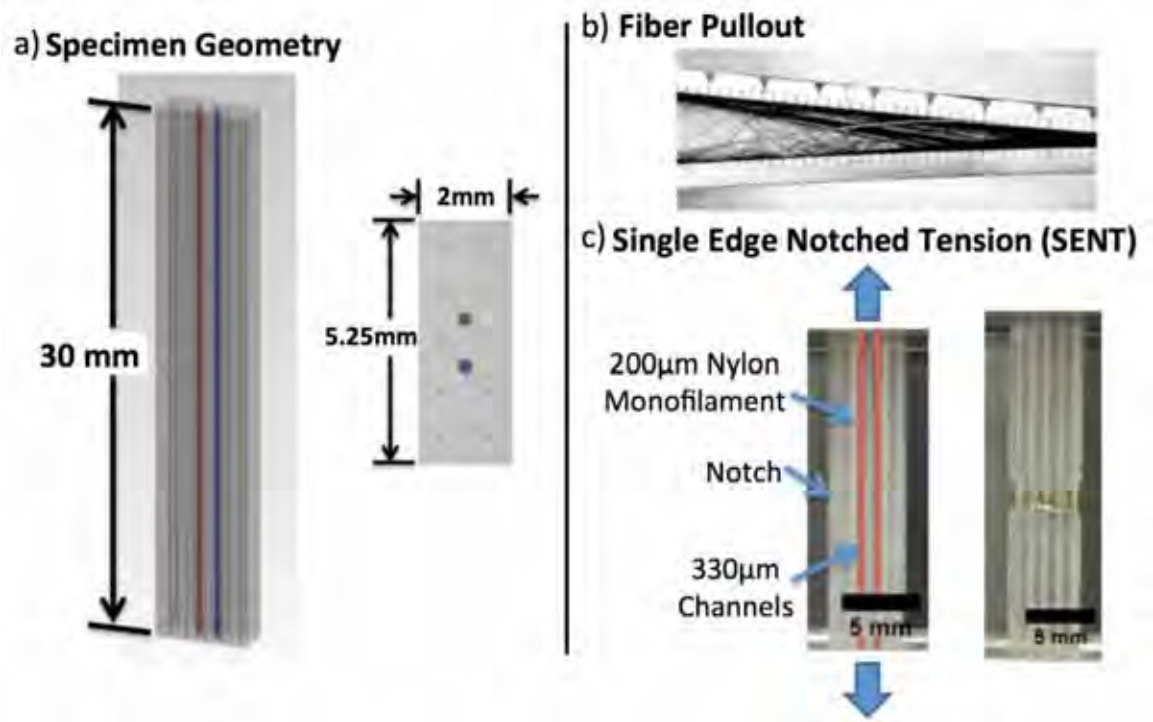

Figure 5. Fiber pullout concept and inspiration. a) Schematic of single edge notched tension (SENT) specimen containing bridging fibers as well as vascular channels running along the long axis of the specimen. b) Double cantilever bending testing of a fiber reinforced composite demonstrating fiber bridging in composite materials. c) Images of specimen prior to initial fracture event and fractured specimen after filling damaged region with healing agent.

The damage was filled with a two part epoxy system first introduced by Toohey et al. [5]. After the damage was filled, and the healing agent was allowed to cure, specimens were evaluated for recovery of elastic modulus using a three point bend testing. A control test in which the damage is filled with a premixed solution of healing agents is depicted in Figure 6, and displayed appreciable recovery of stiffness over an unhealed control.

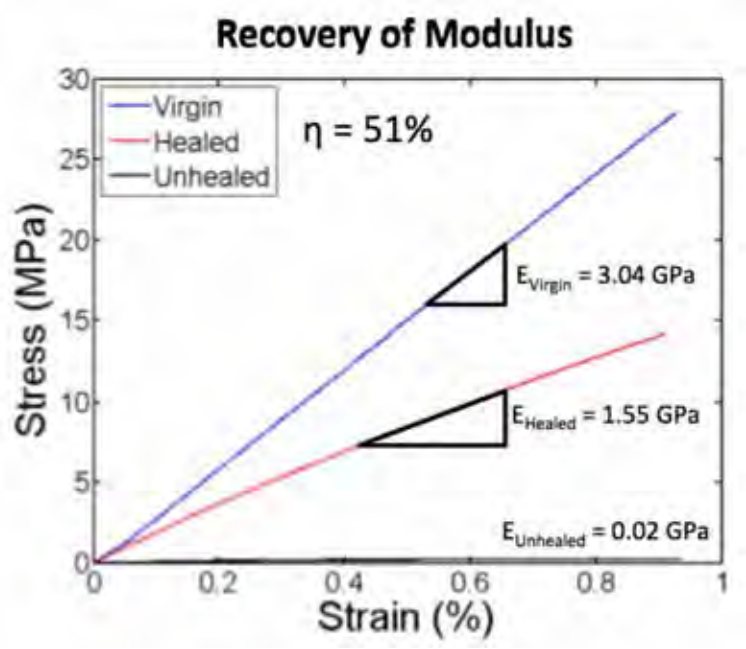

Figure 6. Stiffness recovery in fiber pullout specimen before and after healing (control specimen). E_{virgin} represents the undamaged specimen, E_{healed} represents the fractured specimen after filling with premixed healing agent and allowing it to cure, $E_{Unhealed}$ represents the fractured specimen which was not filled with healing agent showing stiffness only due to bridging fibers.

2.1.3. PDMS hole sealing

Beiermann et al investigated a capsule-based approach to healing mm-scale puncture damage in thin elastomer sheets [6]. Volumetric recovery was limited to a damage size of less than 2 mm due to fluid delivery limitations in microcapsule self-healing systems. Vascular systems are able to supply larger volumes of healing agent from external reservoirs. To test the damage volume limits of a microvascular system, sheets of Sylgard 184 polydimethylsiloxane (PDMS) elastomer were fabricated containing two parallel microchannels. A cylindrical damage volume was induced with the use of Uni-Core biopsy punches (Ted Pella, Redding CA) of increasing diameter. The damage was positioned such that intersection of both microvascular channels occurred. A two-part PDMS healing chemistry (Sylgard 170) was injected into the damage volume. In cases where the damage region filled, the healing agent was allowed to cure for 24 hours and room temperature and pressure tested at 100 kPa (1 atm) for leakage. By implementing microvascular delivery, damage regions up to 3.5 mm in diameter (Figure 7a) were recovered and sealed at a rate of 60% (Figure 7b). Healing agent supply was virtually unlimited, and thus recovery size was instead limited by surface tension and gravity.

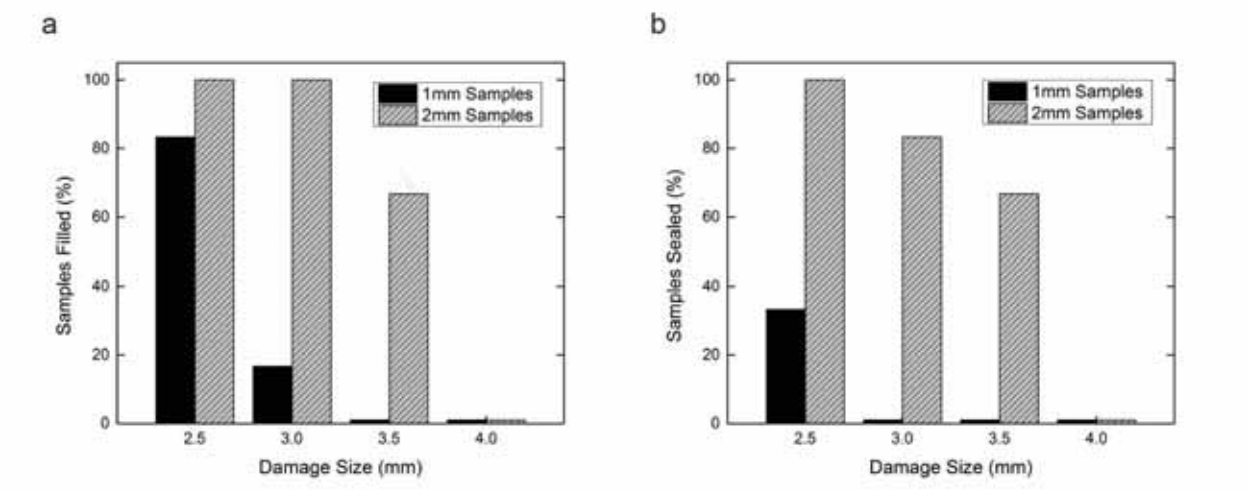

Figure 7. Large damage volumes in PDMS sheets. a) Damage size dependency of fill rate of PDMS sheets for 1 mm and 2 mm thick vascularized specimens. b) Damage size dependency of seal rate of PDMS sheets that filled for 1mm and 2mm thick vascularized specimens.

2.1.4. Restoration of large damage volumes in polymers (WSC)

The regenerative power of tissues and organs in biology has no analog in synthetic materials. Whereas biology achieves regeneration through vascularization and recruitment of stem cells [7–9], engineering materials are generally avascular, with a limited ability to self-heal [10,11]. A variety of repair strategies exist for microscopic defects and cracks [1,12–15], but autonomic restoration of materials that suffer large-scale damage and associated mass loss has not been realized. Restoration requires overcoming the interplay of mass transport, environmental factors, intrinsic forces (such as surface tension), and extrinsic forces (such as gravity) that act on liquid reagents and the chemical reactions associated with damage repair.

Our restoration concept for structural materials is illustrated in Figure 8. The strategy is predicated on the delivery of reactive fluids through two independent vascular networks to the site of damage. Events that lead to substantial mass loss (such as ballistic impact) trigger release of fluids, subsequent mixing, and initiation of the restoration process. A reactive system that progresses from liquid to gel (gel stage) and gel to polymer (polymer stage) is hypothesized to deliver low-viscosity fluids to the site of damage, initially resulting in a shape-conforming yet self-supporting viscoelastic scaffold. Addition of new material proceeds until the damaged region is fully filled and complete replacement of lost mass is achieved. Transformation of the gel into a stiff polymer then allows for recovery of the mechanical properties of the original material.

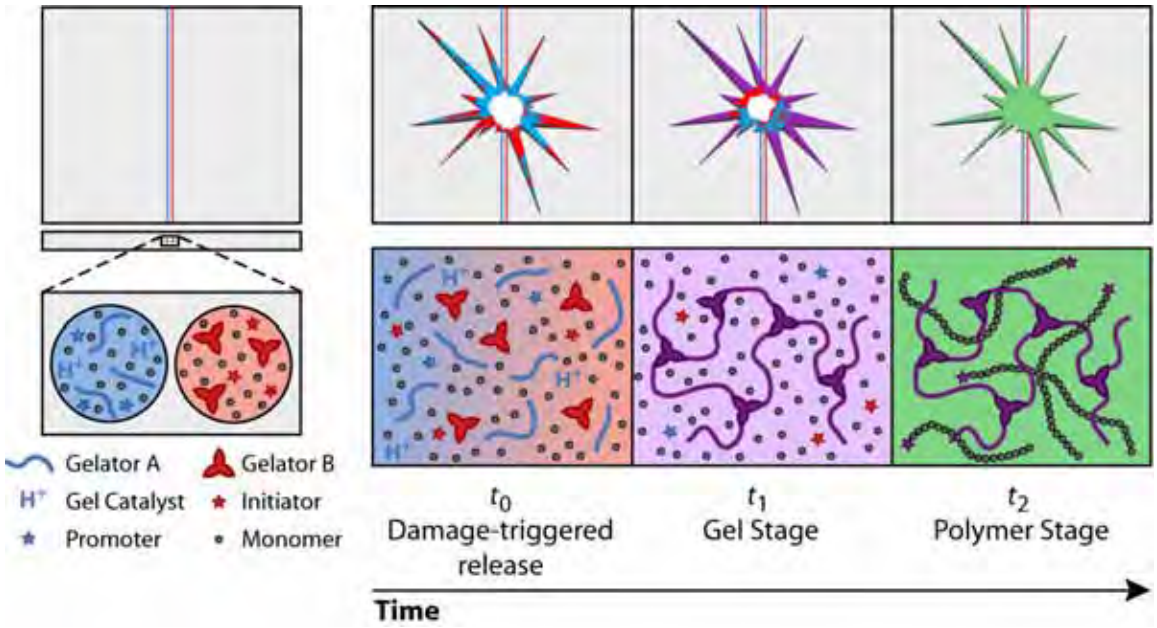

Figure 8. Two-stage restoration strategy. Reactive monomer solutions are incorporated into a vascularized specimen (blue and red channels). Time t_0: impact damage initiates fluid release into the damage region. Time t_1: gel stage (purple) occurs by acid-catalyzed cross-linking of gelators A and B. Deposition of fluid and subsequent gelation continues until the void is filled. Time t_2: the polymer stage (green) occurs by monomer polymerization, resulting in recovery of structural performance.

We developed a two-stage polymer chemistry in which catalyzed gelation of liquid monomer is followed by bulk polymerization to a structural solid (Figure 8). The reactive monomer solutions are stable and low-viscosity (time t_0) until damage-triggered release initiates the chemical processes. A relatively fast gel stage (time t_1, from 30 s up to 28 min) creates a semisolid scaffold on which additional solution is deposited. Gelators A, a bis-acylhydrazine–terminated poly(ethylene glycol), and B, a tris[(4-formylphenoxy) methyl]ethane, form a cross-linked network of dynamic acylhydrazone bonds through acid-catalyzed condensation (Figure 9) [16]. This chemistry is capable of gelling a wide range of organic liquids, including acrylic and thiol-ene monomers. Monomer gelation accomplishes the need to fill gaps stemming from mass loss, and conversion to polymer completes the restoration process. Polymerization kinetics on a timescale > t_1 (hours) avoids premature stiffening of the restored material. Room-temperature polymerization is achieved with judicious choice of radical initiators, promoters, and inhibitors.

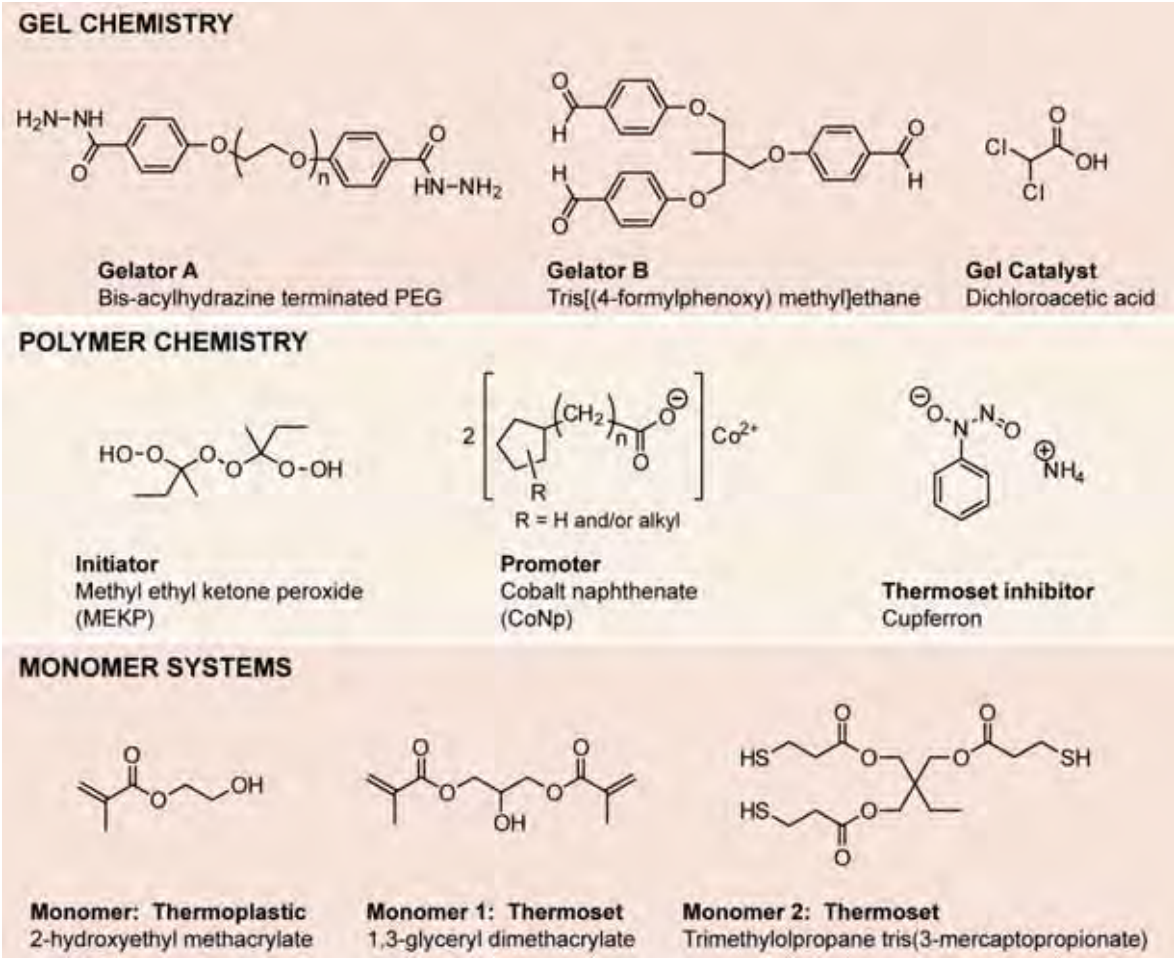

Figure 9. Chemical structures of the two-stage components.

Although biological systems require a complex and highly regulated system of biochemical processes to achieve regeneration [17–24], our strategy produces reliable performance with relatively simple synthetic reagents. The properties of the structural polymer are tailored by selection of the monomer, as demonstrated below with two examples. In one example, 2-hydroxyethyl methacrylate (HEMA) was polymerized with a methyl ethyl ketone peroxide (MEKP) initiator and cobalt naphthenate (CoNp) promoter to give a thermoplastic material;[25] in a second example, liquid thiol-ene agents 1,3-glyceryl dimethacrylate and trimethylolpropane tris(3-mercaptopropionate) react to form a thermosetting material (Figure 9).

Monomers were selected to fulfill a stringent set of requirements, including high boiling points, nonwetting properties, low viscosities, favorable cure kinetics, and the ability to dissolve gelators. The reagents required for each monomer system are mutually compatible with the reagents used for gelation chemistry. Independently tunable chemical triggers selectively control the rates of both gelation and polymerization. The components for both examples are strategically divided into two stable solutions and loaded into separate microchannels (Figure 8).

Oscillatory rheology confirmed the separate occurrence of gelation and polymerization stages as well as the ability to regulate the reaction kinetics of each stage (Figure 10). A representative reaction shown in Figure 10a shows the evolution of storage (G') and loss (G'') moduli of a 12 weight percent (wt %) gelator solution in HEMA. The first plateau of G' reflects monomer

gelation to a ~10^4 to 10^5 Pa semi-solid. Onset of the gel stage (t_1) was defined as the crossover of G' and G''. The second modulus plateau, several orders of magnitude higher, reflects a slower transformation from gel to structural polymer. Polymerization onset (t_2) was designated as the peak of the loss factor (tan δ = G''/G').

Rates of gelation and polymerization are largely independent, which enables precise control of t_1 and t_2 by varying the concentrations of catalyst for the gelation reaction and initiating components for the polymerization reaction. Plots of the time scales of staged transitions for the HEMA example are shown in Figure 10b and c. Gelation rate is dependent on catalyst concentration and determines the scaffold-forming ability. Gel times are controlled from 30 s up to about 30 min (Figure 10b). Control of polymerization was achieved by varying promoter concentration in an inert environment, with the polymer stages taking hold in anywhere from 80 to 180 min (Figure 10c). However, free-radical polymerizations of acrylates are sensitive to atmospheric oxygen. In contrast, the thiol-ene thermoset chemistry is oxygen-tolerant and cures in ambient environments. Thiol-ene polymerizations produced rapidly and overshadow the gel stage even when performed without initiators [26]. To allow sufficient time for gel formation, the radical inhibitor cupferron was used to slow the polymerization rate (Figure 11a) [27,28]. Without inhibitor, the polymerization occurs in less than 10 min. The immediate polymer stage prevents formation of the scaffold and obstructs further delivery of healing agents. Using small amounts of inhibitor (0.02–0.05 wt%), the gel stage is recovered (Figure 11a). Polymerization time is readily controlled from 8.5 to ~100 min by inhibitor concentration (Figure 11b).

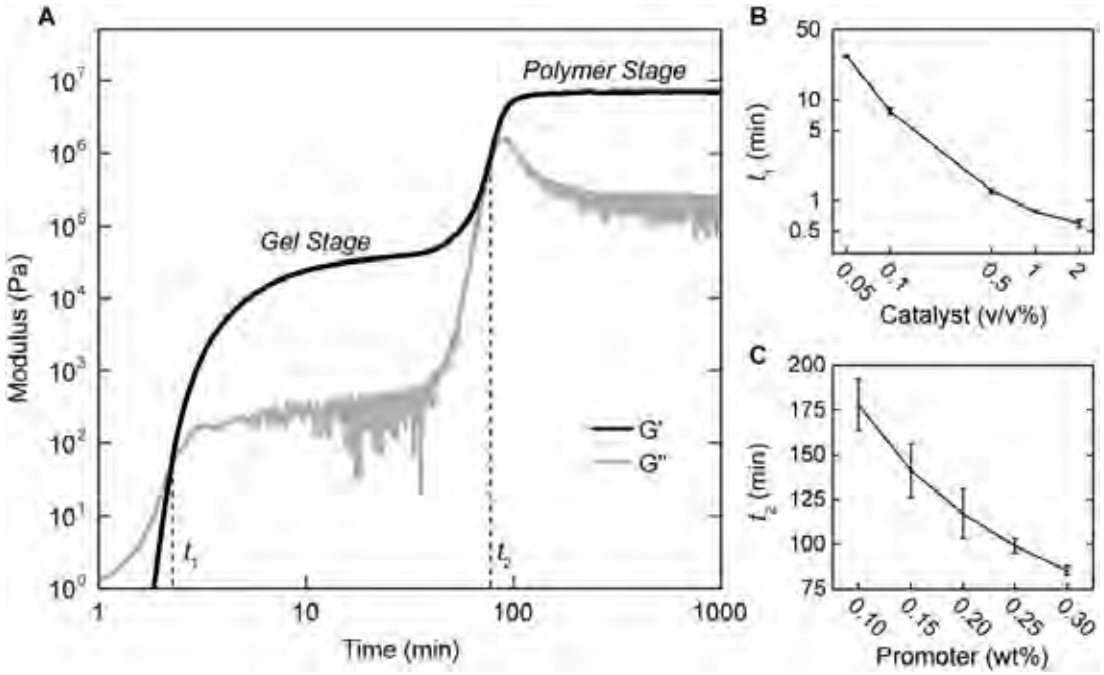

Figure 10. Characterization of the two-stage process. Solutions contain gelators in HEMA (monomer) with dichloroacetic acid (catalyst), methyl ethyl ketone peroxide (initiator), and cobalt naphthenate (promoter). a) Rheological properties of the restorative reagents over time display both the fast formation of the organogel (t_1, seconds to minutes), and slower reaction rate to polymer (t_2, hours) controlled by the concentrations of chemical triggers. b) Control of gel-stage kinetics by varying catalyst concentration (1.5 wt% initiator, 0.1 wt% promoter). c) Control of polymer stage kinetics by varying promoter (2 v/v% catalyst, 1.5 wt% initiator).

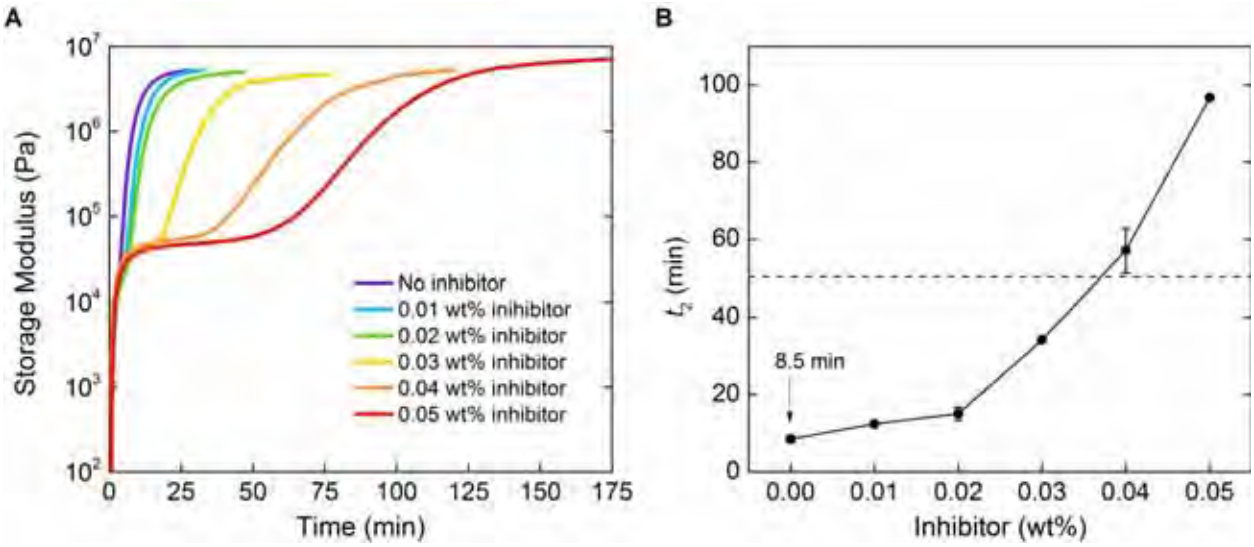

Figure 11. Rheology measurements for controlled two-stage thermoset polymerizations showing control over polymerization kinetics by changing inhibitor concentration. a) Recovery of gel stage by increasing inhibitor concentration. b) Control of the t_2 by cupferron inhibitor concentration. A concentration of 0.04 wt% was used in regeneration experiments to allow for sufficient time (> 45 min) between the gel and polymer stages.

Gelation allows deposition of material beyond that which is dictated by surface tension alone. When damage size exceeds a certain threshold, surface tension is insufficient to retain unreacted fluid, and gravity pulls it out of the damage zone. The boundary between surface tension and gravity-dominated regimes (described by Tate's Law and the drop-weight method of analysis) [29–31] was validated for our experimental setup with standard test fluids (Figure 12).

In contrast to these nonreactive fluids, the gel deposition volume exceeds that expected from Tate's Law by over an order of magnitude. Two formulations containing different gel fractions are plotted in Figure 12, with the greater gel fraction producing a larger deposition volume. The increase in volume retained over inert fluids is due to the mechanical support of the *in situ*–formed gel. Since gelation and deposition occur on the same time scale, the growing material is not only retained by the surface tension of the fluid; it is also retained by the cohesion of the restored material and its adhesion to the deposition surface.

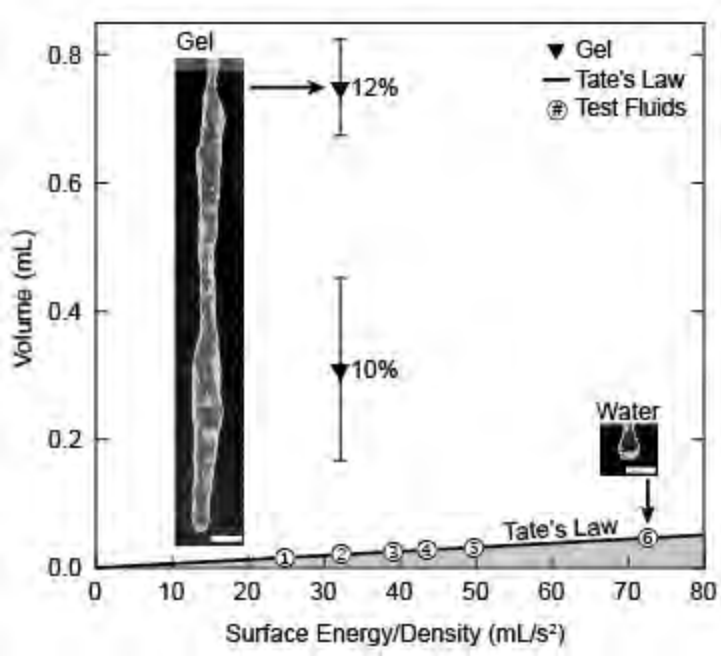

Figure 12. Volume deposited by using restorative gel chemistry (HEMA gel, 2 v/v % catalyst, no initiator or promoter). Tate's Law describes the limiting volume of a nonreactive fluid that can be retained with surface tension; standard test fluids confirm this relationship (1, pentane; 2, HEMA; 3, dimethylsulfoxide; 4, ethylene glycol; 5, glycerol; and 6, water). Two-stage chemistry far exceeds this limit, but deposition is dependent on the concentration of gelators. The inset optical image on the left shows the volume deposited by 12 wt% gelators, whereas the inset optical image on the right shows water test fluid. Scale bars, 5 mm.

Development of the two-stage polymers into a viable healing chemistry requires minimizing cross reactions between components and maintaining low solution viscosities. Both gelation and polymerization reactions are triggered by the combination of at least two compounds. Therefore, stable two-part solutions were prepared by separating the gelation catalyst from the gelators and the polymerization initiator from promoter. In addition, the initiator was separated from the catalyst to prevent premature decomposition. By mass, Gelator A comprises most of the gelator weight fraction, and was split into both solutions to give equal 1:1 volume ratio solutions.

The stability of the solutions was assessed by measuring solution viscosity over a 6 h period for gel only (no initiator or promoter) and two-stage formulations, shown in Figure 13. Both formulations exhibited the same viscosity profile (Figure 13a and b), with Part A and Part B initial viscosities of around 20 mPa·s. However, the viscosity of the Part B solution increased for the first ~1 h before plateauing around 55 mPa·s from some uncatalyzed acylhydrazone formation between the gelators.

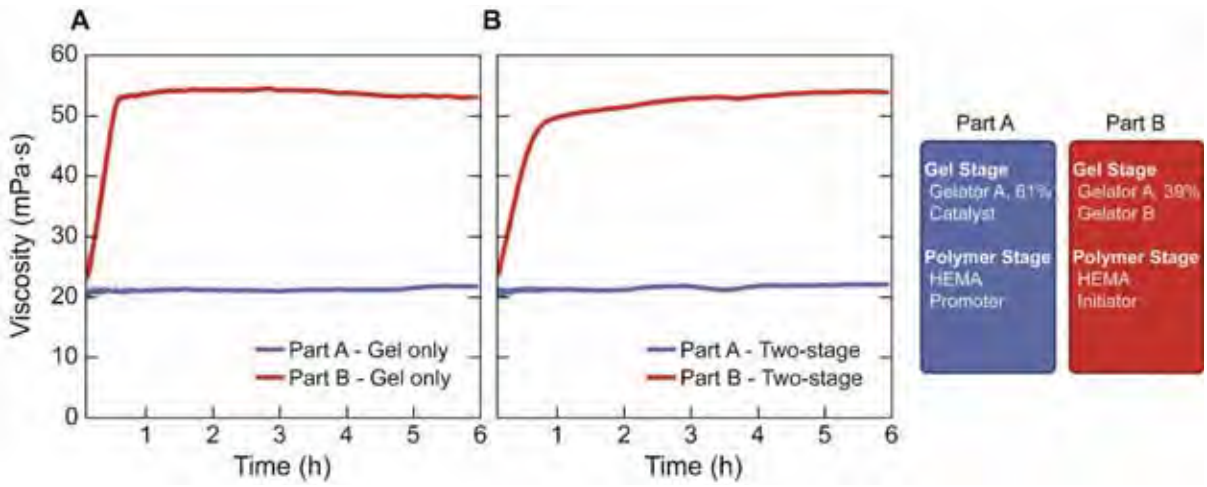

Figure 13. Stability of the HEMA thermoplastic system as Part A-Part B solutions. Viscosity was measured at a shear rate of 5 s^{-1} over 6 h for HEMA solutions containing 0.0001 wt% carbon black in a) gel only formulations (gelators and catalyst) and b) two-stage formulations.

Two-part solutions for the thermoset polymer system were prepared in a similar manner with Gelator A (61%), catalyst, and promoter in Part A; and Gelator A (39%), Gelator B, and initiator in Part B (Figure 14). Unlike the HEMA thermoplastic system, the monomer composition differs between the two solutions. The thiol monomer trimethylolpropane tris (3-mercaptopropionate) (TMPTMP) was exclusively added to Part A due to poor solubility of Gelator B. The dimethacrylate monomer 1,3-glyceryl dimethacrylate (GDMA) was divided between the solutions (30% in Part A, 70% in Part B) to preserve 1:1 volume ratios. Stability was again assessed by monitoring the viscosity over 6 h. Viscosities were significantly higher than for the HEMA thermoplastic system with initial viscosities of 240 and 110 MPa·s for Part A and Part B, respectively. Part A maintained its viscosity for the test duration; however, Part B viscosity doubled over the course of 3−4 hours. Due to the relative instability of the thermoset chemistry, the HEMA thermoplastic system was more thoroughly investigated as a restorative healing agent while the thermoset chemistry was evaluated only for maximum fill capacity in the following sections.

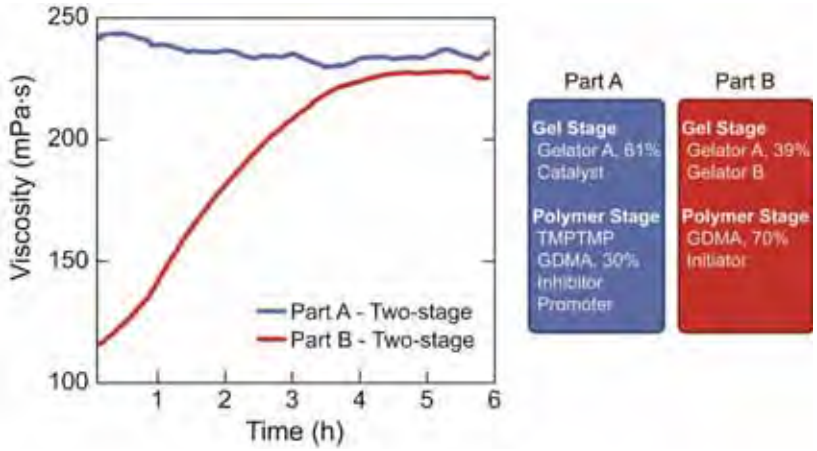

Figure 14. Stability of the two-stage thiol-ene thermoset system as Part A-Part B solutions. Viscosity was measured at a shear rate of 5 s^{-1} over 6 h.

Analysis of Restorative Capacity

In our model damage-filling experiments, the restorative reagents span gaps and fill large damage volumes by forming a free-standing, dynamic gel scaffold on which continued material deposition occurs. We used an open cylinder (sample dimensions are 52 x 52 x 3 mm thick, 330-μm-diameter parallel channels) as a model geometry to test the filling of large-scale damage in thin epoxy sheets. Solutions of HEMA containing gelators, acid catalyst, and fluorescent dye (Nile Red and perylene) were delivered to the damage area via separate microchannels (Figure 15a). A computer-controlled, pressurized system ensures reagents are delivered at 1:1 volume ratios. Upon entering the damaged region, the components quickly mix and wet the inner surface of the sample owing to low viscosity and a low fluid-substrate contact angle. Rapid gelation forms a scaffold on which additional fluid from the microvascular channels is deposited. The faceted appearance of the recovering damage region (Figure 15a) reflects the mechanical stiffness of the developing gel because an ideal liquid would assume a smooth circular shape to minimize surface energy. Gelled material grows inward, and the entire damage region is filled as the process of deposition and gelation continues. The dynamic nature [32] of the gelator chemistry enables continuous (defect-free) gel interfaces and the formation of a monolithic plug in place of the original void.

Restoration to full mechanical function was accomplished by replenishing lost mass and transforming the gelled monomer to a fully polymerized solid. The filling performance of gelling and nongelling controls is compared for increasing damage area in Figure 15b. The area fill ratio (AFR) is calculated for each damage area as the ratio A_{fill}:A_0, where A_{fill} is the area filled by the restorative solutions and A_0 is the total damage area. The control solutions achieve an AFR of 1 only for diameters up to 6.3 mm. For larger diameters, the effect of gravity exceeds surface tension and causes the controls to drip out of the damaged region, which results in incomplete filling. In contrast, gelling solutions fill to capacity (AFR = 1) for damage diameters up to 9.0 mm by overcoming gravity and circumventing failure by dripping. Damage size diameters exceeding 8.0 mm do not reliably fill for all replicates because gravity causes gel material to grow downward rather than toward the damage center; however, the AFR remains substantially higher than that of control solutions because of superior material retention.

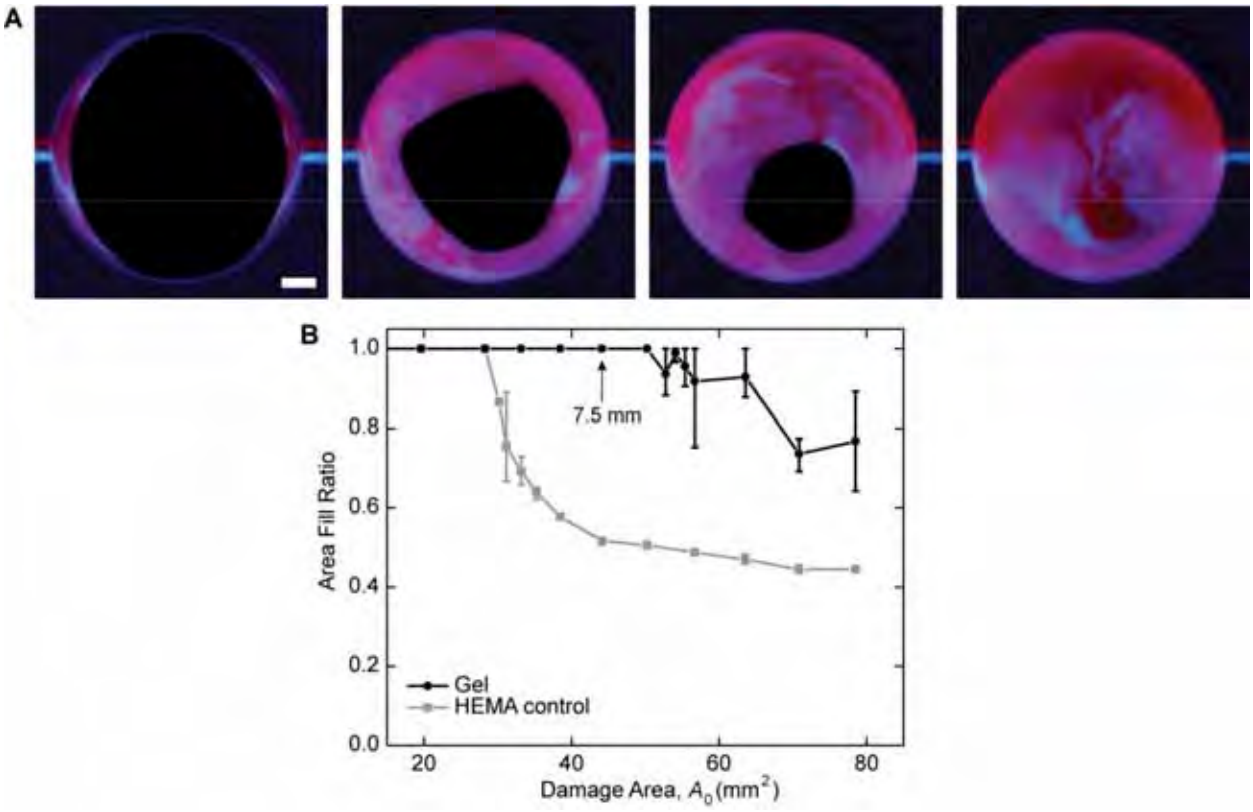

Figure 15. Restoration performance testing with cylindrical damage geometry. a) Optical images of 7.5-mm-diameter open-cylinder damage geometry after 1, 3, 7, and 13 min (left to right) pressurized delivery of HEMA gel solutions (2 v/v% catalyst, no initiator or promoter). Blue liquid is Part A [HEMA, Gelator A (61% of total Gelator A), DCA catalyst] dyed with perylene, and red liquid is Part B [HEMA, Gelator A (39% of total Gelator A), Gelator B] dyed with Nile Red. Scale bar, 1 mm. b) Fill performance achieved for cylindrical holes of increasing size for HEMA gel and a non-gelling neat HEMA control. AFR = A_{fill}/A_0.

A pressure cell was used to verify mechanical recovery of our system by applying 345 kPa of nitrogen to one side of a damage sample and monitoring leakage on the opposite side [6]. Because only a completely filled damage region will withstand pressurization, we tested the maximum damage areas at which each restorative system attained complete filling for each of five replicates (Figure 16). All gelling systems are able to fill larger damage areas than can non-gelling solutions but do not provide mechanical recovery without a second transition to polymer. Only the thermoplastic and thermoset two-stage polymers combine filling performance with mechanical recovery. A standard two-part epoxy resin is presented for comparison, and neither fills a substantial damage area nor seals after a 24-hour room temperature cure. As demonstrated with both larger-area fill ratios and higher seal rates, two-stage polymers provide restoration performance superior to traditional healing chemistries [5]. The final mechanical properties of the two-stage polymer systems are comparable with commercial poly(methyl methacrylate) (PMMA) polymers [33]. Quasistatic tensile testing of the two-stage thermoplastic (HEMA) system yields an elastic modulus of 1.8 GPa and a tensile strength of 45 MPa (Table 1).

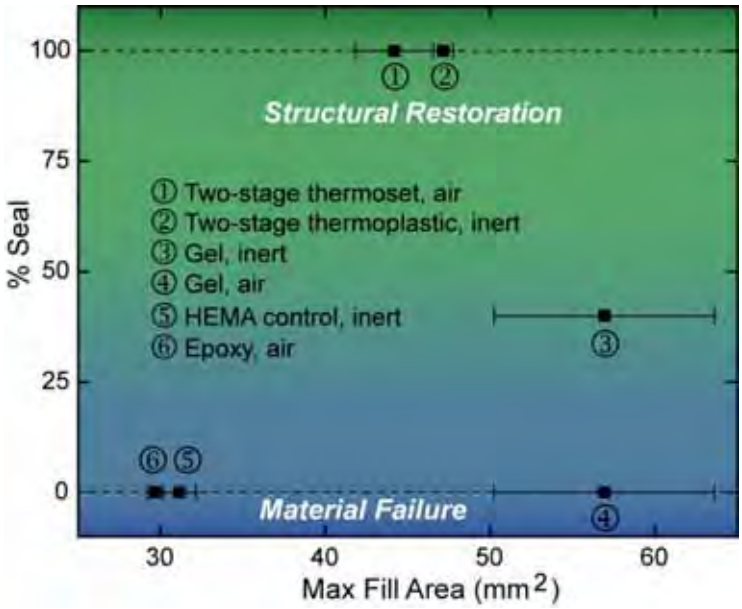

Figure 16. Restoration performance of various healing systems after a 24-hour room temperature cure, with the curing atmosphere indicated in the legend. Samples are subjected to 345 kPa nitrogen pressure loading. Restoration requires both a complete fill and recovery of full mechanical function.

Table 1. Tensile modulus and strength for substrate epoxy and two-stage thermoplastic with slower gelation time used for impact. Modulus determined using a linear fit between 0.1−0.5%. Tested according to ASTM D638, type V at 100 mm/min.

Sample name	Modulus (GPa)	Tensile Strength (MPa)	Number of Specimens
Epoxy substrate (EPON 828 / Epikure 3230)	2.54 ± 0.09	83.3 ± 1.5	3
Two-stage thermoplastic, slow	1.79 ± 0.07	44.9 ± 0.5	3

To test more realistic damage modes, we impacted and punctured specimens using a drop tower apparatus. The multiscale damage present in impact specimens represents a substantial challenge and requires chemistry that can both regrow the lost mass as well as penetrate into microcracks to create a pressure-tight seal. Dropping a striker with a hemispherically shaped tip at 6.26 J (Figure 17a) creates a central puncture and radiating cracks, with damage spanning ~35 mm in diameter. We implemented the same pressurized delivery scheme to fill the damage post-impact. A dye (Oil Blue N) was used to observe the deposition process, which included wicking into the radiating cracks (Figure 17b and c). Although fast gelation chemistry is advantageous for the regrowth of lost mass, it does not provide sufficient time for the reagents to fully penetrate into radiating microcracks. By slowing the gelation kinetics to around 8 min, we were able to achieve gap-filling and partial penetration of radial microcracks emanating from the central hole. Pressure testing of impact samples yielded ~60% sealing success, with most failures attributed to incomplete sealing of the dense network of radiating microcracks. After restoration of impact damage, we reimpacted specimens using the same testing protocol and measured 62% recovery of total absorbed energy in comparison with the initial impact test. The restored material performed on par (76%) with control specimens in which the native substrate material was injected into the damage and cured at a high temperature (Table 2).

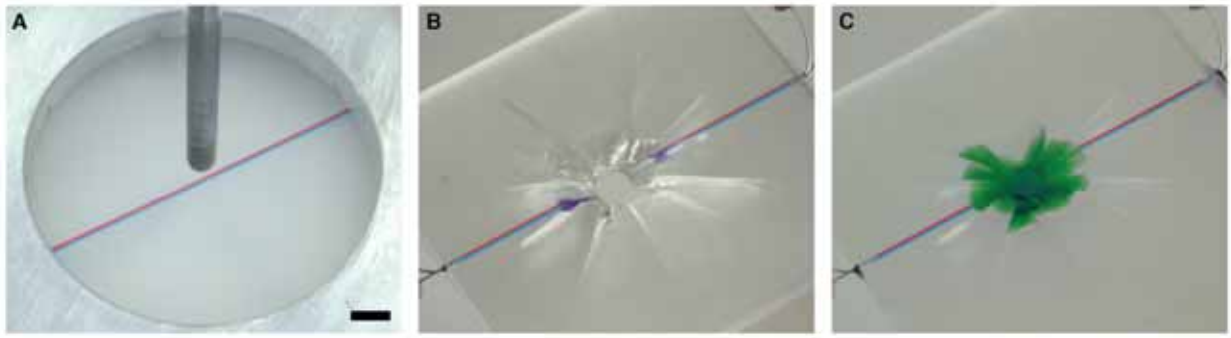

Figure 17. Restoration of impact damage. Perspective views of impact specimen restored with two-stage thermoplastic (HEMA) system (0.1 v/v% catalyst, 1.5 wt% initiator, 0.1 wt% promoter). Both components of two-part solutions are dyed and recolored for visualization. a) Specimen mounted into impact test fixture; 4-mm striker with a hemispherically shaped tip suspended over specimen. b) and c) Impact damage with central puncture and radiating cracks b) before filling and c) after filling. Scale bar, 5 mm.

Table 2. Average energy absorption from impact testing, error represents standard deviation.

Sample	Total energy absorbed (J)		% energy [vs. epoxy substrate]	% energy [vs. epoxy substrate, epoxy injected control]	# of Specimens
	initial impact	re-impact			
Epoxy substrate	0.92 ± 0.21		----	-	30
HEMA control substrate	0.58 ± 0.22		63%	77%	6
Two-stage thermoplastic control substrate	0.82 ± 0.39		89%	109%	3
Epoxy substrate, restored with two-stage thermoplastic		0.57 ± 0.34	62%	76%	5
Epoxy substrate, epoxy injected control		0.76 ± 0.39	82%	-	4

We have demonstrated a vascular approach to damage restoration using a polymer that replaces lost mass and recovers structural performance. Our two-stage chemistry makes use of both a rapid gelation (gel stage) for gap-filling scaffolds and a slower polymerization (polymer stage) for restoration of structural performance. When damage is unpredictable and uncontrolled, more complex and interconnected vascular networks [34] will be necessary to provide sufficient vascular coverage and redundancy to circumvent channel blockage. Truly regenerative polymers may be possible in the future via on-demand delivery of the chemical components of the native substrate polymer coupled with tunable gel and polymer transitions.

2.1.5. Enhanced design and performance of restorative polymer systems

The rapid gelation of the two-stage polymer healing agent is the distinguishing feature of the system that enables the recovery of large damage volumes. Without formation of the gel, liquids are mobile and more susceptible to external forces that may draw the healing agents away from large, open damage volumes. Healing chemistries that polymerize too slowly lead to a "bleed-out" condition where liquids continually drip from the damage zone rather than filling the defect to restore component function.

The initial test geometry (Figure 18a-d), consisting of a 3 mm thick epoxy sheet with two parallel vascular channels, achieved a 97% increase for maximum damage area recovered in a through-thickness cylindrical defect geometry for a gelling healing chemistry compared to non-gelling controls [35]. Beyond 9.0 mm damage diameter, samples only partially filled due to three failure modes illustrated in Figure 18e.

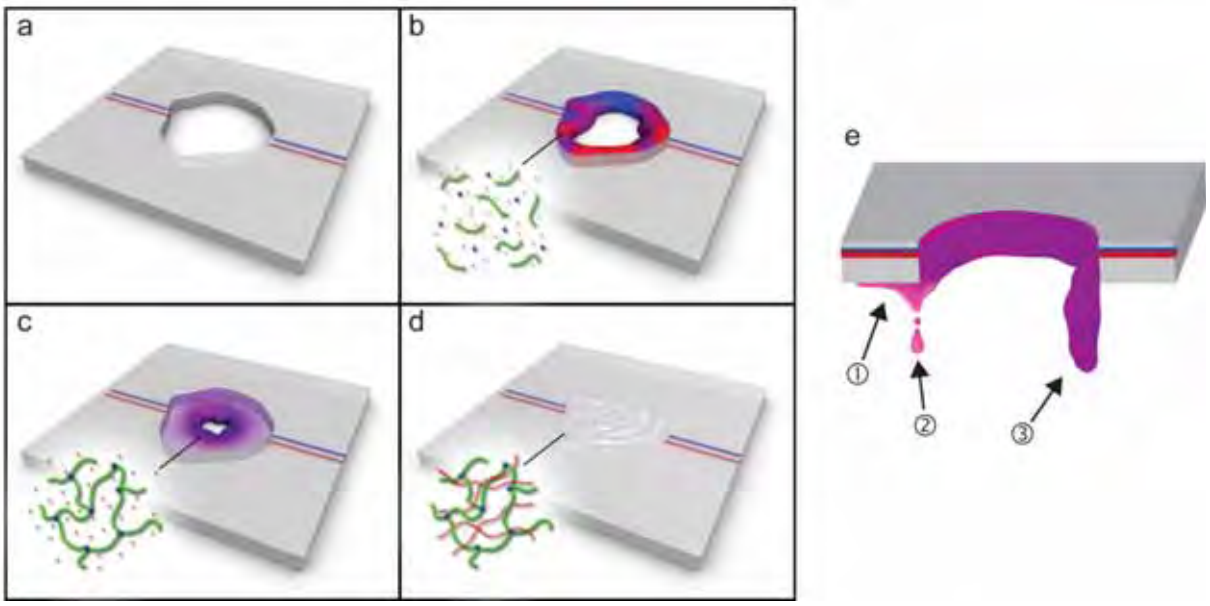

Figure 18. Schematic showing the polymer restoration process for a two-stage healing agent system. a) A damage event caused a large, open wound in microvascular material, b) Two-part chemical healing system was released into the damage volume where mixing occurred. Green segments represent gelator A [PEG-based oligomer], blue dots represent gelator B (aldehyde crosslinker) and the red dots represent the monomer solvent. c) Gelation occurred rapidly via acid-catalyzed reaction of the dissolved gelators. d) Polymerization of the monomer solvent into a structural material. e) Failure modes observed during the fill process: ① surface wetting; ② ungelled reagent dripping; and ③ deflection of the gel.

First, wetting of the healing agents on either the top or bottom surface of the sample wicked un-gelled healing agents out of the damage volume by capillary forces(①). Second, gel formation inhibited microvascular delivery and interfered with proper mixing, preventing gelation of the system. Without gelation, the components of the two-stage chemistry bled out from the damage volume(②). Finally, the growing gel mass sometimes deflected downward rather than closing the gap in the center of the damage volume(③).Results were reported for a single test protocol and the influence of experimental design on these failure modes was not tested.

Characterization of Recovery process

We must mitigate the inherent limitations of liquid healing agents in order to obtain fluid retention sufficient to heal large damage volumes. The cohesive and adhesive forces of gelling healing agents were previously demonstrated to extend the deposition volume by superseding gravitational and surface tension forces in a pendant drop experiment [35]. To test this effect in an actual damage geometry, we recorded the progression of damage area recovery as a function of time in a series of overhead images (Figure 19). Fill progress was assessed by defining an Area Fill Ratio (AFR),

$$AFR = \frac{A_{fill}}{A_0} \qquad (1)$$

where A_{fill} is the damage area recovered by healing agents as viewed from above and A_0 is total area of the original damage zone. AFR data for non-gelling controls and a rapidly gelling system are shown in Figure 19a and b (blue lines), respectively. The non-gelling control repeatedly reached an AFR of ~0.59 before gravity pulled the healing agents from the damage volume and reduced the AFR to ~0.33. In contrast, the gel followed a steady progression toward a complete fill of the damage area, demonstrating the ability of the two-stage chemistry to recover large damage volumes through the formation of a dynamic gel network [16].

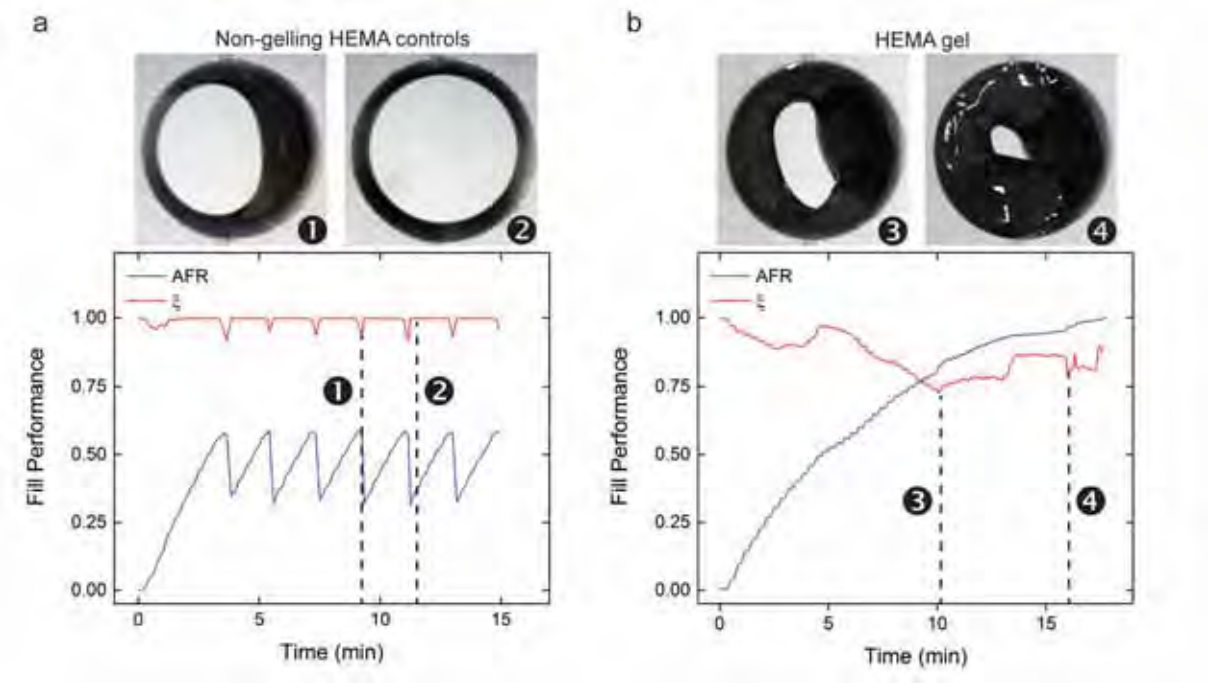

Figure 19. Fill characteristics of large-scale damage filling process a) Non-gelling HEMA controls showed limited AFR and near unity circular deviation. b) HEMA gel system reached a complete fill and showed a significant deviation from circular shape. Damage diameter is 7.0 mm.

For the cylindrical damage geometry, liquid healing agents appeared as an annulus when viewed from above with a circular open damage area present in the center of the damage region. The extent to which the healing agents conformed to a circular contour was calculated from the shape of the unfilled portion of the damage geometry [36],

$$\xi = 1 - \frac{\sqrt{\dfrac{\sum_{i=1}^{N}\left[\left(x_i - A_0\right)^2 + \left(y_i - B_0\right)^2 - {R_0}^2\right]^2}{4{R_0}^2 N\left(1 - \dfrac{3}{N}\right)^2}}}{R_0} \qquad (2)$$

where ξ is the deviation from circularity, x_i and y_i are the coordinates of points around the contour of the unfilled portion of the damage geometry, A_0 and B_0 are the center coordinates of a best fit circle calculated for the unfilled portion of the damage geometry, R_0 is the radius of the best fit circle, and N is the number of points used to construct the best fit circle. ξ was formulated to return a value between 1 (perfect circle) and 0.

Figure 19a and b (red lines) show the difference in ξ between the liquid controls and gel system, respectively. The fill shape of the control fluid is dictated by surface tension, appearing as an annulus until immediately preceding a drip when gravity dominates and pulls the liquid into an oblong shape. In great contrast, the gel material deviates significantly from circularity at the onset of the test and follows no predictable trend, indicating the shape of the gel is not dominated by surface tension.

Healing Agent Delivery Schedule

Delivery schedule was varied for restoration experiments to gauge the effect on maximum fill size. Three pumping protocols were prescribed to alter the cadence of flow while maintaining the overall cycle time and average delivery rate. As with previously described work, one delivery schedule consisted of the following cadence: 1 s pulsed delivery of 1 μL solution B, 3 s delay, 1 s pulsed of 1 μL solution A, and a 15 s delay for a total cycle time of 20 s. Two additional pumping protocols were examined for comparison (Figure 20a). The first was a simultaneous pumping schedule which delivered solutions concurrently. The second was a double frequency alternating schedule with 4 alternating pulses each of 0.5 μL volume. In all three cases, the gel filled a larger area than the control. The original alternating delivery schedule demonstrated the highest fill performance followed by the double frequency alternating schedule and finally, the simultaneous delivery schedule (Figure 20b).

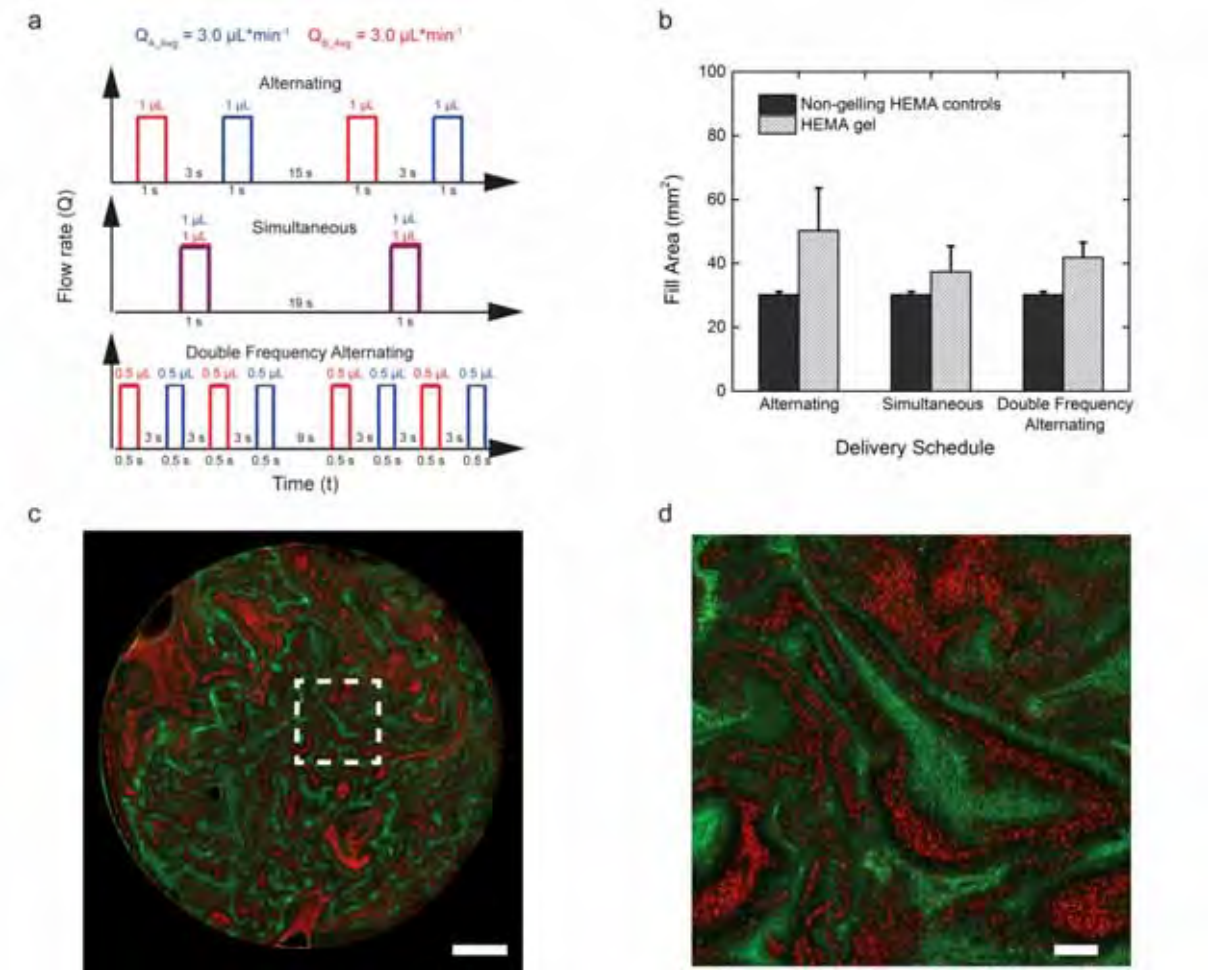

Figure 20. Effects of different delivery schedules. a) Graphical representation of 2 cycles of each schedule. Red lines represent "solution b" and blue lines represent "solution a" (Table 3) b) Fill performance of samples tested under various delivery schedules. c) Micrograph from scanning laser confocal microscope showing a representative distribution of fluorescent nanospheres (red = Rhodamine; green = fluorescein) with an alternating delivery schedule (scale bar = 1 mm). d) Higher magnification region indicated by dotted box in Figure 3c, showing the fluorescent striations (scale bar = 150 μm).

Table 3. Two-part solution composition for two-stage healing agents containing 1.5 wt% initiator, 0.1 wt % promoter, and 2 v/v% catalyst with respect to monomer. Representative values are given for a solution volume of 2 mL total monomer (1 mL per part).

	Component	Amount
Solution Part A	Gelator A[a] (61%)	0.146 g
	Catalyst	40.8 µL
	Promoter[b]	2.1 µL
	HEMA[c,d]	1 mL
Solution Part B	Gelator A[a] (39%)	0.093 g
	Gelator B	0.053 g
	Initiator[b]	31.0 µL
	HEMA[c]	1 mL

a) 12 wt% gelators (3:2 mol ratio A:B) which were divided for equal volume Part A and Part B.
b) Solutions for fill experiments did not include initiator or promoter.
c) HEMA used in making solutions for fill analysis contained 0.0001 wt% carbon black as a contrast agent.
d) HEMA used in making solutions for mixing analysis contained .01 wt% fluorescent nanospheres.

Optimizing two-part healing agent mixing through controlled delivery has been shown to result in superior mechanical performance [34,37–39]. Likewise for a rapidly gelling healing chemistry, performance discrepancies in fill size could be due to different levels of mixing between the two components. Gel time of the healing chemistry is greatly affected by the stoichiometric ratio of the solutions (Table 4). Although each of the schedules was calibrated to deliver 1:1 ratios of solutions, the local stoichiometry of a poorly mixed sample impacted gel time and fill performance.

Table 4. Gel time for vary solution ratios as determined by inversion test. Error is one standard deviation (n = 3).

Solution Ratio (A:B)	Gel Time (s)
2:1	39.7 ± 2.5
1.5:1	32.0 ± 6.2
1:1	29.0 ± 2.0
1:1.5	44.7 ± 3.5
1:2	51.7 ± 1.5

Evaluation of Degree of Mixing

Confocal fluorescent microscopy was used to analyze the position of fluorescent dyed nanospheres to gain a direct indication of mixing. Fluorescent silica nanospheres (~300 nm) containing either Rhodamine B or Fluorescein were synthesized [40,41] and suspended in each of the healing agent components (Rhodamine - Part A, Fluorescein – Part B). As the two-part system mixed during delivery, gelation locked the nanospheres in place and the nanosphere silica shell prevented diffusion following deposition of the healing agents. After allowing the healing chemistry to fully cure into a rigid polymer, confocal micrographs of polished surfaces had a striated appearance with notable concentrations of each nanosphere species (Figure 20c and 20d). The striated appearance of the fluorescent microspheres is indicative of the layer-by-layer growth of the gel mass and provided an opportunity for quantitatively assessing the level of mixing.

We evaluated the distribution of the dyed nanospheres by converting each channel into a binary image (Figure 21a and 21b), overlaying a 30x30 cell grid (cell size ~200 μm x 200 μm, Figure 21c), and calculating cell concentrations of each dye via MATLAB. Lacey described a statistical method to determine the degree of mixing between two particulate species [42],

$$M = \frac{\sigma_0^2 - \sigma^2}{\sigma_0^2 - \sigma_R^2} \qquad (3)$$

where M is the Lacey Mixing Index, σ_0 is standard deviation of cell concentration in a completely unmixed sample, σ is the standard deviation of cell concentration in the actual sample, and σ_R is the standard deviation of cell concentration in a perfectly mixed sample. M will approach unity for a perfectly mixed sample. As opposed to other methods that rely on circumstantial evidence of mixing from mechanical data [5,34,39], our analysis achieves a direct assessment of healing agent placement during fluid delivery.

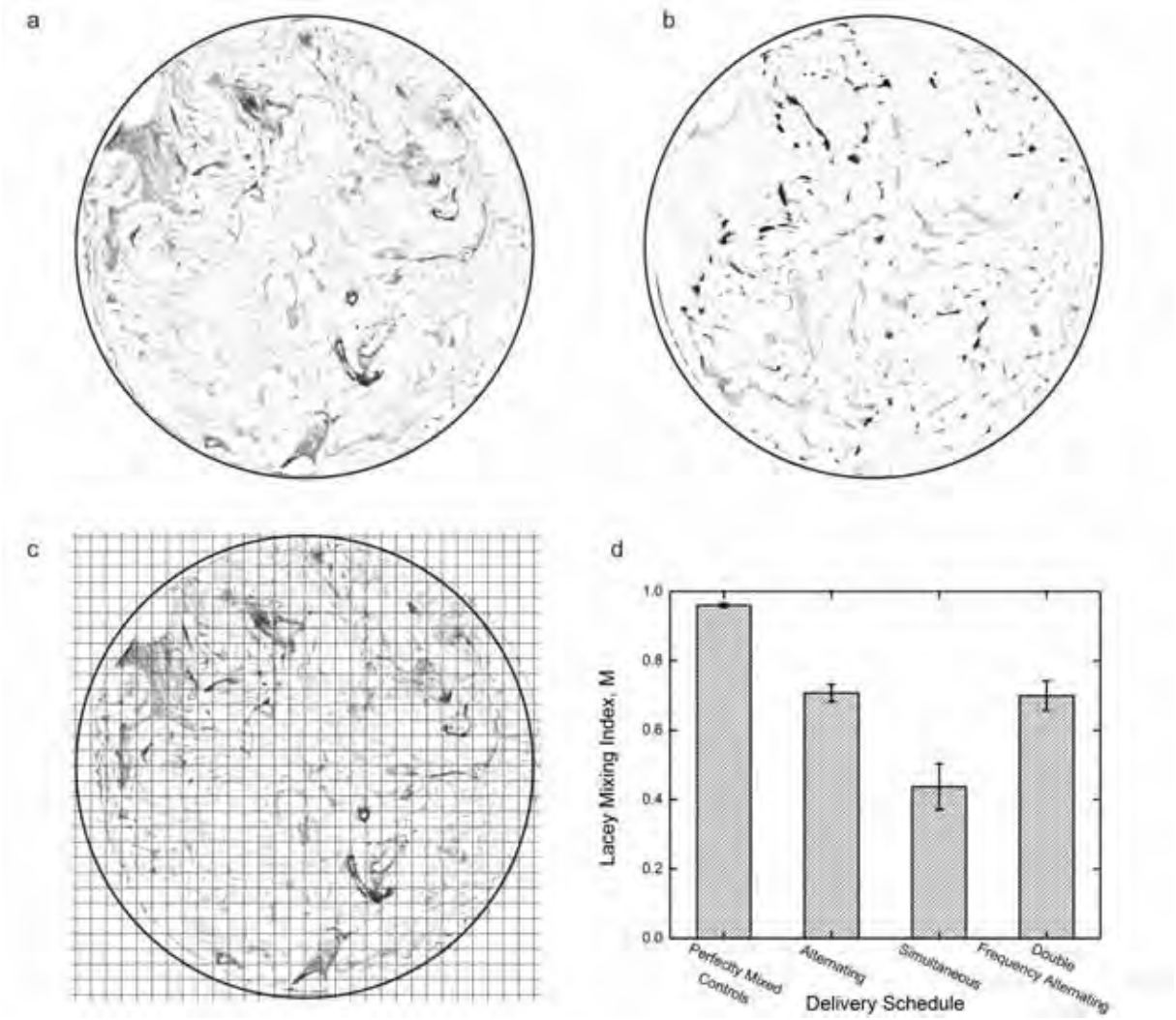

Figure 21. Evaluation of mixing. a) Binary conversion of rhodamine (red) channel from Fig 3C (diameter = 6.5 mm). b) Binary conversion of fluorescein (green) channel from Fig 20c. c) Representative 30x30 grid overlaid on Rhodamine channel. Cells with less than 1.5 % concentration of either component were omitted from mixing index calculations d) Lacey mixing index for each delivery schedule (n = 3 for each schedule, error bar is one standard deviation).

Samples that were premixed with a vortex mixer ("perfectly mixed controls") and manually injected into damage volumes approached M values of unity as expected (Figure 21d). In agreement with fill performance, simultaneous delivery schedule showed the lowest degree of mixing. However, alternating and double frequency alternating schedules showed similar degrees of mixing despite differences in fill performance. A closer look at each sample (Figure 22) revealed the double frequency alternating samples contained larger regions of single-dye composition and lower regional mixing even though overall mixing is equivalent. Hence, mixing influenced fill size but other factors such as local viscosity changes or dynamic contact angle of healing agents could also impact delivery and flow of healing agents in the damage volume to influence the fill performance.

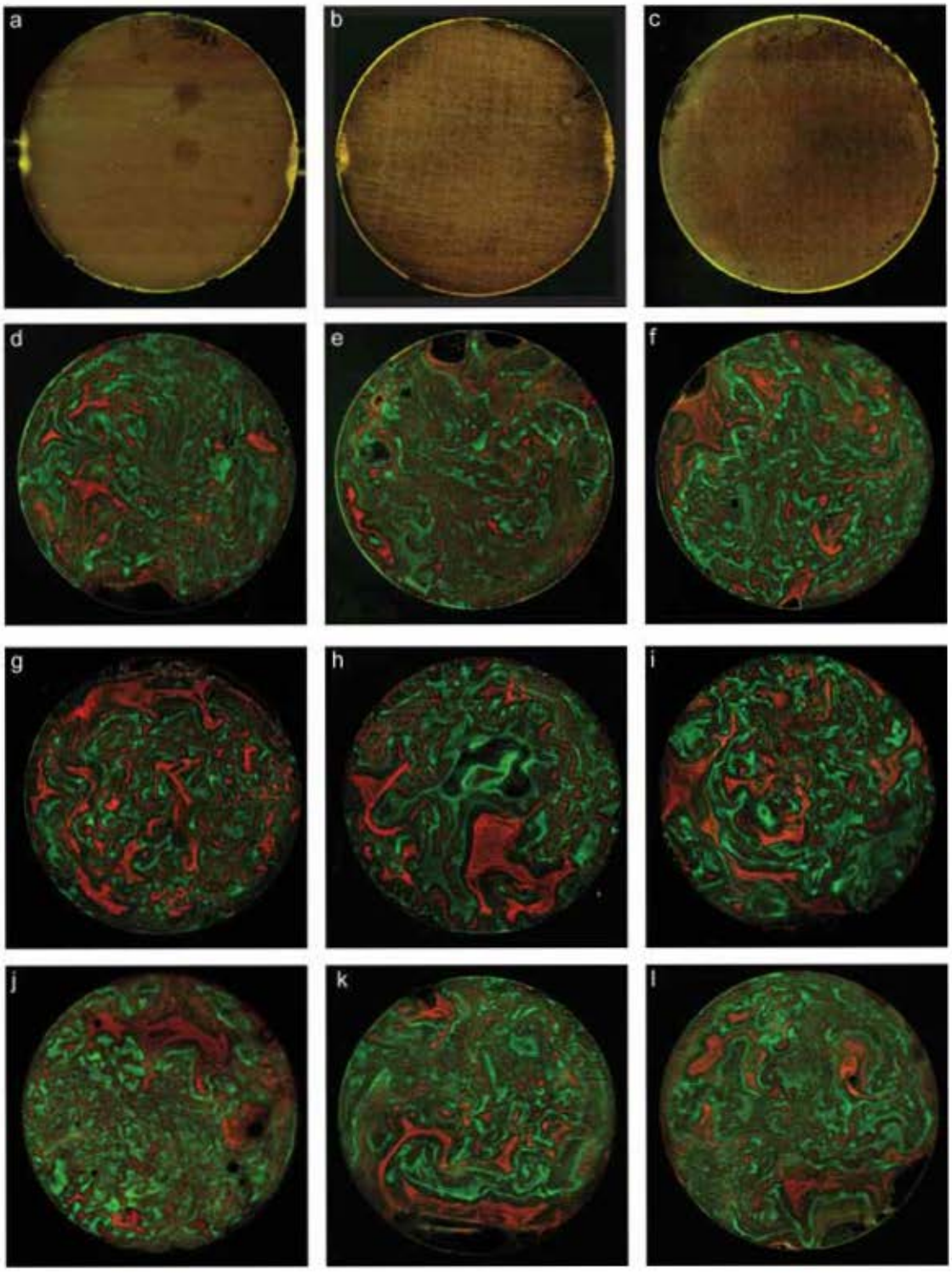

Figure 22. Confocal fluorescence micrographs with Rhodamine (red) and fluoresceine (green) dyed nanospheres. a) – c) Perfectly mixed control, d) – f) alternating delivery schedule, g) – i) simultaneous delivery schedule, j) – l) double frequency alternating delivery schedule. Circle diameter = 6.5 mm

Sample Thickness and Orientation

We investigated the effects of substrate thickness and sample orientation on maximum fill size to determine whether the surface area available for gel accretion or the direction of gravity would influence regeneration performance. The effect of sample thickness on maximum fill area is shown in Figure 23a. Sample thickness is varied from 1-3 mm while holding microchannel position constant with respect to the upper surface. Increasing sample thickness resulted in an increased fill size for both non-gelling controls and gelling healing agents. Improved performance with increasing thickness is expected since the greater sample thicknesses provide a larger surface area for healing agents deposit, spread, and gel to delay failure by deflection. The fill size of the gelling healing agents increased more rapidly with thickness than the non-gelling controls. The controls experienced only marginal benefit from thicker samples because gravity still dominated retention limitations.

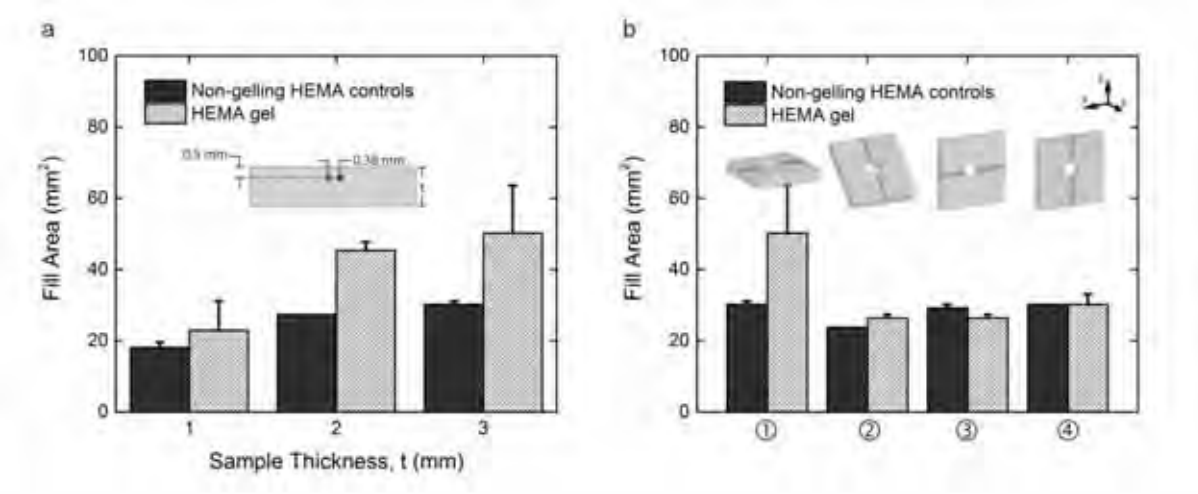

Figure 23. Effect of thickness and orientation on fill performance. a) Fill area of controls and gel for each sample thickness b) Fill area of samples with following orientations: ① 0°, ② 45° vertical channels, ③ 90° horizontal channels, ④ 90° vertical channels.

The fill performance of the gelling healing agents under different damage orientations was investigated to better understand the effect of gravity on the healing process. Figure 23b shows the fill performance of non-gelling controls and gelling healing agents in four different sample orientations: ① 0°, ② 45° tilt with veritcal channels, ③ 90° with horizontal channels, and ④ 90° with vertical channels. The 0° orientation far outperformed all other orientations for the gel. As expected, the controls were largely unaffected by damage orientation. The gel only provided a marginal benefit over controls for the 45° tilt with vertical channels and 90° with horizontal channels. The controls slightly outperformed the gel for the 90° with vertical channels test case.

In all orientations other than the 0° case, one or more of the channels became blocked by the formation of gel. Consequently, the blockage resulted in poor mixing and/or inadequate ratios of components delivered to the damage region which decreased the fill performance. In the 0° orientation, liquids were distributed and retained around the entire circumference of the damage zone awaiting gelation. In all other orientations, healing agents pooled at the bottom of the damage geometry, only covering a relatively small portion of the damage circumference. Healing agents with faster gel times could potentially be used to mitigate orientation challenges if

gelation occurs before healing agents accumulate on the lowest surface. The introduction of additional channels may also help the system resist failure due to channel blockage.

Surface Wetting

We investigated the effect of specimen coatings on the surface wetting failure mode and the maximum damage fill size. The contact angle of HEMA varied drastically with coating, eliciting wetting (θ = 18°), near oleophobic (θ = 72°), and super oleophobic (θ = 163°) responses for bare, Frekote, and UED coated samples, respectively (Figure 24a-c). Liquid on a wetted surface crossed the sample edge to wet the adjacent surface if the "Gibbs inequality condition" [43] (Figure 25) was exceeded,

$$\theta_1 \le \theta_0 \le (180 - \phi) + \theta_2 \qquad (4)$$

where θ_1 is the equilibrium contact angle of the wetted (damage) surface, θ_0 is the contact angle at the edge, Φ is the angle between the two surfaces, and θ_2 is the equilibrium contact angle of the non-wetted (top or bottom sample) surface. θ_1 is 18° for all samples because damage exposes bare epoxy and Φ is 90° because damage is created perpendicular to the channels. However, θ_2 varies and is represented by the contact angle of the various coating conditions.

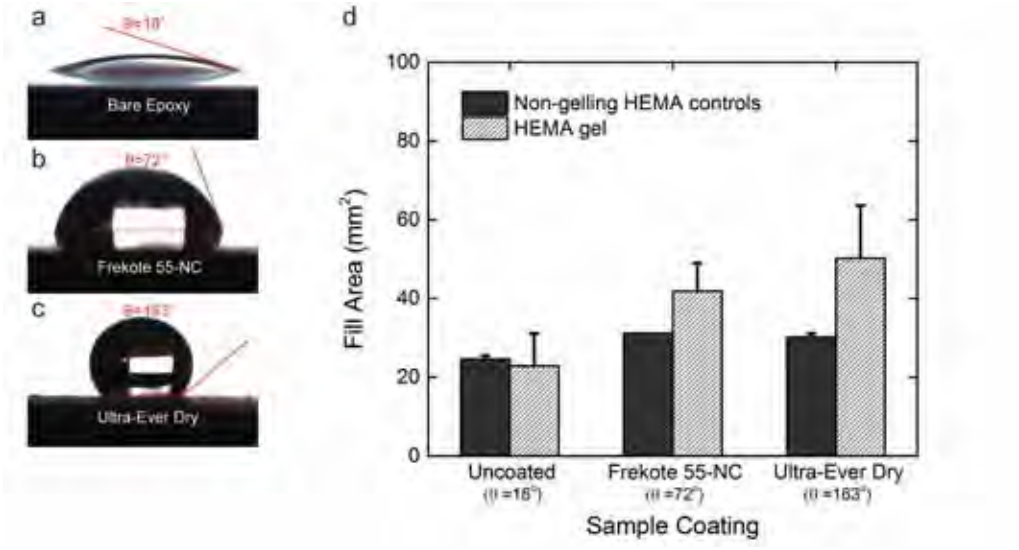

Figure 24. Effect of surface modification on wetting and fill performance. a) Contact angle of HEMA on uncoated epoxy, b) Frekote 55-NC, and c) Ultra-Ever Dry. d) Fill performance of samples at varying surface contact angles.

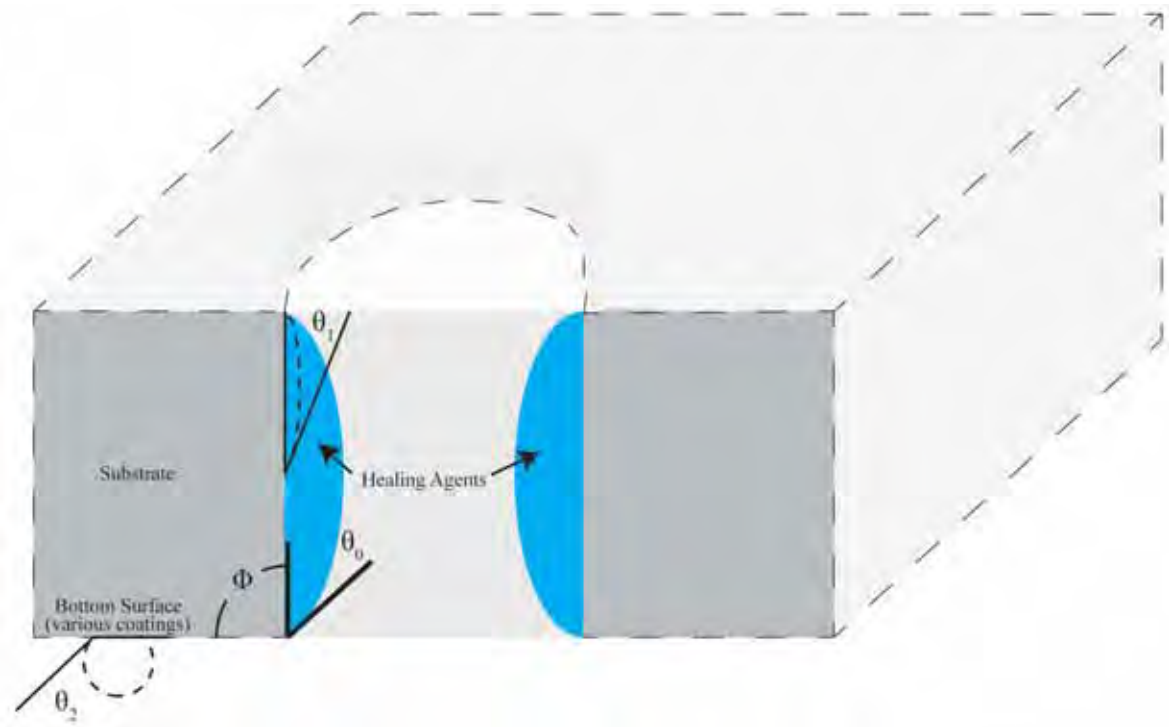

Figure 25. Schematic showing variables included in the Gibbs inequality condition (Equation 4). Droplet outlines represent the low equilibrium contact angle for the damage (uncoated) surface and the bottom (uncoated, Frekote 55-NC, or Ultra-Ever Dry) surface of the sample. As θ_2 increases, the specimens increasingly resist failure by wetting.

Figure 24d compares the fill performance for each coating condition. Bare epoxy samples were prone to wetting failure for both the non-gelling controls and gelling healing agents, resulting in only a marginal performance increase for the gel compared to controls. Healing agents often wetted the bottom surface of the sample prior to gelation. Both Frekote and UED coated samples achieved equivalent fill results for control liquids because the coatings eliminated the wetting failure mode. In contrast, gel fill performance increased with contact angle. Gel buildup hindered and deflected the flow of healing agents to cause occasional wetting failure on Frekote samples, but this event was not observed with UED samples. The selective phobicity of the surface redirects fluids [44,45] and better retains healing agents within the damage volume.

Concentration of Vascular Channels

Samples with 2, 4, and 8 intersecting channels were fabricated and evaluated for fill performance. Cylindrical damage volumes were created at the intersection of the channels (the damage event split each channel in half; E.g. the 2-channel specimens had 4 half-channels delivering fluids) and the healing agent delivery rate was held at 3 $\mu L*min^{-1}$ per channel for each experimental configuration. Figure 26a shows an image sequence of the fill process for an 8-channel specimen with a 10.5 mm damage diameter. We observed more deposition with higher microvascular concentration, leading to enhanced restoration performance (Figure 26b). The maximum fill size of controls was largely unchanged by increasing the number of channels, but gel performance of the 8-channel specimens achieves 164% improvement (11.2 mm damage diameter) in fill area over the 2-channel sample geometry and 197% improvement over controls.

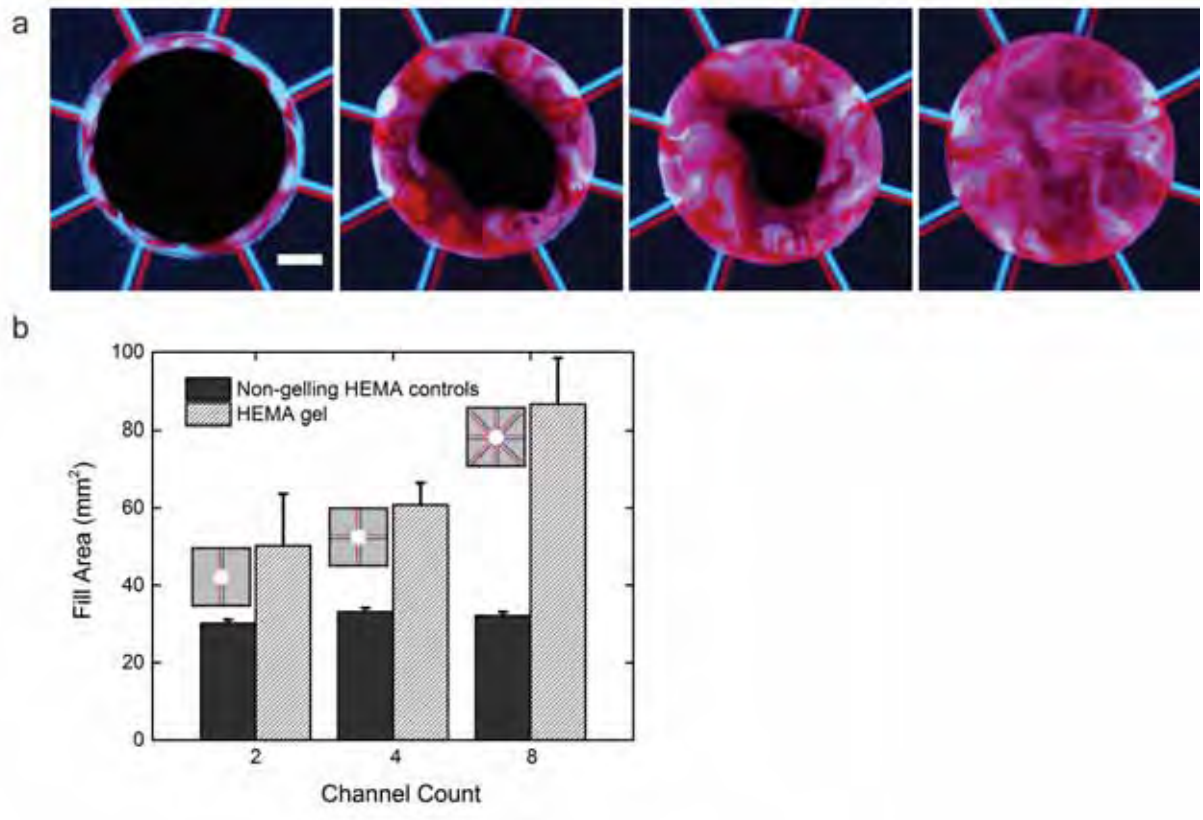

Figure 26. Effect of number of delivery channels on fill performance. a) Fill process for a 10.5 mm diameter sample shown after 1, 5, 8 and 10 minutes into the fill process (scale bar = 2 mm). b) Fill performance of samples with varying channel count.

Overall Fill Performance

The HEMA gel system is a versatile strategy to address large damage volumes as demonstrated by the superior fill results compared to non-gelling control fluids. Table 5 contains numerical values comparing the relative performance of all test conditions. The restoration performance was calculated as a normalized value of gel performance compared to non-gelling controls with respect to the maximum fill area obtained,

$$\zeta = \frac{\alpha_{gel} - \alpha_{control}}{\alpha_{control}} \qquad (5)$$

where ζ is the performance increase, α_{gel} is the maximum fill size attained by HEMA gel for a given experimental protocol (delivery schedule, sample geometry, sample orientation, surface coating, and microvascular density), and $\alpha_{control}$ is the maximum fill size attained by non-gelling controls for the same protocol. The gel outperformed the non-gelling control fluids for every test case ($\zeta > 0$) except for the 90° oriented test configuration with horizontal channel positioning ($\zeta = -0.09$). The performance increase was greatest for samples with an alternating pumping schedule, largest thickness, 0° orientation, superoleophobic surfaces, and highest concentration of microvascular channels. Under these conditions, the gel exceeded the maximum fill size of non-gelling controls by a margin of 3:1.

Table 5. Maximum fill size attained for each test condition.

		HEMA Controls		HEMA Gel		
		Diameter (mm)	Area (mm^2)	Diameter (mm^2)	Area (mm^2)	Performance Increase, ζ
Standard Specimen[a]		6.3	31.2	9.0	63.6	1.04
Experimental Series[b]	**Variables**					
Delivery Schedule	Simultaneous	6.2	30.2	7.6	45.3	0.50
	Double Frequency Alternating	6.3	31.2	7.7	46.5	0.49
Thickness	1 mm	5.0	19.6	6.3	31.2	0.59
	2 mm	5.9	27.3	7.8	47.8	0.75
Orientation	45°, Vertical Channels	5.5	23.7	5.9	27.3	0.15
	90°, Horizontal Channels	6.2	30.2	5.9	27.3	-0.09
	90°, Vertical Channels	6.2	30.2	6.5	33.2	0.10
Surface Coating	θ = 18°	5.7	25.5	6.3	31.2	0.22
	θ = 72°	6.3	31.2	7.9	49.0	0.57
Channel Count	4 Channels	6.6	34.2	9.2	66.4	0.94
	8 Channels	6.5	33.2	11.2	98.5	1.97

a) Standard sample consists of alternating delivery schedule, 3 mm thickness specimens, 0° orientation, superoleophobic surface coating, and 2 microvascular channels.
b) Test conditions conform to the "standard sample" in all respects other than the one specified.

2.1.6. Impact damage restoration (RCRG)

The initial study of restoration of large damage volumes in polymers (section 2.1.4) introduces the performance metrics for restoration of impact damage. Subsequent experimentation probes methods to improve both recovered impact energy absorption when a restored specimen is subjected to a repeat impact, as well as sealing of microcracks when a static pressure is applied to one side of the specimen and leakage is monitored on the opposite side (Figure 27). Variations in the 2-stage restoration chemistry are tested, affecting the mechanical properties of the resulting polymer. Multiple configurations of the bulk substrate are fabricated and tested: changing the type of polymer, and including microcapsules.

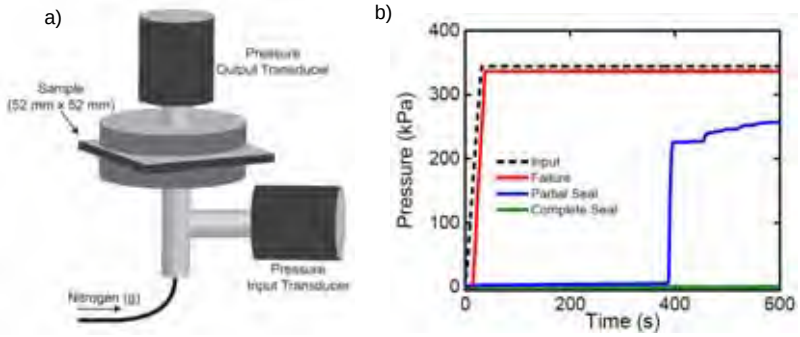

Figure 27. Pressure testing: a) schematic of pressure cell, b) example pressure profiles [35].

Formulation of healing chemistry to improve energy absorption on re-impact

After restoration of impact damage using 2-stage restoration chemistry, specimens were re-impacted using the same testing protocol to determine their recovery of impact energy. With the objective of improving the energy absorption, the formulation of the monomer using in the 2-stage healing chemistry was varied. One promising result was obtained using a mixture of two monomers 2-hydroxyethyl methacrylate (HEMA, used in the previous study), and 2-hydroxyethyl acrylate (HEA), which results in a acrylate copolymer. The chemical formulation of these monomers is shown in Figure 28. The mechanical properties of various weight ratios of these two monomers were studied using dynamic mechanical analysis, and the resulting storage moduli at 1 Hz are shown in Figure 29a.

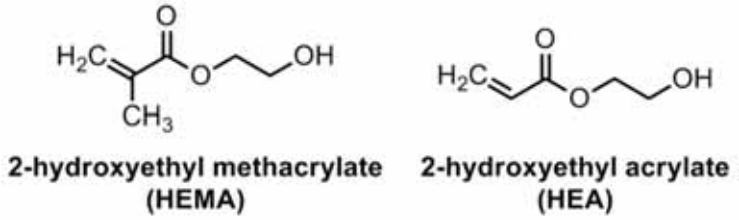

Figure 28. Monomers used in the formulation of acrylate copolymers for energy absorption study.

Experiments were performed to determine the effect of varying the monomer feed ratio, and effectively the mechanical properties of the cured regeneration material on the impact energy absorption when restored specimens were re-impacted. Impacted epoxy sheet specimens were manually injected with premixed 2-stage restoration chemistry and allowed to cure. The injected material was retained in the damage region using a silicone sheet clamped to one side of the specimen. After curing, the specimens were re-impacted. The percent recovery of energy absorption relative to the initial impact is given for the three formulations tested in Figure 29b. The 70:30 ratio of HEMA:HEA, which exhibited a storage modulus of 0.64±0.05 GPa, showed over 100% recovery of impact energy absorbed. When specimens were filled using the in-situ pumping protocol described previously and the 70:30 ratio of HEMA:HEA, they exhibit 82±33% recovery of absorbed impact energy.

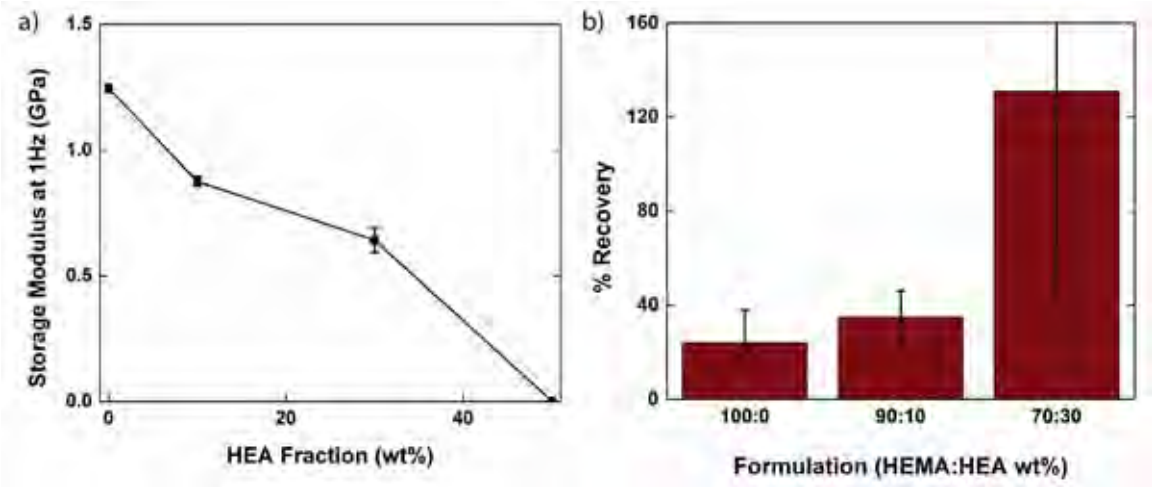

Figure 29. Energy absorption, manually injected controls.

Thermoplastic matrix system for dual healing pathways: 2-stage chemistry, and solvent-based self-healing.

Previously in Section 2.1.4 the substrate chosen for recovery of impact damage an epoxy polymer. Replacement of the substrate with a thermoplastic, specifically an acrylic, enables dual healing pathways: (1) via the reaction of the two parts of the 2-stage chemistry, and (2) solvent healing via the solvation of the substrate and re-entanglement of polymer chains. While the 2-stage chemistry is required for the retention of material in the central lost volume, cracks will be solvent healed by a single component. Previous investigations have used solvents such as methanol or ethanol and the addition of heat for solvent healing of PMMA [46–52].

Previously, the gel time was reduced to improve sealing of impacted epoxy substrates using the HEMA 2-stage chemistry. However, when implementing the slow gelling HEMA 2-Stage chemistry in PMMA substrates, no sealing was observed when specimens were filled the in-situ pumping protocol described previously. It was observed that the HEMA monomer induces solvent cracking of PMMA. An alternative monomer, 2-phenoxyethyl methacrylate (PEM), that does not show solvent cracking was tested. Control experiments were performed in which the 2-stage solution was manually injected into a simple cylindrical drilled hole and allowed to cure (Table 6). As observed in the previous study, 100% of the drilled hole specimens with epoxy substrates filled with the slow gelling 2-stage chemistry sealed. In addition, it should also be noted that all specimens (epoxy substrates) from the previous study sealed when filled with fast gelling formulation and HEMA as a monomer. The specimens in PMMA substrates filled with 2-stage solutions with HEMA as a monomer show very low fractions of specimens sealing, consistent with the failure to seal in the in-situ pumped specimens and the notion that solvent cracking reduces likelihood of sealing. The PMMA substrate specimens that were filled with 2-stage solutions with PEM as a monomer do not show 100% of specimens in sealing. The marginal increase in fraction of specimen sealing may indicate that non-solvent cracking effect of the PEM monomer improves sealing. The cause of the poor sealing fraction in PMMA substrates is certainly due poorer bonding between the healing agent and substrate after the healing agent has cured, but the underlying cause has yet to be determined.

Table 6. Control fills of drilled hole specimens, with various healing agents. Premixed 2-stage healing agent components were injected into hole and allowed to cure.

Specimen Type Substrate/Healing Agent	% of Specimens Sealed	Number of Specimens
Epoxy/2-Stage HEMA Slow	100%	3
PMMA/2-Stage HEMA Slow	17%	6
PMMA/2-Stage HEMA Fast	33%	6
PMMA/2-Stage PEM Fast	50%	6

Hybrid system incorporating both a vascular network and capsules

Despite the positive effect of improving sealing performance by slowing the gelation speed using the HEMA 2-stage chemistry in section 2.1.4, there is one significant disadvantage. Slower gelation reduces the size of through hole that can be filled. The size reduction can be partially combatted by tuning the pumping protocol to suit the slower gelling chemistry. However, such tuning further extends the fill time. The rapid gelling chemistry was well characterized in the previous study, however it did not successful seal impact specimens, presumably due to unfilled radiating microcracks. There are several examples of previous

research in self-healing materials that have successfully demonstrated healing of cracks using microcapsules, both for recovery of fracture toughness [1,15,46,53–57] and for sealing functions [6,58]. In addition, by incorporating capsules into the bulk polymer, the transport distance of the healing agent is greatly reduced, since microcapsules are located all along the microcracks. Thus, it is desirable to combine a vascular network and capsules to separately address the different length scale damage present in impact puncture damage. In this case, the rapidly gelling 2-stage HEMA chemistry is employed to fill the central damage and lost volume with the pumping protocols optimized for the system. Radiating microcracks are repaired via the rupture of microcapsules, and re-bonding of crack surfaces (Figure 30).

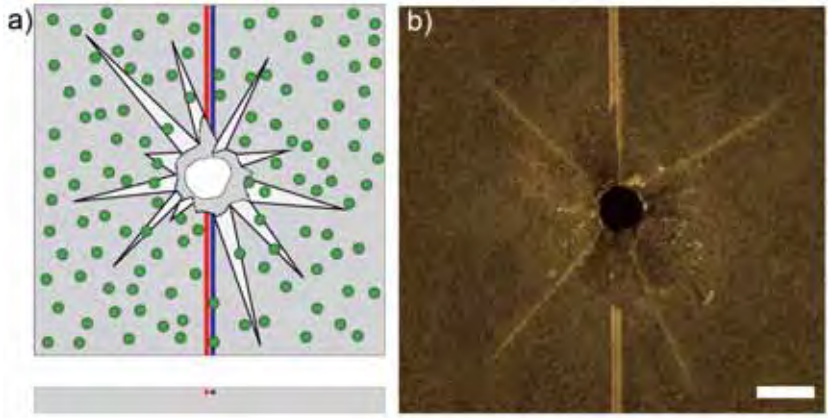

Figure 30. a) Schematic of hybrid system containing vascular channels and capsules (not to scale), showing impact damage. Primary delivery channels for filling of central damage shown in red and blue. Capsules shown in green. b) Top view of impacted specimen containing primary delivery channels and capsules (scale bar = 5 mm).

The solvent-epoxy single capsule system introduced by Caruso demonstrated ~100% recovery of fracture toughness [56]. Capsules containing 97 wt% ethylphenylacetate and 3 wt% Epon 862 (Diglycidyl Ethere of Bisphenol F), and sieved to 75-250 μm (diameter = 190 ± 30 μm) were incorporated at 10 wt% into specimens with the same configuration of vascular network as was implemented in section 2.1.4 (Figure 30). In addition control specimens using capsules containing hexyl acetate (HA, the control used in work by Caruso et. al.) were also fabricated. All specimens were impacted, a manually injected with premixed 2-stage solution, and allowed to cure. Pressure testing showed 100% sealing in the capsule filled specimens, both the self-healing and control, while the no-capsule case showed no sealing (Table 7). The source of the sealing in control specimens is yet to be determined, but may be caused by either a change in the damage geometry that facilitates sealing using only the 2-stage chemistry, or the potential that HA may be inducing crack healing. In addition, impact energy absorption was measured both in the initial impact (virgin energy absorption) as well as after filling. Importantly, the epoxy matrix required for this healing system shows lower virgin energy absorption than the previous system (~0.92 J) faciliting a larger % recovery of energy absorption (~200% for 97:3 self-healing capsules). In addition, specimens containing 10 wt% 97:3 EPA:Epon 862 were filled using the in-situ pumping protocol described previously and the fast gelling HEMA 2-Stage chemistry. The results showed 100% sealing and ~50% recovery of energy absorption.

Table 7. Manual injection fills of capsule filled specimens, Sealing and Energy absorption.

Capsules	2-Stage Filing Agent (HEMA)	Number of Specimens	Sealing%	Virgin Energy Absorption (J)	Filled Energy Absorption (J)	%Recovery
10 wt% 97:3 EPA:862	Fast (2 v/v% DCA)	5	100%	0.22 ± 0.03	0.41 ± 0.09	190 ± 50%
10 wt% 97:3 EPA:862	Slow B (0.05 v/v% DCA)	5	100%	0.24 ± 0.04	0.54 ± 0.19	210 ± 110%
No capsules	Fast (2 v/v% DCA)	3	0%	0.34 ± 0.03	0.26 ± 0.02	76 ± 4%
10 wt% Hexyl Acetate (HA)	Fast (2 v/v% DCA)	8	100%	0.24 ± 0.04	0.28 ± 0.06	125 ± 40%

2.2. New Healing Chemistries

The regeneration and remodeling grant resulted in the development of several new healing chemistries. Each chemistry is highlighted in the following sections.

2.2.1. UV curable healing agents (RCRG)

We sought a one-part healing agent, to preclude the challenges imposed by two-part chemistries. Specifically one-component UV curable healing agents were explored to polymerize under ambient conditions, without intervention. In photo-initiated reactions UV light cleaves covalent bonds, producing active species that induce polymerization [2,59–61]. Furthermore, photocurable chemistries can be selected to harness the UV light available in sunlight, removing the need for a non-autonomous post cure [2]. In our experiments we used a UV lamp with comparable UV irradiance comparable to sunlight (Figure 31).

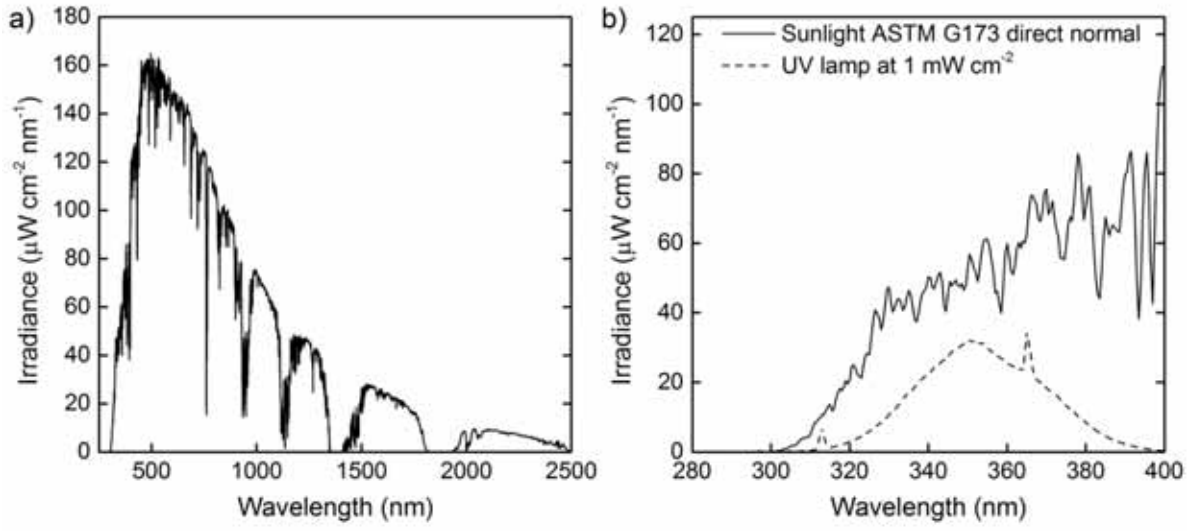

Figure 31. a) Irradiance spectrum of sunlight from ASTM G173 [62], direct normal irradiance, b) Irradiance spectrum of sunlight, UV regime compared to that of UV lamp (365 nm peak irradiance).

Two classes of photoinitiator were explored, cationic and radical. Radical photoinitators are more commonly used, and posses sensitivity to longer wavelengths, however radical polymerizations are inhibited by oxygen. Cationic photopolymerization, however is insensitive to oxygen and will cure under ambient sunlight, but at a slower rate [59,61]. The absorption spectra of an example cationic and radical photoinitiator are shown in Figure 32.

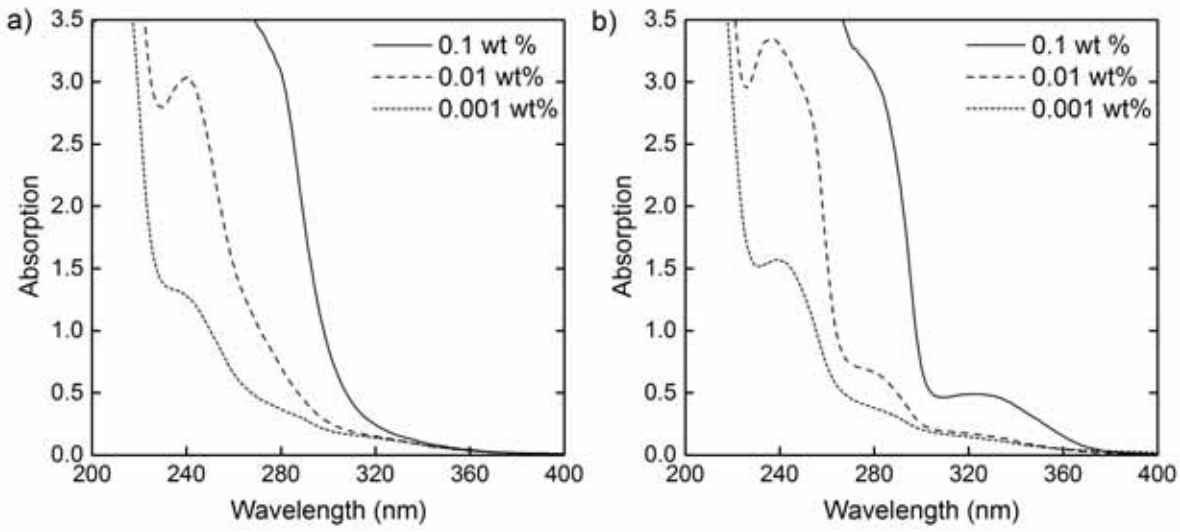

Figure 32. Absorption spectra of example a) cationic (Irgacure 250, BASF) and b) radical (Irgacure 184, BASF) photoinitiators. Collected using a UV-Visible Spectrophotometer (model UV-2401PC, Shimadzu) in Acetonitrile. Peaks in the absorption spectra represent wavelengths to which the photoinitiator is sensitive.

A commonly used phenomenological model for UV curing in polymers comes from work in sterolithography [63]. This equation describes the depth to which a photocurable polymer will cure (cure depth = C_d) with a given exposure to UV light (dose = E_{max}):

$$C_d = D_p \ln\left(\frac{E_{max}}{E_c}\right) \quad (6)$$

The values of D_p, the depth of penetration, and E_c, the critical dose necessary for gelation are experimentally determined for the system. While depth of penetration and critical dose are normally taken as constants for a given formulation, they can also be related to variations in formulation such as concentration of photoinitiator. In Figure 33, measurements of the cure depth were taken for a given dose, where the dose is the product of the intensity of the light source and the time of exposure. Importantly all of the tests were performed with UV irradiances similar or less than that found in sunlight (<1 mW cm^{-2}).

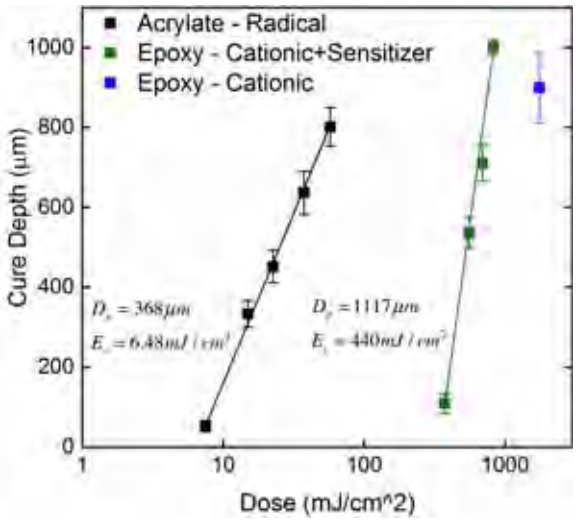

Figure 33. Cure depth characterization of a UV curable healing agents. Formulations: Acrylate – Radical (32 wt% Urethane Acrylate (Ebecryl 1290), 64 wt% trimethyl propane triacrylate (TMPTA), 4 wt% photoinitiator (Irgacure 184)); Epoxy – Cationic+Sensitizer (96 wt% Epon 815C, 3 wt% photoinitiator (Irgacure 250), 1 wt% sensitizer (Darocur 1173)); Epoxy – Cationic (97 wt% Epon 815C, 3 wt% photoinitiator (Irgacure 250)).

Considering this model, one can tune the depth of cure by controlling the exposure to UV light. However, the unmet challenge remains: how does one limit the desired curing to the coating and prevent it from propagating into the underlying vasculature? The solution sought by using surface valves in section 2.1.1 precludes the necessity for any control over depth of cure by isolating uncured material released to the damage site from the underlying vasculature. The polymer is simply required to cure under the intensity of UV light available in sunlight. The epoxy-cationic system was selected due to its insensitivity to atmospheric oxygen [2].

2.2.2. Epoxy-thiol healing chemistry

Two-part healing agents provide an effective, robust, and rapid means to achieve self-healing in microvascular self-healing systems [5,34,35,37,38]. Chemistries are chosen to fit specific applications using properties such as mechanical properties, reaction kinetics, viscosity, and wetting (surface tension) behavior. An epoxy-amine two-part system consisting of EPON 8132 and EPIKURE 3274 (Momentive, Columbus, OH) has proven versatile in multiple healing geometries including surface coatings [5] and fiber-reinforced composite double cantilever beams (DCB) [34]. For the DCB geometry, this epoxy-amine system achieved more than 100% recovery of fracture toughness (G_{IC}) as compared to mode-I delamination of the virgin composite. Although effective, a cure of 2 days at 30°C was required to obtain this performance, at which point a 78% degree of cure was reached.

Carioscia et al. have demonstrated thiol-ene/thiol-epoxy hybrid polymers that achieve >70% conversion in 1 hour at room temperature in the presence of an amine catalyst [64,65] with the epoxy-thiol portion obtaining greater than 90% conversion. We modified this system to develop a healing agent based on thiol-epoxy networks. The system contains a common epoxy resin, EPON 828 (Bisphenol A diglycidyl ether, Momentive); a reactive diluent, Epodil 750 (1,4-Butanediol diglycidyl ether, Air Products and Chemicals, Allentown PA); a tetrathiol crosslinker, Pentaerythritol tetrakis(3-mercaptopropionate (Sigma, Milwaukee, WI); and a tertiary amine catalyst, N,N-Dimethylbenzylamine or (Dimethylaminomethyl)phenol (Sigma) (Figure 34).

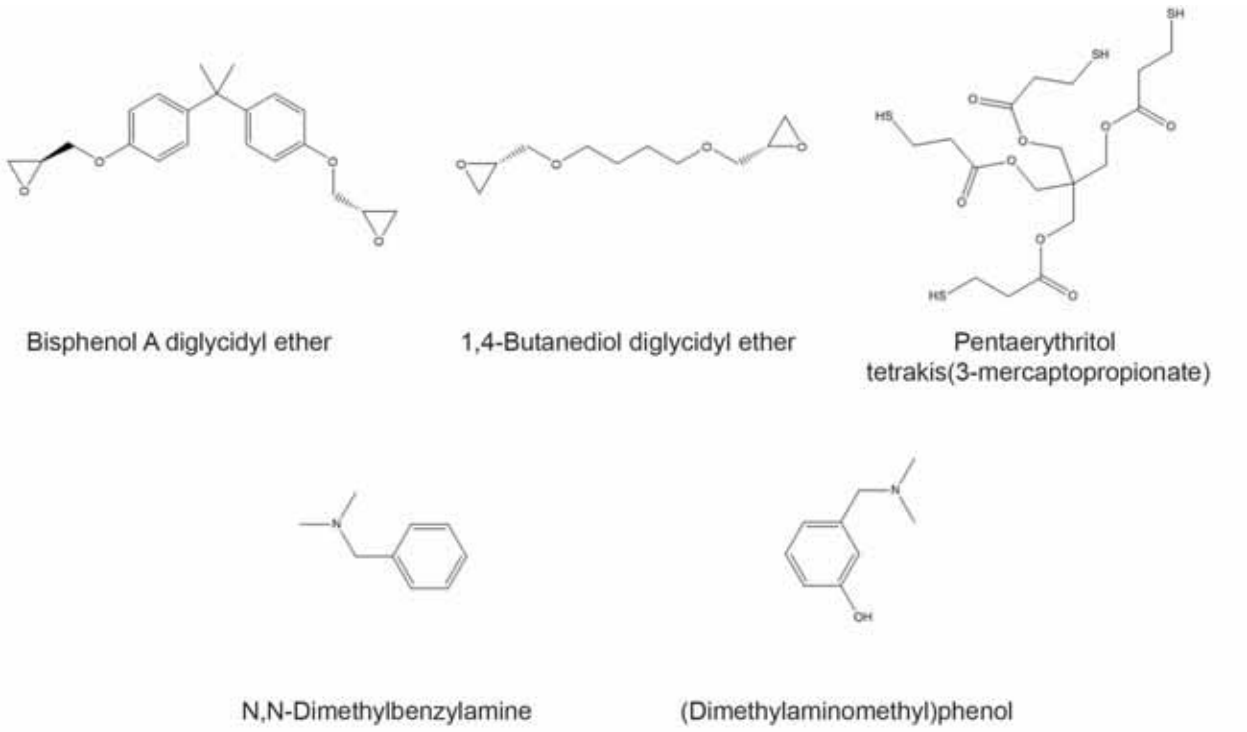

Figure 34. Components of thiol-epoxy healing agent.

The healing agent can be split into two solutions (one containing EPON 828, Epodil 750 and the other containing Tetrathiol, amine catalyst). Table 8 below shows the measured viscosity and surface energy properties of these constituents as well as the measured properties of a blend of 75% Epon 828/25% Epodil 750 (Epoxy Blend). All properties were measured at room temperature. The surface energy was determined via Tate's Law [29–31] and viscosity was determined via a strain sweep on an AR-G2 (TA Instruments, New Castle DE) outfitted with 25 mm diameter parallel plate geometry.

Table 8. Maximum fill size attained for each test condition

Component	Surface Energy (dyne*cm^{-1})	Viscosity (cPs)
Epon 828	45.4 ± 0.2	19,500
Epodil 750	37.0 ± 0.1	17
Epoxy Blend	42.3 ± .1	574
Tetrathiol	47.1 ± 0.2	495
N,N-Dimthylbenzylamine	26.0 ± 0.1	2
(Dimethylaminomethyl)phenol	32.9 ± 0.3	36

A time sweep experiment on an AR-G2 outfitted with 25 mm parallel plates also demonstrated the ability to control reaction kinetics by varying the amount of amine catalyst. Stochiometric samples containing EPON 828/Epodil 750 (75%/25% by weight), tetrathiol, and catalyst were tested under static flow conditions (Figure 35). Experiments were terminated once the mixture viscosity reached 100 Pa*s (100,000 cps). N,N-Dimethylbenzylamine resulted in a much more rapid cure for the same concentration of catalyst compared to (Dimethylaminomethyl)phenol. Pot life fell between 10 minutes and 130 minutes depending on catalyst type and concentration.

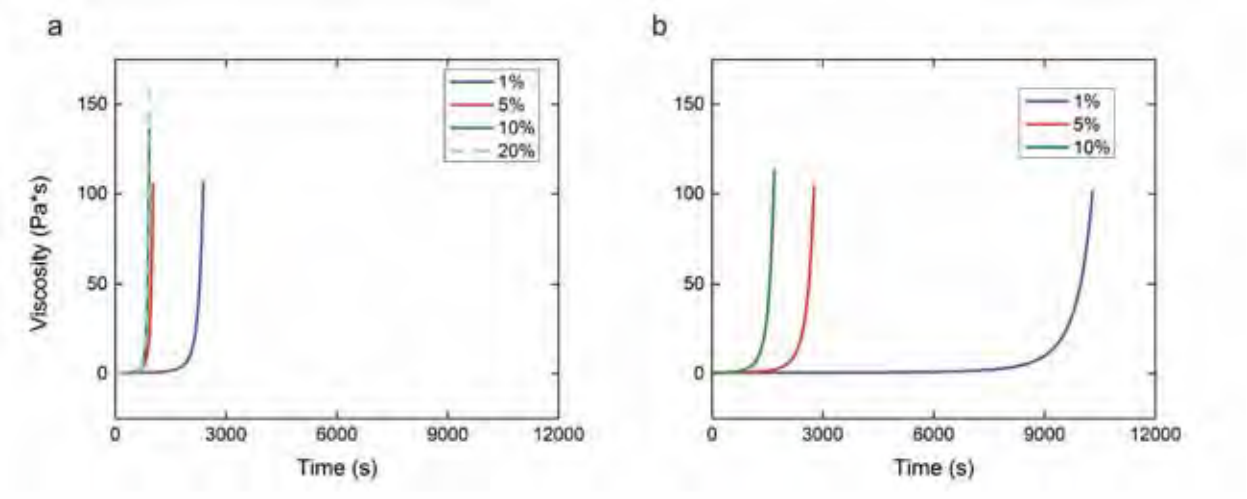

Figure 35. Viscosity as a function of time for epoxy-thiol healing agent consisting of EPON 828/Epodil 750 (75%/25% by weight) and tetrathiol in stoichiometric proportions with a tertiatry amine catalyst. a) Cure rate as a function of catalyst concentration for N,N-Dimethylbenzylamine. b) Cure rate as a function of catalyst concentration for (Dimethylaminomethyl)phenol.

Patrick et al. reported a theoretical maximum healing efficiency of EPON 8132/EPIKURE 3274 of 130% based on G_{IC} calculations for the DCB geometry after a 48-hour cure at 30° C [34]. Using identical fracture procedures, a healing agent consisting of EPON 828/Epodil 750 (75%/25% by weight), and tetrathiol mixed at stoichiometric proportions with 3 wt% (Dimethlaminomethyl)phenol catalyst resulted ~150% healing efficiency after a 24-hour room temperature cure, demonstrating its promise as a high performance healing agent (Figure 36).

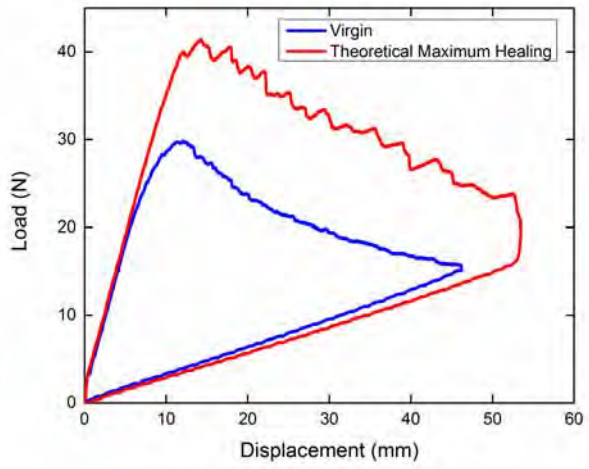

Figure 36. DCB theoretical maximum performance of an epoxy-thiol healing agent system in a controlled injection experiment. EPON 828/Epodil 750 (75%/25% by weight), and tetrathiol mixed at stoichiometric proportions with 3 wt% (Dimethlaminomethyl)phenol catalyst.

2.2.3. Reversible chemistries

In biological systems, regeneration is often aided by scaffolds providing support and structure to facilitate infiltration of blood vessels and promote cell growth [66]. These porous scaffolds are typically composed of a network of proteins, or synthetic mimics, which are used in the recovery of bone or cartilage [67]. Furthermore, marine barnacles utilize elastic polymer networks in a secreted adhesive to strongly adhere to hard surfaces [68]. Following these examples, the first attempts to create synthetic scaffolds for regeneration focused on dynamic materials that change in response to their environment. These smart materials contain a trigged solid-to-fluid transition that incorporates a mechanism to restructure like their biological counterparts.

The first scaffold materials explored utilize dynamic, reversible bonds, i.e. bonds that are formed and broken under equilibrium conditions. Scaffolds were constructed through weak covalent crosslinking of poly(vinyl alcohol) (PVA) polymers with borate anions (Figure 37a). Low concentrations of borate (0.08−0.3 M) instantly crosslink and gel PVA solutions through formation of a didiol complex [69]. The gelation is also pH reversible which facilitates a potential mechanism for controlled deposition or removal of the scaffold. The viscoelastic properties of the PVA-borate gels were investigated using rheology. Higher concentrations of borate increase the modulus of the gel by increasing the crosslink density (Figure 37b). While the elastic (storage) modulus reaches ~10^4 Pa, the bonds are highly dynamic such that the viscous (loss) modulus, G”, is also large. Consequently, PVA-borate gels do not hold their shape and were unsuccessful as scaffolds.

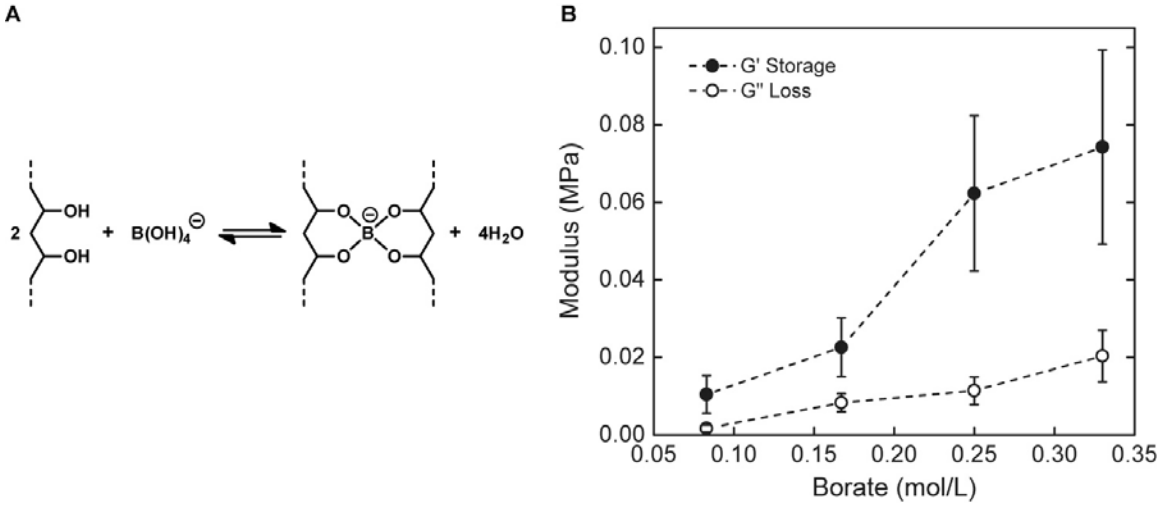

Figure 37. Poly(vinyl alcohol)-borate gels. a) Dynamic crosslinking mechanism of two PVA chains with a borate anion. b) Increasing shear modulus of a 12.5 wt% PVA solution with borate anions. Average is reported after the gel reaches a plateau modulus.

Two methods were investigated to increase the rigidity of the gel scaffold (Scheme 1). Hyperbranched polyether dendrimers (PGly) were synthesized as additional crosslinking sites for the borate ion (Scheme 1A) [70,71]. Dendrimers of various sizes (M_n 1000–1600 g/mol) and concentrations were screened in PVA-borate gels. However, there was no increase in gel rigidity for any combination; the gel properties actually decrease when the dendrimers were added. Another approach employed functionalizing the PVA polymer with pendant groups styrylpyridinium, SbQ (Scheme 1B) [72,73]. SbQ-functionalized PVA polymers will gel after photoinduced crosslinking, but the new polymers were incompatible with the borate salt and

precipitate out of solution. Another drawback to PVA-borate gels is the near instantaneous crosslinking when the borate is added. As a result, the microvascular channels used to deliver the scaffold would easily clog. Attempts to slow the gelation with pH buffers were unsuccessful. Further investigation into PVA-borate scaffolds was stopped in favor of more rigid and controllable polymer gels.

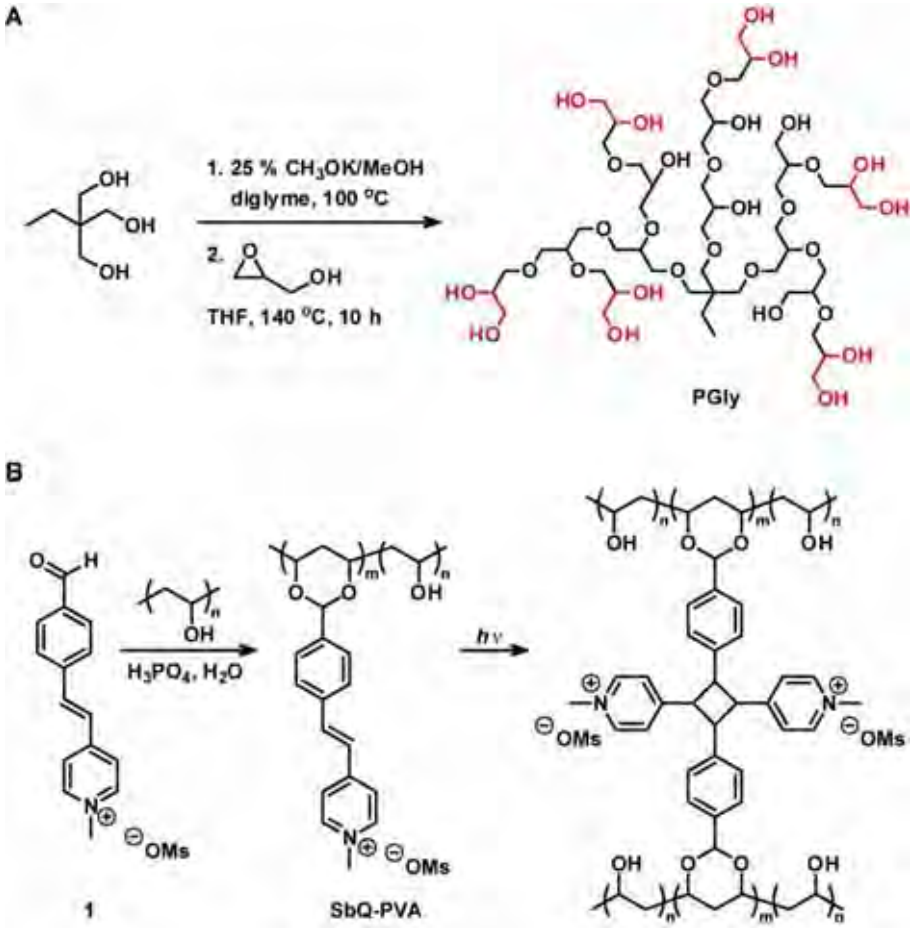

Scheme 1. Methods of improving PVA-borate gel rigidity through a) polyglycerol (PGly) dendrimers [70,71] and b) UV-initiated crosslinking of SbQ (styrylpyridinium) functionalized PVA [72,73].

Organogel scaffolds were created through the catalyzed gelation of Gelators A, *bis*-acylhydrazine terminated poly(ethylene glycol), and B, tris[(4-formylphenoxy) methyl]ethane, in organic solvents (e.g. DMF, dichloromethane) (Figure 38) [16]. The resulting network of acylhydrazone bonds could be reversibly decomposed and reformed 7 times by changing the apparent pH of the organic solvent. More importantly, the acid catalyzed sol-to-gel transition gives a mechanism for controlling scaffold formation. The gel is also chemically robust and retains its shape (G' >> G").

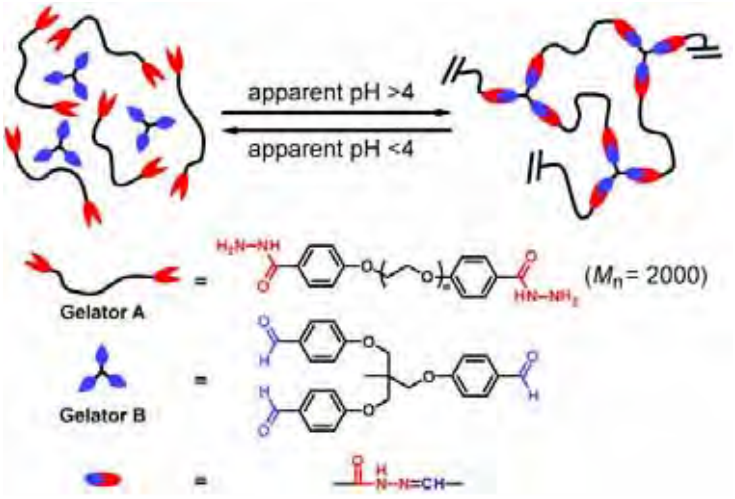

Figure 38. Reversible organogel formation using an end-functionalized poly(ethylene glycol) oligomer and tri-aldehyde crosslinker. Apparent pH was measured in DMF [16].

Although the chemical gel provided a strong scaffold material with control over the sol-gel transition, the gel solvent in both PVA-borate and the organogel poses a significant challenge. Our initial approach to regeneration deposits a scaffold first and then infiltrates the network with healing agents. However, the gel solvents were largely incompatible with the healing chemistries. Diluting structural resins with water or organic solvents yielded brittle and weak final materials (Figure 39). In addition, solvent evaporation caused the scaffolds to shrink and collapse before the resin could be incorporated.

Figure 39. PVA-borate gel scaffolds. b) Vascular specimen containing PVA solution (blue), borate solution (red) and carrier fluid (green). b) Gel deposition and growth on top of the vascular network. c) Image of a cured healing resin after incorporation of water from the hydrogel scaffold. Scale bar 0.5 cm.

To overcome the challenges with incompatible materials, a new regenerative chemistry was required that combines scaffold forming gelation with liquid healing agents. By replacing the organogel solvent with a monomeric solvent, both stages could be accomplished using a single system. Combining the two stages (gel scaffold and polymer healing agents) eliminates the need for infiltration with resin, avoids shrinking of the scaffold between stages, and simplifies the overall regeneration design.

2.2.4. Two-stage polymer chemistry

Traditional healing chemistries, such as epoxy, transform from a viscous liquid solution to a final structural polymer in a single step. In contrast, a two-stage (scaffold and healing) chemistry undergoes two transformations accomplished on different time scales (Figure 40). A rapid, catalyzed gelation event forms the scaffold and is followed by a gel-to-polymer transformation to fully regenerate the damaged material. The gel scaffold consists of a network of acylhydrazone bonds formed by acid-catalyzed condensation of Gelator A, *bis*-acylhydrazine-terminated poly(ethylene glycol), and B, tris[(4-formylphenoxy) methyl]ethane. Subsequent room temperature redox free-radical polymerization of the monomeric solvent affords the final regenerated material. This chemistry allows for the generation of materials with tunable properties and is highly adaptable with independent control over the kinetics of both stages without relying on external stimuli (i.e. heat and light). Low concentrations of chemical triggering agents determine the onset of each stage. For the gel stage, changes in acid catalyst concentration tune the gelation time, t_1, from a few seconds up to multiple days [16,35,74]. In our previous work, this control enabled the healing chemistry to adapt to multiple damage modes including microcracks, where infiltration of cracks was aided by slower gel times, and large through-hole voids, where faster gel times were advantageous [35]. Carefully tuning the polymerization kinetics prevented premature hardening of the healing agent which obstructs further scaffold deposition.

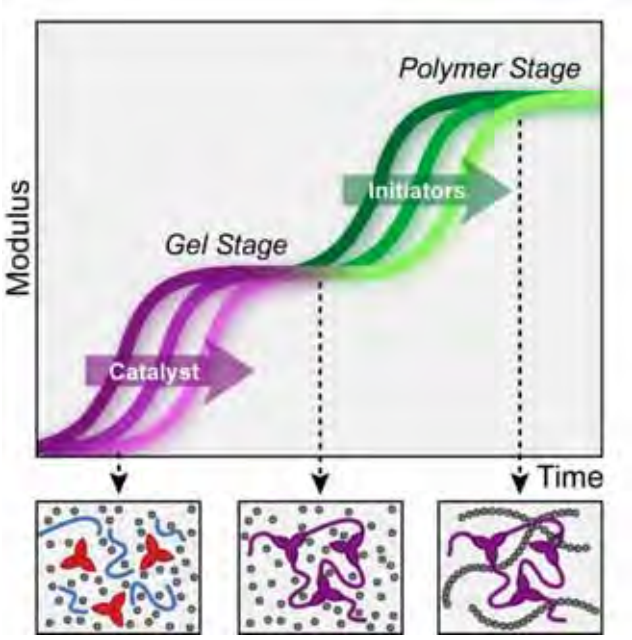

Figure 40. Two-stage rheological properties. Independent, temporally controlled material transitions from sol-to-gel and gel-to-polymer achieved by varying gelation catalyst and polymerization initiator concentrations.

Using this two-stage chemistry with 2-hydroxyethyl methacrylate (HEMA), damage area recovery was increased by 51% in non-scaffold forming healing agents [35]. However, solutions containing only the gelation chemistry (no polymer stage) are able to fill areas 82% larger. The addition of the polymerization components negatively affects the gel stage and limits the fillable area in two-stage formulations. Herein, a new polymer stage initiating chemistry was investigated to improve the independence of the two stages. Furthermore, we demonstrate the versatility of our two-stage polymer chemistry by exploring the gel-forming ability in a variety of monomeric solvents. Of these, five vinyl monomers were selected for an in-depth rheological study comparing temporal control (gel time, t_1, and subsequent polymerization onset, t_2) with the improved and previously reported autonomic initiating systems. Finally, the two-stage polymers were evaluated as potential regenerative healing agents based on their wetting properties, stability and mechanical performance.

The versatility of our two-stage chemistry is demonstrated by its wide range of material properties. The gelation chemistry (see Figure 42) is broadly compatible with a variety of organic solvents. In particular, the high solubility of the poly(ethylene glycol) backbone of Gelator A allows for the formation of free-standing gels in more than 35 vinyl liquids including (meth)acrylates, acrylamides, styrenes, and vinyl ethers. Figure 41 shows gels formed in 24 different monomers using dichloroacetic acid (DCA) as the gelation catalyst. Monomers suitable as regenerative healing agents must readily solvate the gelators and exhibit high boiling points, low viscosities, and curing kinetics favorable for bulk polymerizations at room temperature. Five monomers were explored as potential two-stage polymers—hydroxypropyl methacrylate (HPMA, #1); 2-hydroxyethyl acrylate (HEA, #3); 2-phenoxyethyl methacrylate (PEM, #5); *N*,*N*-dimethylacrylamide, (NN-DMA, #18); and methacrylic acid (MAA, #24) (numbers correspond to gels in Figure 41).

Figure 41. Gelation of monomeric solvents. Gels formed using 12 wt% gelators and 0.1 v/v% dichloroacetic acid catalyst. 1) hydroxypropyl methacrylate, HPMA; 2) hydroxypropyl acrylate; 3) 2-hydroxyethyl acrylate, HEA; 4) glycidyl methacrylate; 5) 2-phenoxyethyl methacrylate, PEM; 6) trimethylolpropane triacrylate; 7) methyl acrylate; 8) methyl methacrylate; 9) ethyl acrylate; 10) styrene; 11) 4-acetoxystyrene; 12) α-methyl styrene; 13) ethylene glycol dimethacrylate; 14) poly(ethylene glycol)-dimethacrylate, Mn ~550; 15) divinyl benzene; 16) 1,4-butanediol diacrylate; 17) *N*-(3-methoxypropyl)acrylamide; 18) *N*,*N*-dimethylacrylamide, NN-DMA; 19) ethylene glycol vinyl ether; 20) *N*-vinyl-2-pyrrolidone; 21) acrylonitrile; 22) 2-carboxyethyl acrylate; 23) acrylic acid; 24) methacrylic acid, MAA.

The ability of our system to regenerate various damage modes (i.e. millimeter-sized gaps and crack planes) originates from the unique temporal control of the sol-to-gel and gel-to-polymer transformations. However, achieving complete distinction between stages has been limited due to the instability of the peroxide initiator. The original initiating system (initiator system I) for the polymerization stage uses methyl ethyl ketone peroxide (MEKP), which is promoted to decompose at room temperature with a metal-salt promoter, cobalt naphthenate (Figure 41). However, MEKP is very sensitive to strong acids which induces decomposition through heterolysis of the oxygen-oxygen bond (−O-OH) [75–77]. Increasing the concentration of

gelation catalyst increases the polymerization time t_2; consequently, the two stages become interdependent. The acid sensitivity of MEKP also affects the gel time, t_1, since gelation occurs faster in a gel-only versus two-stage formulation [35].

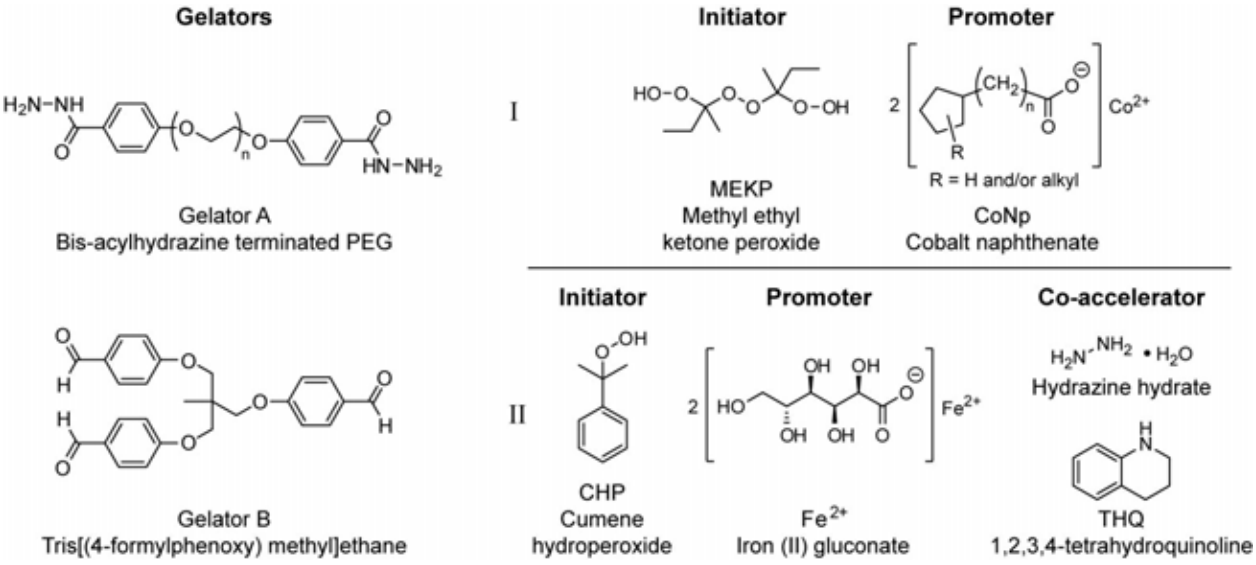

Figure 42. Gelation chemistry and free-radical redox initiator systems. Acid-catalyzed gelation through condensation of Gelator A (M_n = 2000) and Gelator B. Promoted room temperature polymerization using initiator system (I) methyl ethyl ketone peroxide and cobalt naphthenate or (II) cumene hydroperoxide, iron gluconate and either hydrazine or tetrahydroquinoline.

Development of an improved initiating system focused on a more stable initiator, cumene hydroperoxide (CHP). CHP has a higher thermal stability than MEKP and does not decompose under mildly acidic conditions [78]. Like MEKP, CHP rapidly decomposes in the presence of a metal-salt via one-electron redox reaction at room temperature:

$$ROOH + M^{n+} \rightarrow RO^{\bullet} + OH^{-} + M^{(n+1)+}$$

$$ROOH + M^{(n+1)+} \rightarrow ROO^{\bullet} + H^{+} + M^{n+}$$

CHP is commonly decomposed by the addition iron (II) or copper (I) cations, both with low energy barriers between oxidation states [79]. We utilized iron (II) gluconate as the promoter in initiator system II (Figure 42). Typical redox initiation of CHP employs various co-accelerators to reduce iron (III) to the more active iron (II) to achieve rapid decomposition, which is mainly attributed to the low oxidation state of the metal ions.[80] Simple screening tests were conducted on common co-accelerators in combination with initiator system II (1:10 and 1:100 mol Fe^{2+}:co-accelerator) in neat monomer (Table 9). The addition of any co-accelerator significantly increased the mechanical properties of the final, cured polymer. In contrast, control reactions with only Fe^{2+} (0.32 wt%) and CHP (1.5 wt%) either did not or only partially polymerized after curing for 16 hours. *N*,*N*-dimethyl-*p*-toluidine (DMPT) was an effective co-accelerator for most monomers but the basic amine slows the acid-catalyzed gel time in two-stage formulations. Sodium hydroxymethanesulfinate (rongalite) was the strongest reducing agent and aided the bulk polymerization of all monomers tested. However, polymerizations were extremely rapid and proceeded instantaneously in NN-DMA and hydroxypropyl acrylate. Neither 1,2,3,4-tetrahydroquinoline (THQ) or hydrazine influenced the gelation chemistry when used in catalytic concentrations and were employed as co-accelerators in initiator system II.

Table 9. Co-accelerator screening in select monomers.

Monomer[a]	Co-accelerator[b]					
	DMPT	THQ	Hydrazine	APH	Rongalite	─
NN-DMA	p	p	p	p	p	wp
HPMA	p	p	p	p	p	n
PEM	n	p	p	wp	p	n
HEMA	p	p	p	p	p	wp
HPA	p	p	p	p	p	n
NVP	n	n	n	n	wp	n
4-AS	n	n	n	n	wp	n

[a]Solutions contain 1.5 wt% CHP, 0.32 wt% Fe^{2+} and 1 v/v% catalyst, cured for 16 hours in a purging nitrogen atmosphere. HEMA = 2-hydroxyethyl methacrylate, HPA = hydroxypropyl acrylate, NVP = *N*-vinyl-2-pyrrolidone, 4-AS = 4-acetoxystyrene. [b]Comprehensive results from concentrations 1:10 and 1:100 Fe^{2+}:co-accelerator. p = hard polymer, wp = weakly/partially polymerized, n = no polymer formed.

Five vinyl monomers were selected as two-stage healing agents for in-depth rheological study of reaction kinetics ─ gel time, t_1, and polymerization onset, t_2. We further compared the temporal control afforded using both initiator systems: MAA and HEA were polymerized using initiator system I, and HPMA, PEM and NN-DMA were polymerized using initiator system II. (Figure 42) The results were compared to the regenerative system containing HEMA (2-hydroxyethyl methacrylate), which was established as a regenerative healing agent previously [35]. Concentrations of promoter and co-accelerator were optimized for optimal control of polymerization and stiffness of the final polymer.

Gel-stage kinetics were varied using DCA catalyst concentrations from 0.05−2 v/v% in gel-only and two-stage formulations (Figure 43a-f). The gel time (t_1), measured by tabletop rheology, steadily decreases in all monomers as more catalyst is added. However, the acid sensitivity of MEKP (initiator system I) is apparent. At low catalyst concentrations, gel times differ by 1−10 minutes between gel-only and two-stage systems in HEA and MAA, and have been shown to vary more than 20 minutes in our previous work using HEMA [35]. Conversely, initiator system II offers a significant improvement in t_1 distinction. For all catalyst concentrations tested in PEM, NN-DMA and HPMA, t_1 was unaffected by the introduction of the initiation chemistry (Figure 42c-e).

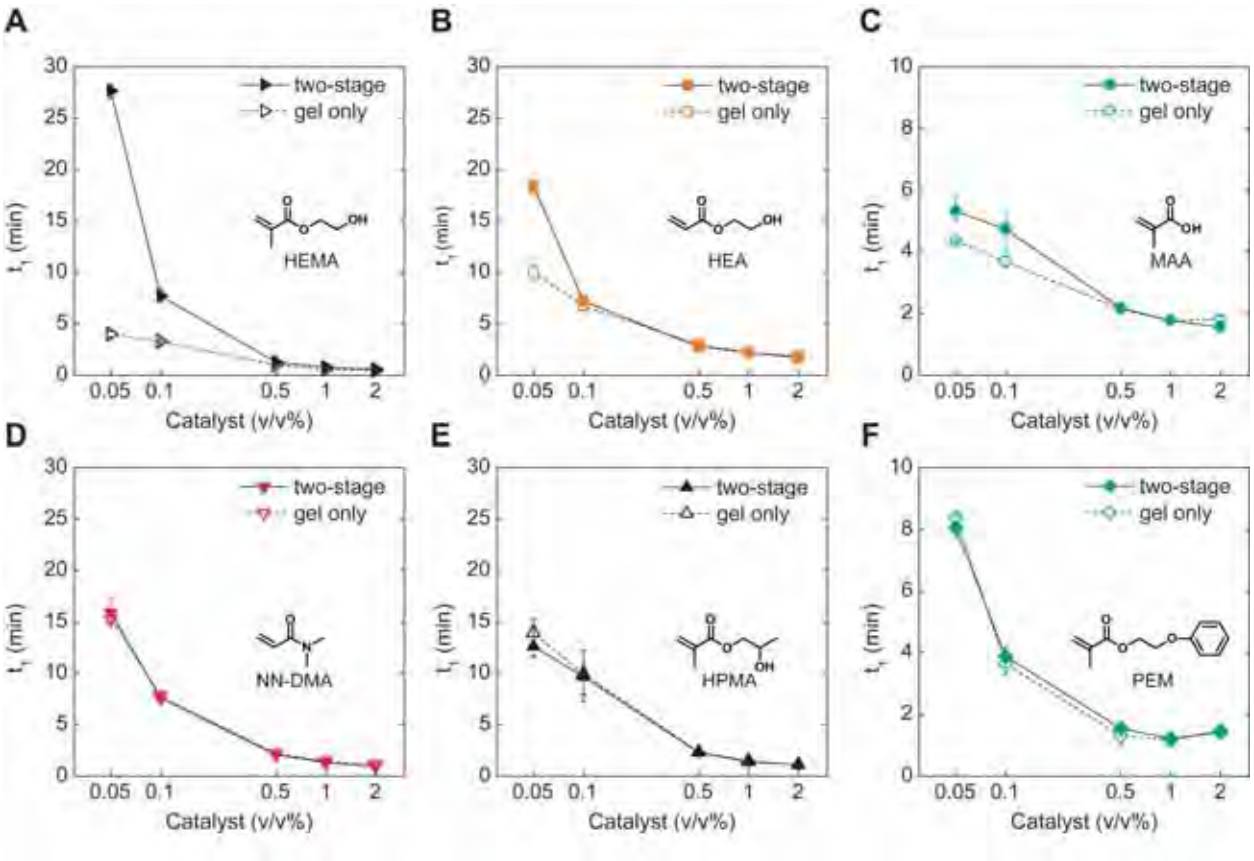

Figure 42. Control of gel stage kinetics via dichloroacetic acid (DCA) catalyst concentration. Gel times, t_1, per catalyst volume percent for formulations containing gel only (no initiators) and two-stage chemistries. Two-stage contains initiator system I for HEMA a), HEA b) and MAA c); initiator system II for NN-DMA d), HPMA e) and PEM f). 12 wt% gel solutions of acidic MAA will gel in 7 min without catalyst. The average is reported with error bars at high and low values. For some data points, error bars are smaller than the symbols. (Direct comparison of HEMA gel times to the new two-stage polymers is not applicable because HEMA used Gelator A with a M_n = 1000 g/mol).

The polymerization rates were measured using oscillatory rheology. Gelation of monomer sol solutions were achieved with 1.0 v/v% catalyst for t_1 values between 1−2.5 min with the gel stage reaching a plateau modulus of 10^4-10^5 Pa. Subsequent onset of polymerization (t_2) was defined as the sharp modulus increase from the gel stage and precisely controlled by varying concentration of initiating components. The gel plateau (t_1─t_2) varied from as little as 16 min to ~2 h for NN-DMA and HPMA, respectively. Controlled onset times are given in Figure 43 and, in general, coincide with the bulk propagation rates of the neat monomer (with the exception of PEM, k_p = 900 L/mol·s at 60 °C) [81]. HEMA, HEA and NN-DMA exhibit the highest k_p values of 1.3 x10^4, 1.0x10^4 and 1.6x10^4 L/mol·s at 25°C, respectively, and the fastest t_2 times [82,83]. Likewise, MAA and HPMA display slow t_2 times and low k_p values of 600 and 790 L/mol·s at 25 °C, respectively [84]. Both initiator systems enable direct control of t_2 through variation of either promoter or co-accelerator concentrations. Precise control of the polymer stage allows for readily adaptable chemistries without external energy input (i.e. light or heat), synthesis of monomers or strict stoichiometric control of monomer components.

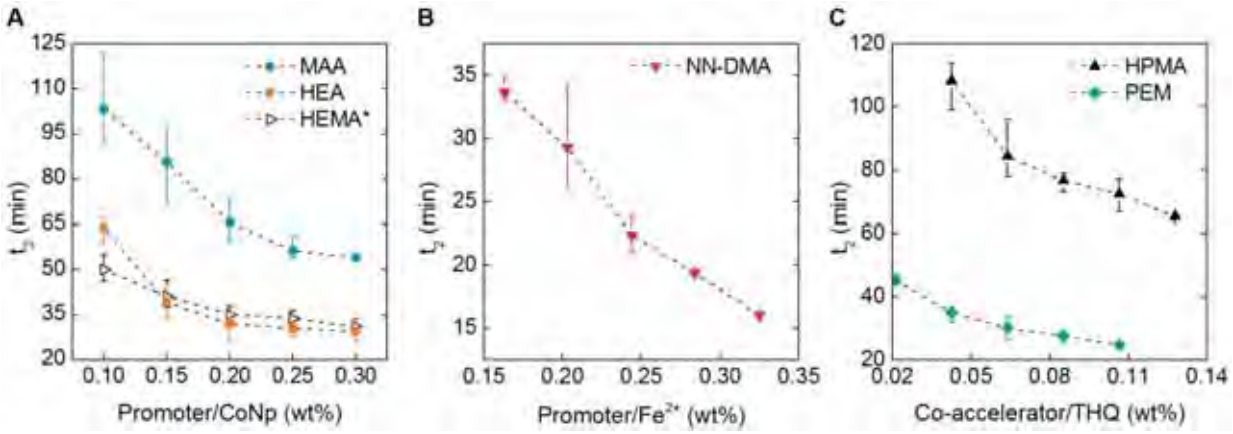

Figure 43. Control of polymer-stage kinetics. Polymerization onset, t_2, varied by promoter or co-accelerator weight percent; all formulations contain 12 wt% gelators, 1 v/v% gel catalyst and 1.5 wt% initiator. Two-stage initiator system I for a) HEMA, HEA and MAA; initiator system II for b) NN-DMA (0.035 v/v% hydrazine), c) PEM (0.08 wt% Fe^{2+}) and HPMA (0.32 wt% Fe^{2+}). *HEMA data from previous work for reference. The average is reported with error bars as high and low values. For some data points, error bars are smaller than the symbols.

Although orthogonal gel and polymer stages are desired, changing acid concentration does influence the time of polymerization onset, t_2, showing interdependence of the two stages. Figure 44 outlines this effect in the two-stage polymerization of MAA (initiator system I) and HPMA (initiator system II) with 0.1 and 1.0 v/v% DCA catalyst. As designed, lowering concentrations of acid increases t_1; however, t_2 also varies. In all monomers polymerized using MEKP-containing initiator system I, high acid concentrations slow t_2. For example, in Figure 44a, the Δt_2 of MAA is 74 min, ~14 times slower with 1.0 v/v% of catalyst loading. In Figure 44b, the CHP-containing initiator system II with 1.0 v/v% catalyst polymerizes ~2 times *faster* than 0.1 v/v% in HPMA. Thus, addition of high concentrations of DCA was anticipated to behave similarly to adding less initiator [75,76,78,85–88]. Instead, the catalyst contributes to the polymerization of monomer in initiator system II by increasing the polymerization rates.

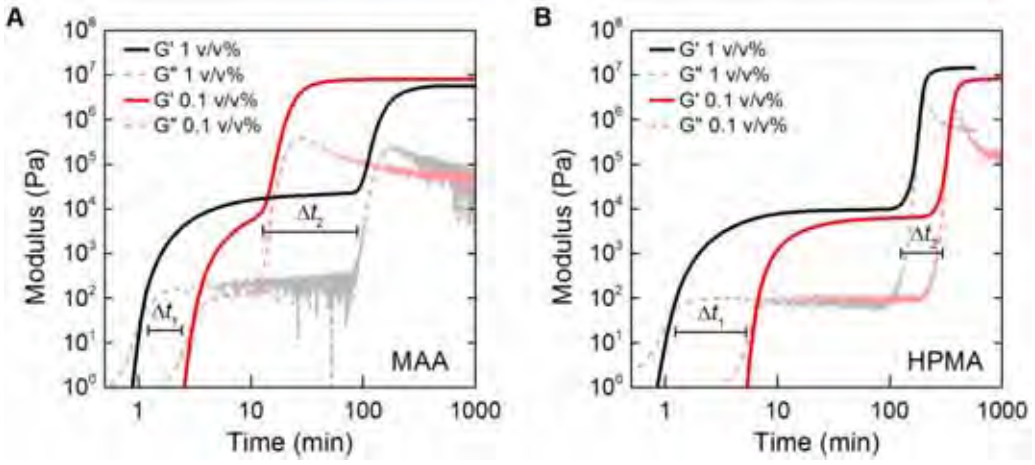

Figure 44. Interdependence of gelation and polymerization kinetics. Gel time shift, Δt_1, and polymerization onset shift, Δt_2, after changing catalyst concentration from 1 v/v% to 0.1 v/v%. a) Effect in MAA using initiator system I. b) Effect in HPMA using initiator system II. MAA contains 1.5 wt% MEKP and 0.15 wt% CoNp. HPMA contains 1.5 wt% CHP, 0.32% Fe2+, and 0.043 THQ%.

Factors contributing to the observed reactivity differences between initiator systems I and II include the decomposition of the hydroperoxide initiator and pH-dependent oxidation state of the metal promoter. Acids lower the activation energy of oxygen-oxygen bond homolysis through protonation of the hydroxyl oxygen of the hydroperoxide. Thus, onset temperatures (T_0) for thermal decomposition decrease upon addition of acid. Table 10 illustrates this effect for MEKP and CHP with 0.1 and 1 v/v% DCA catalyst additives. The thermal stability of both initiators decreases by 17 and 54 degrees with the addition of 1 v/v% DCA for MEKP and CHP, respectively. It is also well known that redox-initiated systems are pH-dependent, which influences the oxidation state of the metal promoter. Iron gluconate (initiator system II) activity may be enhanced in acidic conditions (Fe^{2+} favored over Fe^{3+}) [89,90] while cobalt naphthenate activity (initiator system I) decreases in acidic solutions. Nevertheless, orthogonality of the two-stage system was improved in the gel stage with the introduction of initiator system II. While the polymer stage is affected by the acid catalyst, the polymerization is promoted, not inhibited, in the improved initiator system II.

Table 10. Thermal decomposition of peroxide initiators with 0.1 and 1 v/v% DCA catalyst. Heating rate 5 °C/min from 25-275 °C.

Sample	T_0 (°C)[b]	
	MEKP	CHP
Neat initiator[a]	128	208
Initiator + 0.1 v/v% DCA	118	177
Initiator + 1.0 v/v% DCA	111	154

[a]10 wt% initiator in dimethylphthalate
[b]Temperatures ± 2 °C

Five new two-stage chemistries were developed and demonstrate time-controlled and triggerable rheological transitions. Further development into a regenerative chemistry requires compatibility with microvascular delivery and effective damage recovery. We have previously described our regeneration concept using two-stage polymer chemistries [35]. Regenerative healing agents are

delivered through vascular channels embedded in an epoxy substrate. A computer-controlled, pressurized system delivers the fluids as low viscosity sol solutions to the damage region. Rapid gelation forms a scaffold that supports the deposition of additional healing agent at volumes an order of magnitude greater than nonreactive fluids [35]. Restoration of mechanical function is accomplished by final transformation to polymer (Figure 45). The regenerative potential of new two-stage polymers must also consider the monomer wetting performance, solution stability and final mechanical properties.

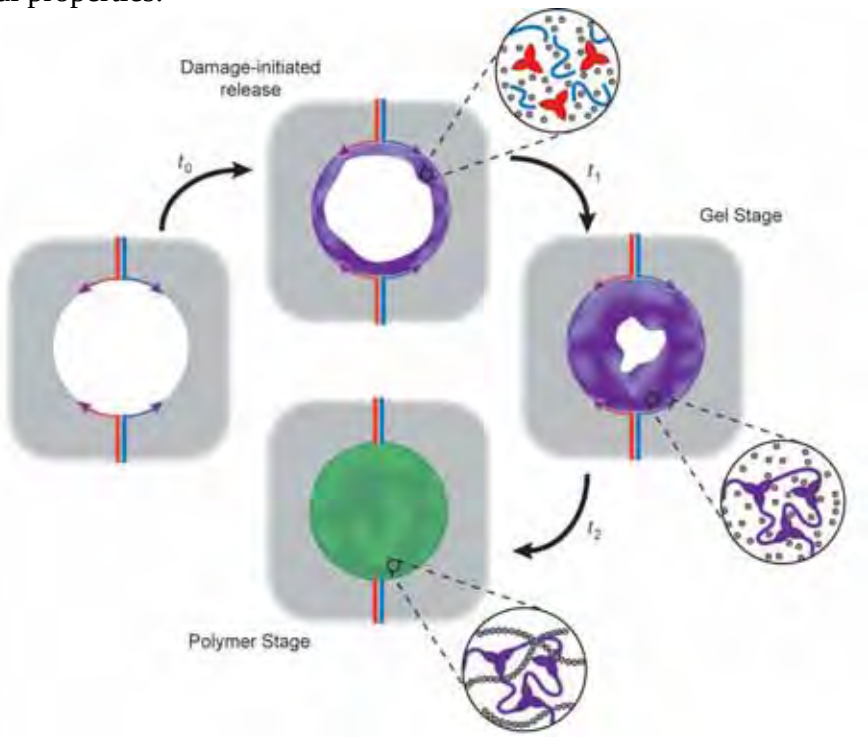

Figure 45. Regeneration concept of the two-stage polymer chemistry. Impact damage creates a through-hole void, initiating release of the healing agents (gelators, red and blue symbols; monomer, gray circles) from embedded vascular channels, time t_0. Time t_1, the gel stage forms a covalent gel scaffold supporting additional deposition of fluids. Subsequent polymer stage at time t_2, recovers mechanical function by polymerization of the healing agent.

In microvascular systems, the surface energy of the healing agents influences wetting of the damage region [5]. For small damage volumes (e.g. crack planes), capillary forces alone are effective to retain healing agents. As the damage region increases to millimeter-sized voids, the healing agents will preferentially wet the material surface rather than remaining in the damage volume. To overcome this challenge, we have previously applied superoleophobic /superhydrophobic coatings to the surface [35]. Using the same non-wetting coating Ultra-Ever Dry®, we measured the monomer contact angles (CA) on both bare and coated epoxy substrates (Figure 45 and Table 11). All monomers readily wet the bare epoxy surface with contact angles <23°. However, the non-wetting performance of the coated surface varied significantly per monomer. HEA (CA 163.8 ± 3.3°) and PEM (CA 145.6 ± 7.5°) were non-wetting on coated surfaces. NN-DMA was exhibited some non-wetting behavior with CA 66.5 ± 21.8°. Conversely, the coating did not effectively prevent wetting of both HPMA and MAA where the latter fully wets the surface.

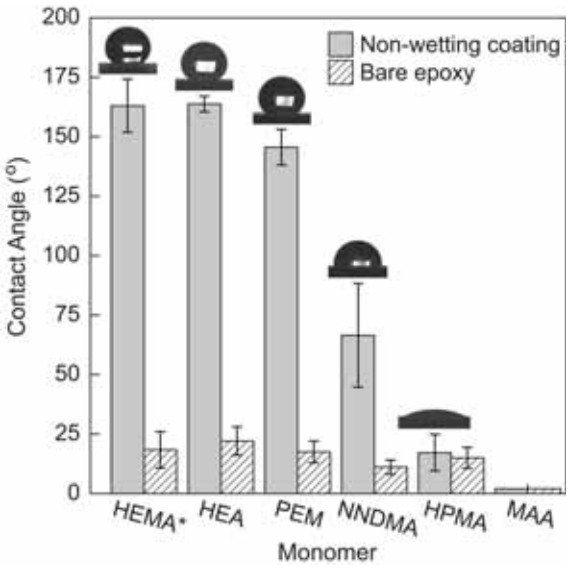

Figure 45. Monomer wetting performance. Static contact angle of monomers on Ultra-Ever Dry® non-wetting coating and bare epoxy. Inset: optical images of monomer droplets on coated surfaces. MAA fully wets both coated and uncoated epoxy samples such that the contact angle could not be measured. *HEMA data is added for reference from Section 2.1.4..

Ease of delivery through microvascular networks and into damage regions requires stable, low viscosity healing agents [5,91]. Many healing systems are delivered as two-part solutions, generally a viscous epoxy resin (~11,000−13,000 mPa·s) which must be modified with a diluent and a lower viscosity curing agent for final solution viscosities of 50−1,400 mPa·s [5]. High viscosity solutions often limit migration into cracked planes and/or poorly heal because of difficulty in mixing, subsequently leading to stoichiometric mismatch [1,5,37]. Viscosity also plays a role in network design and ease of delivery, requiring larger channels or higher pressures for delivery [1]. In contrast, viscosities of the two-stage solutions range from as little as 8 to 37 mPa·s (Table 11). Stability of the healing solutions is achieved by segregating the reaction-triggering compounds; as long as the gel catalyst is separated from Gelators A & B and the initiator is separated from the promoter, the solutions are non-reactive until mixed. Working stability was tested by measuring the Part A and Part B solution viscosities over 8 hours with a shear rate of 1 s^{-1} (Figure 46). Monomers with both high polarity and the lowest viscosity, NN-DMA and MAA, were the most stable and act as the best gelator solvents. Part A solutions maintained a constant viscosity in all monomers, except in HPMA where at this concentration Gelator A self-assembled after 30 min. The gelators are split to yield equal solids by weight in the two-part solutions; thus both gelators are in Part B. Lack of catalyst and off-stoichiometry prevent the gelators from crosslinking (in acidic MAA, off stoichiometry alone hinders gelation). However, viscosity of Part B solutions increases to ~10 mPa·s in poorer solvents (HEA, PEM and HPMA), likely caused by bond formation. The viscosity levels after 8 h, however, and remain well below the viscosity range of healing agents used in previous microvascular systems.

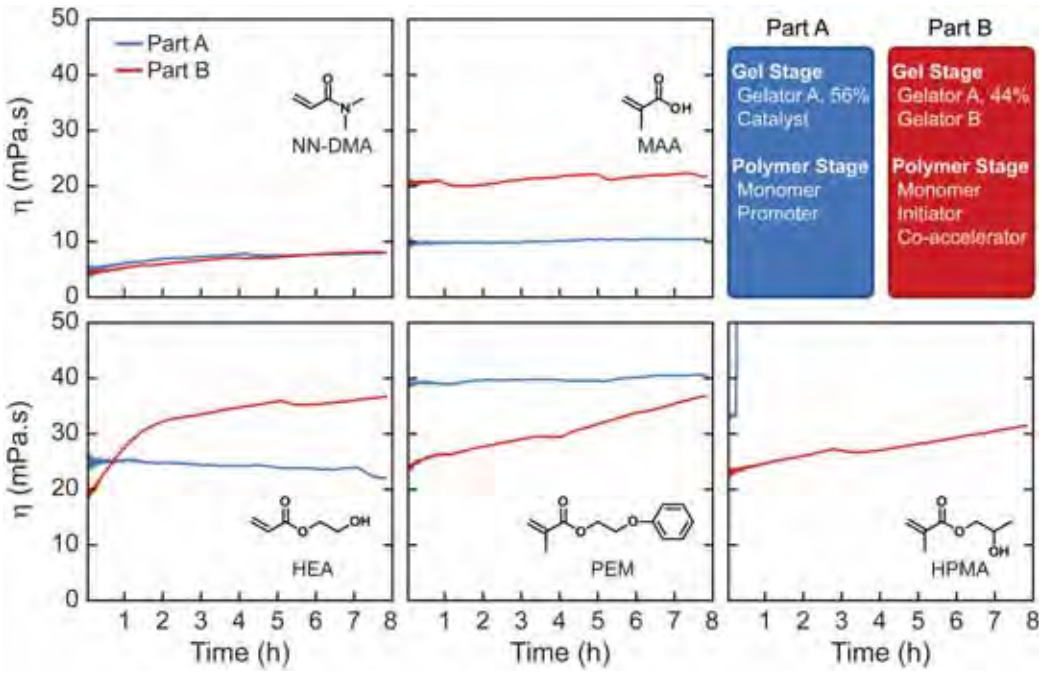

Figure 46. Stability of two-stage healing agents as Part A-Part B solutions. Composition of each solution given in upper right, only initiator system II contains co-accelerator (NN-DMA, PEM, HPMA). Viscosity measured at a shear rate of 1 s^{-1}.

Material regeneration requires the combination of gel and polymer stages. Without transformation to the polymer stage, the gel chemistry fills large damage volumes but does not recover the mechanical properties of the substrate [35]. Final moduli of the two-stage polymers were investigated using dynamic mechanical analysis. Two-part solutions of each monomer system were mixed by mechanical stirring and quickly poured into a mold. Samples were cured in a purging nitrogen environment for 24 h (PEM, HPMA, MAA) or 48 h (HEA, NN-DMA). The tensile storage modulus (E') was recorded as a function of frequency from 0.1−100 Hz on samples cut into thin bars (20 x 5 x 0.5 mm). Moduli at 1 and 10 Hz are given in Table 4.3. Both PEM and HPMA have storage moduli above 1 GPa, similar to commercial PMMA [33] and many structural adhesives [92]. The stiffness of NN-DMA and MAA are an order of magnitude lower followed by HEA which reached a storage modulus of 3.31 ± 0.33 MPa at 10 Hz. Although the mechanical performance of some monomers was poor due to incomplete curing, the modulus of each two-stage system increased by at least two orders of magnitude from the gel stage.

Table 11. Wetting, stability, and mechanical performance of two-stage systems. *HEMA data is added for comparison. Viscosity and storage modulus data for HEMA contained Gelator A (M_n 1000 Da) and 2 v/v% DCA catalyst.

Two-stage system	Monomer Contact Angle (°)		Solution Viscosity at 8 h (mPa·s)[a]		Two-stage Polymers E' (GPa)	
	Coated	Bare Surface	Part A	Part B	1 Hz	10 Hz
HEMA*	163.0 ± 11.2	18.4 ± 7.6	22	54	0.91 ± 0.12	1.16 ± 0.11
PEM	145.6 ± 7.5	17.5 ± 4.5	40	37	1.09 ± 0.10	1.34 ± 0.12
HPMA	17.2 ± 7.7	15.0 ± 4.4	gel	31	1.06 ± 0.12	1.32 ± 0.14
NN-DMA	66.5 ± 21.8	11.1 ± 3.0	8	8	0.24 ± 0.10	0.32 ± 0.10
MAA	—	—	10	22	0.13 ± 0.04	0.17 ± 0.04
HEA	163.8 ± 3.3	22.1 ± 6.0	22	36	2.77 ± 0.27 MPa	3.31 ± 0.33 MPa

[a]Viscosity data ± 2 mPa·s

In summary, five two-stage chemistries were developed, each employing a combination of versatile gelation chemistry and polymerization of monomeric solvents. Both stages were designed with specific reaction triggers (i.e. acid-catalyzed gelation and promoted radical initiation) to provide temporal control of the rheological transitions. Orthogonality of the stages was improved by introducing a stable initiator system based on cumene hydroperoxide. Each two-stage chemistry exhibits tunable rheological transitions displaying induced gelation within 18 min, followed by subsequent gel-to-polymer hardening via polymerization over 2 hours. Some of the monomer systems discussed may serve as regenerative healing agents, as they exhibit favorable wetting performance, remain stable liquid states over 8 h, and afford final polymers with high moduli.

2.3. Advanced Vascular Delivery

Despite recent advancements in self-healing vascular materials, the delivery methods applied are relatively simple compared to natural analogs. The following sections highlight the development of advanced systems for improving the vascular delivery of reactive chemistries for healing and damage restoration.

2.3.1. Fluid-mediated delivery

Rapidly reacting chemistries such as PVA-Borate (see previous Figure 37) present a challenge for microvascular delivery. Upon contact, the PVA and Borate solutions instantly gel, which impedes further mixing of the two solutions and may result in channel clogs. One method to mitigate this challenge is through the use of microfluidic emulsions. A carrier fluid of mineral oil was implemented as a continuous phase in a microvascular network while dilute PVA and borate solutions were injected in order to create an emulsion (Figure 47). The emulsive droplets are prevented from merging while in the microchannel due to the immiscible carrier fluid. Once the fluids have reached an open surface, the reactive droplets can recombine and react. In addition to promoting mixing of the two components, this technique prevents the channels from clogging. Carrier fluids can furthermore purge the channels and allow delivery of additional components. Acid was delivered to the PVA-borate mass post-gelation, which converted the system to a sol and allowed for removal of the sol via the microvascular network.

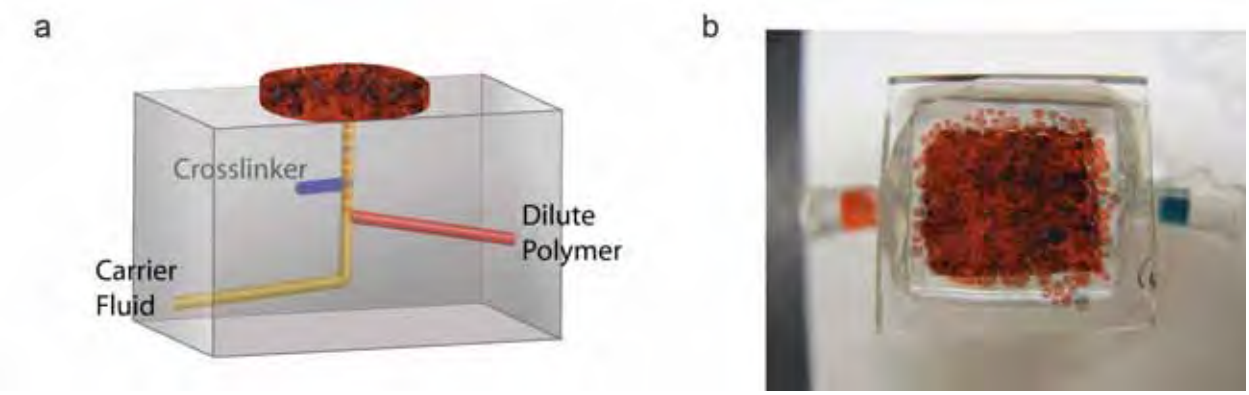

Figure 47. Fluid-mediated delivery. a) Schematic of delivery system showing an immiscible carrier fluid separating disparate reactive components. b) Image of microvascular device showing delivery and gelation of PVA and borate solutions.

Some epoxy resins (EPON 828) and amine hardeners (diethylenetriamene, m-xylylenediamine) are both immiscible with alkanes (hexane, penate) and compatible with this delivery technique. Volatile alkanes evaporate upon exit of the microvascular network, leaving the epoxy and amines to react.

2.3.2. Air assisted reagent delivery

Air can be used to separate reactive components to achieve a single-channel healing agent delivery of reactive species (Figure 48). Air pressure transports fluids down the length of the microchannel and keep reactive species out of contact until they have exited the channel. Performance is improved by creating a super-phobic surface on the interior of the channels to reduce contact area of the fluid with the channel walls. Ultra Ever-Dry (Ultratech International, Jacksonville FL) provides a super-phobic surface of fluids with surface energy ~37 dyne*cm^{-1} and above and is easily applied to the interior surfaces of microchannels.

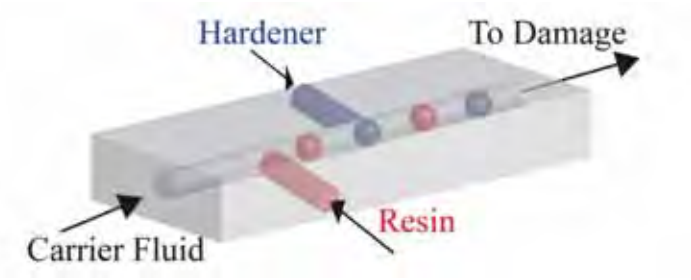

Figure 48. Schematic depicting air-assisted reagent delivery.

2.3.3. Accumulators for healing agent sequestration

While significant work has been devoted to the development of vascularized self-healing materials, most do not offer autonomous control of the volume released after a damage event. Instead, repair requires a scheme to manually regulate the flow with a prescribed pumping schedule. In the abrasive damage of coatings introduced in section 2.1.1, the damage is isolated from the vascular network, enabling easier testing of repeat healing cycles. However, like many other vascular self-healing schemes, control of volume release is manual. In the case of coatings, without intervention the resulting coating thickness is poorly controlled, limiting its autonomy. In this work, an accumulator is developed to release a controlled volume of material in response

to damage. The accumulator is integrated into the coating/pressure sensitive valve concept presented in section 2.1.1. The ability to autonomically release a controlled volume of material is investigated.

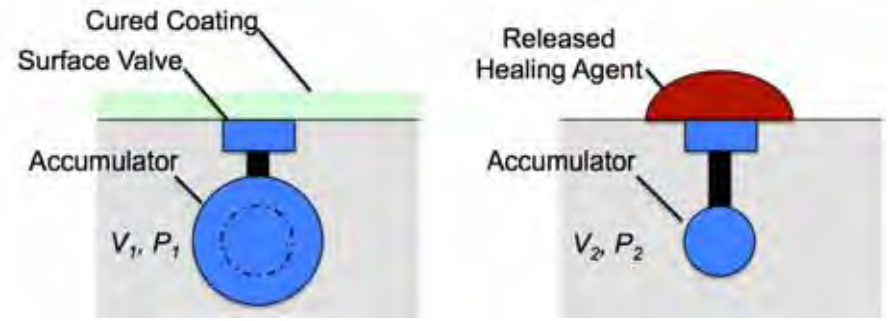

Figure 49. Schematic segregated system containing a valve and pressurized accumulator.

In section 2.1.1, the valve was responsible for both protection of the underlying vasculature, as well as control of volume deposition. Here a system is proposed in which the functions of protection and volume control are decoupled (Figure 49). The protection of the vascular channels and the healing agent contained within them is accomplished by a surface valve similar to that described in section 2.1.1. The function of volume control is regulated by an accumulator. The geometry and material properties of the accumulator and the system pressure regulate the volume deposited. Upon static pressurization, deformation of the accumulator results in a defined stored volume. When the abrasive damage results in opening of the integrated surface valve, the volume of healed material is released and pressure within the accumulator decays. Relative to Figure 49, the volume deposition is:

$$V_{deposited} = V_1 - V_2 \qquad (7)$$

Integrated valve + accumulator prototype

A specimen consisting of a deflecting membrane accumulator and a valve embedded in epoxy was fabricated (Figure 50). The specimen is similar to the previous single valve type shown in Figure 2d in section 2.1.1. Two valve geometries, and two accumulator geometries were subsequently fabricated and tested.

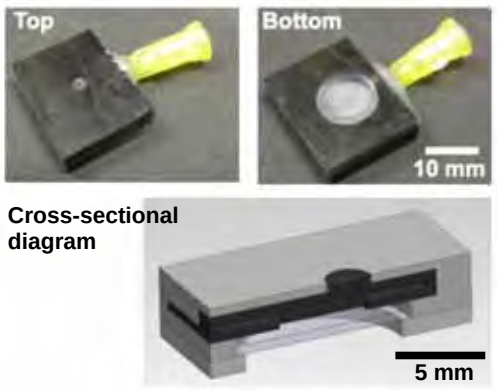

Figure 50. Integrated valve + accumulator prototype

System design: valve and accumulator geometry

The previous valve design has a conical interior, as shown in Figure 51b. This shape results in a slowly decaying release profile. The revised flat top valve (Figure 51c) is a more compliant design and produces a more a more rapid release of healing agent. Such a rapid action will result in the entire volume of healing material being released prior to the curing reaction, which may improve the control of volume released. The effect on system pressure decay (indicating release profile) when the valve geometry is changed is measured (Figure 51a).

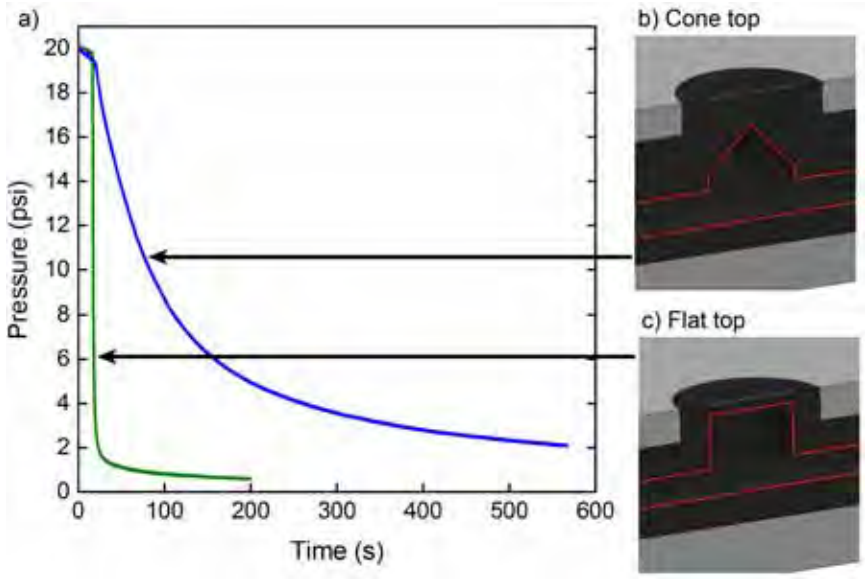

Figure 51. Cross-sectional diagrams of valve interior and a) associated release profile. b) Cone top valve as used in study described in section 2.1.1. c) Proposed flat top valve.

The geometric design parameters for the accumulator influence the total volume released. The deposition volume (ΔV) of a circular deflecting membrane accumulator can be estimated by assuming the deflected membrane takes the form of a spherical cap with volume given by:

$$\Delta V = \frac{\pi}{6} w_0 \left(3r^2 + {w_0}^2\right) \tag{8}$$

where r is the radius of the membrane and w_0 is the deflection of the center point of the membrane given by [93]:

$$w_0 = 0.662 r \sqrt[3]{\frac{rP}{Eh}} \tag{9}$$

where P is the pressure, E is the Young's modulus of the membrane material and h is the membrane thickness. Two different accumulator geometries (specifically changing accumulator diameter) were fabricated and tested for volume release and compared to the analytical model Figure 52. Currently the analytical model and experimental data do not show good agreement. The source of this discrepancy lies in the assumptions of the model, stemming from the fact that the model is limited to much smaller strains. A hyperplasic model would likely more accurately represent the data.

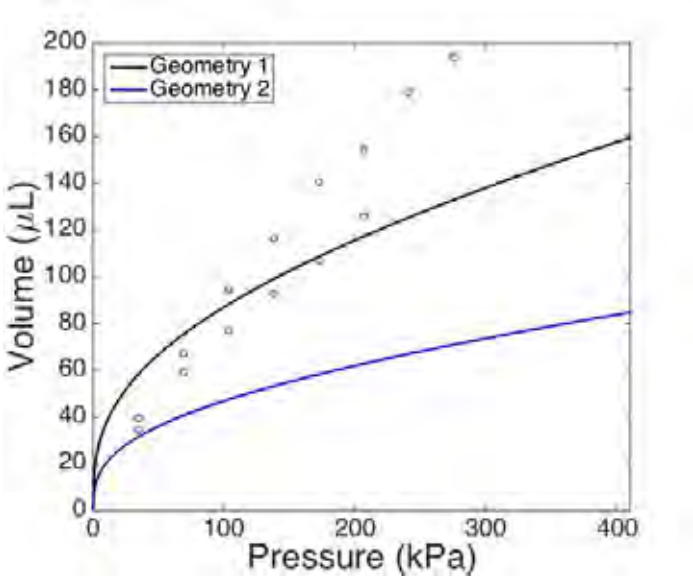

Figure 52. Volume release for given pressure and 2 different accumulator geometries: Geometry 1: 9 mm diameter, Geometry 2: 7 mm diameter. Open circles are experimentally measured data; solid lines are analytical model.

3. References

[1] B.J. Blaiszik, S.L.B. Kramer, S.C. Olugebefola, J.S. Moore, N.R. Sottos, S.R. White, Self-Healing Polymers and Composites, Annu. Rev. Mater. Res. 40 (2010) 179–211. doi:10.1146/annurev-matsci-070909-104532.

[2] J. V. Crivello, R. Narayan, S. Sternstein, Fabrication and mechanical characterization of glass fiber reinforced UV-cured composites from epoxidized vegetable oils, J. Appl. Polym. Sci. 64 (1997) 2073–2087. doi:10.1002/(SICI)1097-4628(19970613)64:11<2073::AID-APP3>3.0.CO;2-G.

[3] S. Kurata, N. Yamazaki, Mechanical Properties of Poly(alkyl a-fluoroacrylate)s as Denture-base Materials, J. Dent. Res. 68 (1989) 481–483. doi:10.1177/00220345890680030901.

[4] J.B. Donnet, ed., Carbon Black: Science and Technology, Second Edition, 2nd ed., Taylor & Francis, 1993.

[5] K.S. Toohey, C.J. Hansen, J.A. Lewis, S.R. White, N.R. Sottos, Delivery of Two-Part Self-Healing Chemistry via Microvascular Networks, Adv. Funct. Mater. 19 (2009) 1399–1405. doi:10.1002/adfm.200801824.

[6] B.A. Beiermann, M.W. Keller, N.R. Sottos, Self-healing flexible laminates for resealing of puncture damage, Smart Mater. Struct. 18 (2009) 085001. doi:10.1088/0964-1726/18/8/085001.

[7] K.D. Birnbaum, A. Sánchez Alvarado, Slicing across kingdoms: regeneration in plants and animals., Cell. 132 (2008) 697–710. doi:10.1016/j.cell.2008.01.040.

[8] M.D.C. Carnevali, F. Bonasoro, E. Lucca, M.C. Thorndyke, Pattern of Cell-Proliferation in the Early Stages of Arm Regeneration in the Feather Star Antedon Mediterranea, J. Exp. Zool. 272 (1995) 464–474.

[9] R.J. Lauzon, K.J. Ishizuka, I.L. Weissman, Cyclical generation and degeneration of organs in a colonial urochordate involves crosstalk between old and new: a model for development and regeneration., Dev. Biol. 249 (2002) 333–348. doi:10.1006/dbio.2002.0772.

[10] E.B. Murphy, F. Wudl, The world of smart healable materials, Prog. Polym. Sci. 35 (2010) 223–251. doi:10.1016/j.progpolymsci.2009.10.006.

[11] R.P. Wool, Self-healing materials: A review, Soft Matter. 4 (2008) 400. doi:10.1039/b711716g.

[12] X. Chen, M.A. Dam, K. Ono, A. Mal, H. Shen, S.R. Nutt, et al., A thermally re-mendable cross-linked polymeric material., Science. 295 (2002) 1698–1702. doi:10.1126/science.1065879.

[13] P. Cordier, F. Tournilhac, C. Soulié-Ziakovic, L. Leibler, Self-healing and thermoreversible rubber from supramolecular assembly., Nature. 451 (2008) 977–980. doi:10.1038/nature06669.

[14] A.C. Balazs, T. Emrick, T.P. Russell, Nanoparticle polymer composites: where two small worlds meet., Science. 314 (2006) 1107–1110. doi:10.1126/science.1130557.

[15] S.R. White, N.R. Sottos, P.H. Geubelle, J.S. Moore, M.R. Kessler, S.R. Sriram, et al., Autonomic healing of polymer composites., Nature. 409 (2001) 794–7. doi:10.1038/35057232.

[16] G. Deng, C. Tang, F. Li, H. Jiang, Y. Chen, Covalent Cross-Linked Polymer Gels with Reversible Sol−Gel Transition and Self-Healing Properties, Macromolecules. 43 (2010) 1191–1194. doi:10.1021/ma9022197.

[17] E. Nacu, E.M. Tanaka, Limb Regeneration: A New Development?, Annu. Rev. Cell Dev. Biol. 27 (2011) 409–440. doi:10.1146/annurev-cellbio-092910-154115.

[18] K. Echeverri, E.M. Tanaka, Mechanisms of muscle dedifferentiation during regeneration, Semin. Cell Dev. Biol. 13 (2002) 353–360. doi:10.1016/S1084952102000915.

[19] J.I. Morrison, S. Lööf, P. He, A. Simon, Salamander limb regeneration involves the activation of a multipotent skeletal muscle satellite cell population., J. Cell Biol. 172 (2006) 433–440. doi:10.1083/jcb.200509011.

[20] J.P. Brockes, A. Kumar, Plasticity and reprogramming of differentiated cells in amphibian regeneration, Nat. Rev. Mol. Cell Biol. 3 (2002) 566–574.

[21] C. Jopling, S. Boue, J.C. Izpisua Belmonte, Dedifferentiation, transdifferentiation and reprogramming: three routes to regeneration., Nat. Rev. Mol. Cell Biol. 12 (2011) 79–89. doi:10.1038/nrm3043.

[22] S.J. Odelberg, Cellular plasticity in vertebrate regeneration, Anat. Rec. B New Anat. 287 (2005) 25–35. doi:10.1002/ar.b.20080.

[23] J.M.W. Slack, Amphibian muscle regeneration--dedifferentiation or satellite cells?, Trends Cell Biol. 16 (2006) 273–275. doi:10.1016/j.tcb.2006.04.007.

[24] A. Kumar, C.P. Velloso, Y. Imokawa, J.P. Brockes, The regenerative plasticity of isolated urodele myofibers and its dependence on Msx1, PLoS Biol. 2 (2004). doi:10.1371/journal.pbio.0020218.

[25] C.S. Sheppard, V.R. Kamath, The Selection and Use of Free Radical Initiators, Polym. Eng. Sci. 19 (1979) 597–606.

[26] C.E. Hoyle, T.Y. Lee, T. Roper, Thiol-enes: Chemistry of the past with promise for the future, J. Polym. Sci., Part A Polym. Chem. 42 (2004) 5301–5338. doi:10.1002/pola.20366.

[27] Y.B. Kim, H.K. Kim, H.C. Choi, J.W. Hong, Photocuring of a thiol-ene system based on an unsaturated polyester, J. Appl. Polym. Sci. 95 (2005) 342–350. doi:10.1002/app.21248.
[28] P. Esfandiari, S.C. Ligon, J.J. Lagref, R. Frantz, Z. Cherkaoui, R. Liska, Efficient stabilization of thiol-ene formulations in radical photopolymerization, J. Polym. Sci. Part A Polym. Chem. 51 (2013) 4261–4266. doi:10.1002/pola.26848.
[29] T. Tate, On the magnitude of a drop of liquid formed under different circumstances, Phil. Mag. S. 27 (1864) 176–180.
[30] W.D. Harkins, F.E. Brown, THE DETERMINATION OF SURFACE TENSION (FREE SURFACE ENERGY), AND THE WEIGHT OF FALLING DROPS: THE SURFACE TENSION OF WATER AND BENZENE BY THE CAPILLARY HEIGHT METHOD., J. Am. Chem. Soc. 41 (1919) 499–524. doi:10.1021/ja01461a003.
[31] J.L. Lando, H.T. Oakley, Tabulated correction factors for the drop-weight-volume determination of surface and interracial tensions, J. Colloid Interface Sci. 25 (1967) 526–530. doi:http://dx.doi.org/10.1016/0021-9797(67)90064-1.
[32] R.J. Wojtecki, M.A. Meador, S.J. Rowan, Using the Dynamic Bond to Access Macroscopically Responsive Structurally Dynamic Polymers., Nat. Mater. 10 (2011) 14–27. doi:10.1038/nmat2891.
[33] J.E. Mark, ed., Polymer Data Handbook, Oxford University Press, New York, 1999.
[34] J.F. Patrick, K.R. Hart, B.P. Krull, C.E. Diesendruck, J.S. Moore, S.R. White, et al., Continuous Self-Healing Life Cycle in Vascularized Structural Composites, Adv. Mater. 26 (2014) 4302–4308. doi:10.1002/adma.201400248.
[35] S.R. White, J.S. Moore, N.R. Sottos, B.P. Krull, W.A. Santa Cruz, R.C.R. Gergely, Restoration of large damage volumes in polymers., Science. 344 (2014) 620–3. doi:10.1126/science.1251135.
[36] I. Kasa, A circle fitting procedure and its error analysis, Instrum. Meas. IEEE Trans. …. (1976) 8–14.
[37] A.R. Hamilton, N.R. Sottos, S.R. White, Self-healing of internal damage in synthetic vascular materials., Adv. Mater. 22 (2010) 5159–63. doi:10.1002/adma.201002561.
[38] C.J. Hansen, S.R. White, N.R. Sottos, J. a. Lewis, Accelerated Self-Healing Via Ternary Interpenetrating Microvascular Networks, Adv. Funct. Mater. 21 (2011) 4320–4326. doi:10.1002/adfm.201101553.
[39] A.R. Hamilton, N.R. Sottos, S.R. White, Pressurized vascular systems for self-healing materials., J. R. Soc. Interface. 9 (2012) 1020–8. doi:10.1098/rsif.2011.0508.
[40] A. Van Blaaderen, J. Van Geest, A. Vrij, Monodisperse colloidal slica spheres from tetraalkoxysilanes: particle formaion and growth mechanism, J. Colloid Interface …. 154 (1992).
[41] N.A.M. Verhaegh, A. Van Blaaderen, Dispersions of Rhodamine-Labeled Silica Spheres : Synthesis , Characterization , and Fluorescence Confocal Scanning Laser Microscopy, 96 (1994) 1427–1438.
[42] P.M.C. Lacey, Developments in the theory of particle mixing, J. Appl. Chem. 4 (2007) 257–268. doi:10.1002/jctb.5010040504.
[43] J. Oliver, C. Huh, S. Mason, Resistance to spreading of liquids by sharp edges, J. Colloid Interface Sci. 59 (1977) 568–581.
[44] Z. Xue, M. Liu, L. Jiang, Recent developments in polymeric superoleophobic surfaces, J. Polym. Sci. Part B Polym. Phys. 50 (2012) 1209–1224. doi:10.1002/polb.23115.
[45] B.P. Casavant, E. Berthier, A.B. Theberge, J. Berthier, S.I. Montanez-Sauri, L.L. Bischel, et al., Suspended microfluidics., Proc. Natl. Acad. Sci. U. S. A. 110 (2013) 10111–6. doi:10.1073/pnas.1302566110.
[46] A.S. Gladman, A.-D.N. Celestine, N.R. Sottos, S.R. White, Autonomic Healing of Acrylic Bone Cement., Adv. Healthc. Mater. (2014) 1–6. doi:10.1002/adhm.201400084.
[47] K. Jud, H.H. Kausch, J.G. Williams, Fracture mechanics studies of crack healing and welding of polymers, J. Mater. Sci. 16 (1981) 204–210. doi:10.1007/BF00552073.
[48] C.B. Lin, S. Lee, K.S. Liu, Methanol-Induced crack healing in poly(methyl methacrylate), Polym. Eng. Sci. 30 (1990) 1399–1406. doi:10.1002/pen.760302109.
[49] T. Wu, S. Lee, Carbon tetrachloride-induced crack healing in polycarbonate, J. Polym. Sci. Part B Polym. Phys. 32 (1994) 2055–2064. doi:10.1002/polb.1994.090321212.
[50] P.-P. Wang, S. Lee, J.P. Harmon, Ethanol-induced crack healing in poly(methyl methacrylate), J. Polym. Sci. Part B Polym. Phys. 32 (1994) 1217–1227. doi:10.1002/polb.1994.090320709.
[51] H.-C. Hsieh, T.-J. Yang, S. Lee, Crack healing in poly(methyl methacrylate) induced by co-solvent of methanol and ethanol, Polymer. 42 (2001) 1227–1241. doi:10.1016/S0032-3861(00)00407-9.
[52] J.-S. Shen, J.P. Harmon, S. Lee, Thermally-induced Crack Healing in Poly(Methyl Methacrylate), J. Mater. Res. 17 (2002) 1335–1340. doi:10.1557/JMR.2002.0199.

[53] C.L. Mangun, a. C. Mader, N.R. Sottos, S.R. White, Self-healing of a high temperature cured epoxy using poly(dimethylsiloxane) chemistry, Polymer. 51 (2010) 4063–4068. doi:10.1016/j.polymer.2010.06.050.
[54] H. Jin, C.L. Mangun, D.S. Stradley, J.S. Moore, N.R. Sottos, S.R. White, Self-healing thermoset using encapsulated epoxy-amine healing chemistry, Polymer. 53 (2012) 581–587. doi:10.1016/j.polymer.2011.12.005.
[55] H. Jin, C.L. Mangun, A.S. Griffin, J.S. Moore, N.R. Sottos, S.R. White, Thermally stable autonomic healing in epoxy using a dual-microcapsule system., Adv. Mater. 26 (2014) 282–7. doi:10.1002/adma.201303179.
[56] M.M. Caruso, B.J. Blaiszik, S.R. White, N.R. Sottos, J.S. Moore, Full Recovery of Fracture Toughness Using a Nontoxic Solvent□Based Self□Healing System, Adv. Funct. Mater. 18 (2008) 1898–1904. doi:10.1002/adfm.200800300.
[57] M.M. Caruso, D. a. Delafuente, V. Ho, N.R. Sottos, J.S. Moore, S.R. White, Solvent-Promoted Self-Healing Epoxy Materials, Macromolecules. 40 (2007) 8830–8832. doi:10.1021/ma701992z.
[58] J.L. Moll, S.R. White, N.R. Sottos, A Self-sealing Fiber-reinforced Composite, J. Compos. Mater. 44 (2010) 2573–2585. doi:10.1177/0021998309356605.
[59] R. Schwalm, UV Coatings: Basics, Recent Developments and New Applications, Elsevier, Amsterdam, 2007.
[60] C. Decker, T. Bendaikha, Interpenetrating polymer networks. II. Sunlight-induced polymerization of multifunctional acrylates, J. Appl. Polym. Sci. 70 (1998) 2269–2282. doi:10.1002/(SICI)1097-4628(19981212)70:11<2269::AID-APP21>3.0.CO;2-D.
[61] J. V Crivello, Photoinitiated Cationic Polymerization, Annu. Rev. Mater. Sci. 13 (1983) 173–190. doi:10.1146/annurev.ms.13.080183.001133.
[62] ASTM_G173, Standard Tables for Reference Solar Spectral Irradiances : Direct Normal and Hemispherical on 37° Tilted Surface, ASTM. (2013). doi:10.1520/G0173-03R12.2.
[63] J.H. Lee, R.K. Prud'homme, I. a. Aksay, Cure depth in photopolymerization: Experiments and theory, J. Mater. Res. 16 (2011) 3536–3544. doi:10.1557/JMR.2001.0485.
[64] J.A. Carioscia, H. Lu, J.W. Stanbury, C.N. Bowman, Thiol-ene oligomers as dental restorative materials., Dent. Mater. 21 (2005) 1137–43. doi:10.1016/j.dental.2005.04.002.
[65] J. Carioscia, J. Stansbury, C. Bowman, Evaluation and control of thiol-ene/thiol-epoxy hybrid networks, Polymer. 48 (2007) 1526–1532.
[66] S. Bose, S. Vahabzadeh, A. Bandyopadhyay, Bone tissue engineering using 3D printing, Mater. Today. 16 (2013) 496–504. doi:10.1016/j.mattod.2013.11.017.
[67] W.L. Grayson, M. Fröhlich, K. Yeager, S. Bhumiratana, M.E. Chan, C. Cannizzaro, et al., Engineering anatomically shaped human bone grafts., PNAS. 107 (2010) 3299–304. doi:10.1073/pnas.0905439106.
[68] B.H. Tan, H. Hussain, K.C. Chaw, G.H. Dickinson, C.S. Gudipati, W.R. Birch, et al., Barnacle repellent nanostructured surfaces formed by the self-assembly of amphiphilic block copolymers, Polym. Chem. 1 (2010) 276. doi:10.1039/b9py00332k.
[69] E. Pezron, L. Leibler, A. Ricard, F. Lafuma, R. Audebert, Complex formation in polymer-ion solution. 1. Polymer concentration effects, Macromolecules. 22 (1989) 1169–1174. doi:10.1021/ma00193a030.
[70] A. Sunder, R. Mulhaupt, Method for Producing Highly Branched Glycidol-Based Polyols, US 2003/0092879 A1, 2003.
[71] A. Sunder, R. Hanselmann, H. Frey, R. Mulhaupt, Controlled synthesis of hyperbranched polyglycerols by ring-opening multibranching polymerization, Macromolecules. 32 (1999) 4240–4246. doi:10.1021/ma990090w.
[72] K. Ichimura, S. Watanabe, Preparation and characteristics of photocross-linkable poly (vinyl alcohol), J. Polym. Sci. Polym. Chem. Ed. 20 (1982) 1419–1432.
[73] K. Ichimura, Photocrosslinking behavior of poly(vinyl alcohol)s with pendant styrylpyridinium or styrylquinolinium groups, Makromol. Chem. 188 (1987) 2973–2982.
[74] F. Liu, F. Li, G. Deng, Y. Chen, B. Zhang, J. Zhang, et al., Rheological Images of Dynamic Covalent Polymer Networks and Mechanisms behind Mechanical and Self-Healing Properties, Macromolecules. 45 (2012) 1636–1645. doi:10.1021/ma202461e.
[75] J.M. Tseng, C.M. Shu, J.P. Gupta, Y.F. Lin, Evaluation and modeling runaway reaction of methyl ethyl ketone peroxide mixed with nitric acid, Ind. Eng. Chem. Res. 46 (2007) 8738–8745. doi:10.1021/ie0614069.
[76] X. Li, H. Koseki, Y. Iwata, Y.-S. Mok, Decomposition of methyl ethyl ketone peroxide and mixtures with sulfuric acid, J. Loss Prev. Process Ind. 17 (2004) 23–28. doi:10.1016/j.jlp.2003.08.003.
[77] J. Sanchez, T.N. Myers, Peroxides and Peroxide Compounds, Organic Peroxides, in: Kirk-Othmer Encycl. Chem. Technol., John Wiley & Sons, 2001: pp. 1–85. doi:10.1002/0471740039.vec1914.

[78] M.S. Kharasch, A. Fono, W. Nudenberg, The chemistry of hydroperoxides I. The acid-catalyzed decomposition of α,α-dimethylbenzyl (α-cumyl) hydroperoxide, J. Org. Chem. 15 (1950) 748–752. doi:10.1021/jo01150a005.
[79] P. Klemarczyk, J. Guthrie, Advances in anaerobic and cyanoacrylate adhesives, in: D.A. Dillard (Ed.), Adv. Struct. Adhes. Bond., Woodhead Publishing Limited, Cambridge, 2010: pp. 96–129.
[80] S. Moane, D.P. Raftery, M.R. Smyth, R.G. Leonard, Decomposition of peroxides by transition metal ions in anaerobic adhesive cure chemistry, Int. J. Adhes. Adhes. 19 (1999) 49–57. doi:10.1016/S0143-7496(98)00056-6.
[81] D.J. Forster, J.P.A. Heuts, T.P. Davis, Conventional and catalytic chain transfer in the free-radical polymerization of 2-phenoxyethyl methacrylate, Polymer. 41 (2000) 1385–1390. doi:10.1016/S0032-3861(99)00292-X.
[82] J. Schrooten, I. Lacík, M. Stach, P. Hesse, M. Buback, Propagation Kinetics of the Radical Polymerization of Methylated Acrylamides in Aqueous Solution, Macromol. Chem. Phys. 214 (2013) 2283–2294. doi:10.1002/macp.201300357.
[83] K. Liang, R.A. Hutchinson, The effect of hydrogen bonding on intramolecular chain transfer in polymerization of acrylates, Macromol. Rapid Commun. 32 (2011) 1090–1095. doi:10.1002/marc.201100224.
[84] A.M. Van Herk, Pulsed initiation polymerization as a means of obtaining propagation rate coefficients in free-radical polymerizations. II Review up to 2000, Macromol. Theory Simulations. 9 (2000) 433–441. doi:10.1002/1521-3919(20001101)9:8<433::AID-MATS433>3.0.CO;2-I.
[85] R.-H. Chang, C.-M. Shu, Y.-S. Duh, J.-M. Jehng, Calorimetric studies on the thermal hazard of methyl ethyl ketone peroxide with incompatible substances., J. Hazard. Mater. 141 (2007) 762–8. doi:10.1016/j.jhazmat.2006.07.062.
[86] S.R. Graham, R. Hodgson, L. Vechot, M. Iqbal Essa, Calorimetric studies on the thermal stability of methyl ethyl ketone peroxide (MEKP) formulations, Process Saf. Environ. Prot. 89 (2011) 424–433. doi:10.1016/j.psep.2011.08.005.
[87] R.A. Sheldon, Synthesis and uses o f alkyl hydroperoxides and dialkyl peroxides, in: S. Patai (Ed.), Chem. Funct. Groups, Peroxides, John Wiley & Sons, Inc., Chichester, UK, 1983: pp. 161–200.
[88] G. Lauterbach, W. Pritzkow, T.D. Tien, V. Voerckel, Studies on the Decomposition of Alkyl Hydroperoxides by different catalysts, J. Prakt. Chem. 330 (1988) 933–946. doi:10.1002/prac.19883300612.
[89] R.G.R. Bacon, The initiation of polymerisation processes by redox catalysts, Q. Rev. Chem. Soc. 9 (1955) 287–310.
[90] E.T. Denisov, T.G. Denisova, T.S. Pokidova, Free radical generation by reactions of ions with molecules, in: Handb. Free Radic. Initiat., John Wiley & Sons, Inc., Hoboken, New Jersey, 2003: pp. 591–653.
[91] K.S. Toohey, N.R. Sottos, J.A. Lewis, J.S. Moore, S.R. White, Self-healing materials with microvascular networks, Nat. Mater. 6 (2007) 581–5. doi:10.1038/nmat1934.
[92] B. Hussey, J. Wilson, Structural Adhesives: Directory and Databook, Chapman & Hall, London, 1996. doi:10.1007/978-1-4613-1203-1.
[93] S.P. Timoshenko, S. Woinowsky-Krieger, Theory of Plates and Shells, McGraw-Hill, New York, NY, 1959.

1.

1. Report Type

Final Report

Primary Contact E-mail

Contact email if there is a problem with the report.

swhite@illinois.edu

Primary Contact Phone Number

Contact phone number if there is a problem with the report

217.333.1077

Organization / Institution name

University of Illinois

Grant/Contract Title

The full title of the funded effort.

Regeneration and Remodeling of Composite Materials

Grant/Contract Number

AFOSR assigned control number. It must begin with "FA9550" or "F49620" or "FA2386".

FA9550-10-1-0255

Principal Investigator Name

The full name of the principal investigator on the grant or contract.

Scott Ray White

Program Manager

The AFOSR Program Manager currently assigned to the award

Dr. Byung-Lip Lee

Reporting Period Start Date

06/01/2010

Reporting Period End Date

05/31/2015

Abstract

The Regeneration and Remodeling of Composite Materials (Regeneration) Program was supported by the Air Force Office of Scientific Research (AFOSR) through a Discovery Grant from 2010-2015. The program was conducted at the University of Illinois at Urbana-Champaign (UIUC). Regeneration was conceived to expand the function of materials containing microvascular networks to achieve autonomous response and adaptation to external stimuli. The central goal of Regeneration was to integrate bio-mimetic functions into synthetic, engineering materials realized through a synergistic combination of expertise in chemistry and engineering. The Regeneration and Remodeling of Composite Materials program was focused on replicating the function of regeneration in which natural systems rebuild or replace macroscopic structures autonomously. Inspired by this biological ability, vascular networks were designed to synthetically regrow load-bearing structures and replenishing protective surface coatings. Multistage polymerization reactions introduced a new paradigm in healing agent conceptual design where rapid rheological transformations and selective wetting resulted in new self-supporting fluids which build upon themselves in an accretive fashion to regenerate lost mass. Experimental procedures were developed to demonstrate system efficacy and repeatability in achieving functional homeostasis of structural materials.

Distribution Statement

This is block 12 on the SF298 form.

Distribution A - Approved for Public Release

Explanation for Distribution Statement

If this is not approved for public release, please provide a short explanation. E.g., contains proprietary information.

SF298 Form

Please attach your SF298 form. A blank SF298 can be found here. Please do not password protect or secure the PDF The maximum file size for an SF298 is 50MB.

SF_298_FA9550-10-1-0255.pdf

Upload the Report Document. File must be a PDF. Please do not password protect or secure the PDF . The maximum file size for the Report Document is 50MB.

AFOSR_Final Report_lowrez.pdf

Upload a Report Document, if any. The maximum file size for the Report Document is 50MB.

Archival Publications (published) during reporting period:

1.H. Jin, K.R. Hart, A.M. Coppola, R.C. Gergely, J.S. Moore, N.R. Sottos, S.R. White, Self-Healing Epoxies and Their Composites, in: W.H. Binder (Ed.), Self-Healing Polymers From Principles to Applications. Wiley-VCH Verlag GmbH & Co. KGaA, Weinheim, Germany, 2013.
2. J.F. Patrick, K.R Hart, B.P. Krull, C.E. Diesendruck, J.S. Moore, S.R. White, N.R. Sottos. Continuous Self-Healing Life Cycle in Vascularized Structural Composites. Advanced Materials, 26 (2014) 4302-4308.
3. S.R. White, J.S. Moore, N.R. Sottos, B.P. Krull, W.A. Santa Cruz, R.C.R. Gergely, Restoration of Large Damage Volumes in Polymers. Science 344 (2014) 620–3.
4. R.C.R. Gergely, S.J. Pety, B.P. Krull, J.F. Patrick, T.Q. Doan, A.M. Coppola, P.R. Thakre, N.R. Sottos, J.S. Moore, S.R. White, Multidimensional Vascularized Polymers using Degradable Sacrificial Templates. Advanced Functional Materials 25 (2015) 1043–1052.
5. B.P Krull, J.F Patrick, K.R. Hart, S.R White, N. Sottos, Automatic Optical Crack Tracking for Double Cantilever Beam Specimens. Accepted by Experimental Techniques 3 March 2015.
6. B.P Krull, R.C.R. Gergely, W.A. Santa Cruz, Y. Fedonina, J.F. Patrick, J.S. Moore, S.R. White, N.R. Sottos, Enhanced Performance of Regenerative Polymers. In Preparation for Advanced Functional Materials.
7. R.C.R. Gergely, N.R. Sottos, J.S. Moore, S.R. White, Regenerative Polymeric Coatings via Pressure Responsive Surface Valves. In Preparation for Advanced Materials
8. W.A. Santa Cruz, B.P. Krull, R.C.R. Gergely, S.R. White, N.R. Sottos, J.S. Moore, Two-Stage Chemical Resins: A Broad Tool for Material Regeneration. In Preparation for ACS Macro Letters.

Changes in research objectives (if any):

Change in AFOSR Program Manager, if any:

Extensions granted or milestones slipped, if any:

AFOSR LRIR Number

LRIR Title

Reporting Period

Laboratory Task Manager

Program Officer

Research Objectives

Technical Summary

Funding Summary by Cost Category (by FY, $K)

	Starting FY	FY+1	FY+2
Salary			
Equipment/Facilities			
Supplies			
Total			

Report Document

Report Document - Text Analysis

Report Document - Text Analysis

Appendix Documents

2. Thank You

E-mail user

Aug 27, 2015 10:32:15 Success: Email Sent to: swhite@illinois.edu